Progress in Nuclear Magnetic Resonance Spectroscopy 64 (2012) 29–69

Contents lists available at SciVerse ScienceDirect

Progress in Nuclear Magnetic Resonance Spectroscopy

journal homepage: www.elsevier.com/locate/pnmrs

Nuclear Magnetic Resonance to characterize and monitor Cultural Heritage

Donatella Capitani *, Valeria Di Tullio, Noemi Proietti

Magnetic Resonance Laboratory "Annalaura Segre", Institute of Chemical Methodologies, CNR Research Area of Rome, Via Salaria km. 29.300, 00015 Monterotondo, Rome, Italy

ARTICLE INFO

Article history:
Received 5 August 2011
Accepted 1 November 2011
Available online 9 November 2011

Dearly dedicated to the memory of Prof. Annalaura Segre

Keywords:
Cultural Heritage
Non-invasive NMR characterization
Micro-invasive NMR characterization
Porous materials
Moisture detection by NMR
Ageing detection by NMR

Contents

Abbreviations: BMA/EA, butyl methacrylate and ethyl acrylate; CMC, carboxymethylcellulose; CPMAS, cross polarization magic angle spinning; CPMG, Carr–Purcell–Meiboom–Gill; DA, diacids; DEPT, distortionless enhancement by polarization transfer; DG, diglyceride; DMA, Dynamic Mechanical Analysis; DOSY, diffusion ordered spectroscopy; DTG, Differential Thermal Gravimetry; EA, ethylacrylate; EDP, efflorescence pathway diagram; ESR, Electron Spin Resonance; FA, fatty acids; HA, hydroxy acid; HDDA, 1,6 hexanediole diacrylate; HOHAHA, homonuclear Hartmann Hahn spectroscopy; HPLC, High-Performance Liquid Chromatography; HRMAS, High Resolution Magic Angle Spinning; HSQC, heteronuclear single quantum coherence; IRT, Infrared Thermography; IT Plot, intensity temperature plot; MA, methylacrylate; MAS, Magic Angle Spinning; MG, Monoglyceride; MIP, Mercury Intrusion Porosimetry; MMA, methylmethacrylate; MOUSE, MObile Universal Surface Explorer; MRI, Magnetic Resonance Imaging; MSD, Mean Squared Displacement; PEG, polyethylene glycol; PFG-NMR, Pulsed Field Gradient Nuclear Magnetic Resonance; TEOS, tetraethoxysilane; TG, tryglyceride; TGA, Thermo Gravimetric Analysis; TMS, tetramethylsilane; 3Q MAS, Triple Quantum Magic Angle Spinning; UPR, unsaturated polyester resins; WISE, WIdeline SEparation; XRD, X-Ray Diffraction Analysis; XRF, X-Ray Fluorescence Analysis.

* Corresponding author. Tel.: +39 0690672700; fax: +39 0690672477.
E-mail address: donatella.capitani@imc.cnr.it (D. Capitani).

0079-6565/$ - see front matter © 2011 Elsevier B.V. All rights reserved.
doi:10.1016/j.pnmrs.2011.11.001

1. Introduction

In the last decades the interest of the scientific community in characterizing, monitoring and conserving objects belonging to Cultural Heritage has continuously increased. In fact there is an always growing understanding that the characterization of the state of conservation, the knowledge of the causes of degradation of materials, the development of new methods and materials aimed at lengthening the life time of the artifacts, are mandatory in the correct safeguard of Cultural Heritage. The monitoring and diagnosting of artifacts is of help in preventing or delaying the degradation. As a matter of fact, artworks are complex heterogeneous systems whose analysis requires a multi-disciplinary approach including physics, chemistry, biology, geology, computer sciences. In addition, the number and the amount of samples collected from precious artifacts to be analyzed must be reduced to a minimum. As a consequence, a methodological approach where micro-destructive, non-destructive, and possibly non-invasive techniques are combined, is advisable.

Although for 50 years Nuclear Magnetic Resonance [1] has been a very powerful tool in many fields, its application to Cultural Heritage is rather recent. One of the reasons is that during its initial decades of existence NMR was mainly a tool for the analysis of samples in the liquid phase, whereas materials of interest for Cultural Heritage, such as paper, wood, stones, textiles, resins, parchment, pottery, glass, leather cannot be solubilized without definitely changing or even fully destroying their molecular structure. Nevertheless some NMR analysis in solution have been carried out to characterize soluble organic residues found in ancient artifacts. Usually in this field, liquid or gas chromatography followed by mass spectroscopy have been applied to separate molecular mixtures into their pure components. Nowadays these techniques are preferred to NMR only when extremely low amount of materials are available. In fact complex mixtures of organic compounds may be successfully analyzed by NMR based on difference in the molecular self diffusion coefficients. As is well known, molecular self-diffusion can be encoded into NMR datasets by means of pulsed-gradients of magnetic field (PFG-NMR) [2]. Diffusion-ordered NMR spectroscopy (DOSY) [3] is a particularly convenient way of displaying the molecular self-diffusion information, organized in a bidimensional array with the NMR spectrum on one dimension and the self-diffusion coefficient on the other one. Mixtures of compounds of different molecular weight can be nicely separated in the DOSY map. After recognizing the presence of different compounds in the analyzed residue, 2D NMR techniques [4] may be applied to identify the structure of compounds.

The required amount of material to be analyzed by NMR in solution may be minimized through the use of the recently developed cryogenically cooled NMR probes (cryoprobes) which take advantage of the fact that the radio frequency electronics generates less noise at low temperature. By reducing the temperature of the NMR detection coil and the preamplifier signal to noise ratio, large increases in NMR sensitivity have been achieved in the last few decades. This net increase in sensitivity enables one to successfully analyze an amount of sample that, just a few years ago, was simply considered too low to be studied by NMR. Cryoprobes and microprobes [5,6] offer the chance to minimize the amount of material needed to perform the NMR analysis down to the microgram scale, making NMR spectroscopy in solution a suitable technique for the analysis of a very low amount of soluble materials of interest for Cultural Heritage.

With the development of high resolution 1D and 2D solid state NMR techniques [7,8] such as high power decoupling, Magic Angle Spinning and cross-polarization to enhance the sensitivity of rare nuclei, and with the development of solid state bi-dimensional techniques, NMR has become a powerful tool also in the characterization of solid materials belonging to Cultural Heritage. Nowadays, almost any element of the periodic table may be analyzed in the liquid as well as in the solid state, the natural isotopic abundance and the sensitivity to the NMR experiment being the only limitation.

Many materials of interest for Cultural Heritage may be considered to be porous, such as porous stones, plaster, mortar, wood, paper, wall painting, fired clays. Therefore, to investigate some properties of these materials, NMR methods used to study porous materials, are applied. The most common NMR methods to probe the structures of porous media are based on the measurement of relaxation times and diffusion coefficients of water inside the porous system. In fact, relaxation times of fluids confined in porous media are strictly related to the geometry of the structure, as water in small pores relaxes rapidly, whereas water in large pores relaxes more slowly. The presence of relaxation sinks at the surface of pore grains and the inhomogeneity of pore dimensions, cause multi-exponential decay of the magnetization and a reduction of relaxation times. In many cases the properties of porous systems may be spatially resolved by means of Magnetic Resonance Imaging (MRI) [9] of fluids introduced in the pores [10].

Since the early days of well-logging NMR, water-saturated natural rocks have been characterized by multi-exponential NMR relaxation behaviour which may be analyzed in terms of distributions of relaxation times [11]. In the literature numerous experiments on water-saturated rocks have shown that relaxation time distributions are similar to pore size distributions obtained by other techniques such as Mercury Intrusion Porosimetry (MIP). For instance, in many sandstones, T_2 distributions correlated well with mercury capillary pressure curves [12]. Obviously, such a similarity is not universal, as NMR measures the size of the pore bodies, whereas MIP measures the size of the pore throat [13]. Besides, the relationship between relaxation times and pore size distributions is actually more complex because of the diffusion associated with internal gradients, such as those induced by magnetic susceptibility contrast between the pore fluid and solid matrix [14].

The introduction of joint probability densities of relaxation times and diffusion coefficients in terms of bi-dimensional distributions [15–19], has been another important development. In fact,

T_1–T_2 or diffusion–relaxation correlation maps have been exploited to study fluids in porous materials [20].

An actual breakthrough for the NMR application to Cultural Heritage has certainly been the development of unilateral NMR sensors. These sensors allow one to study arbitrarily sized objects non-invasively by combining open magnets and surface RF coils to generate a sensitive volume external to the sensor and inside the object under investigation [20–23], but the price to be paid is the inhomogeneity of the magnetic field. The availability of this instrumentation makes it nowadays possible to measure NMR parameters such as proton density, relaxation times, diffusion coefficients, and even to collect correlation maps of unmovable and precious artifacts and monuments belonging to Cultural Heritage. Usually, with these devices, to reach different depth of measurements inside the investigated object, the tuning frequency must be electronically switched. For instance, different probeheads, each one tuned at the proper frequency, are used to measure at selected depths.

Much work has been done to find relationships between NMR signals obtained in homogeneous and inhomogeneous fields and the geometrical and transport parameters of disordered media [24]. The effect of relaxation which complicates the self-diffusion measurements in the presence of a strong magnetic field gradient has been overcome by constant relaxation methods [25]. These methods are based on pulse sequences with a constant evolution time to avoid encoding T_2, any gradient that is on during the application of an RF pulse must have a constant amplitude, any gradient that is switched in the course of an experiment must always be switched at the same time and at a constant time with respect to all subsequent pulses, and, finally, the number of RF pulses must be constant. An experiment that meets these criteria may consist of an excitation pulse followed by two spin echoes with echo time T_1 and T_2 respectively, during which a magnetic field gradient of constant strength is applied. The total time $2(T_1 + T_2)$ must be constant, thus keeping the extent of signal attenuation due to transverse relaxation constant. By varying T_1 and T_2 while maintaining the total time constant the extent of diffusion attenuation of the observed signal is changed, and, consequently, the diffusion coefficient can be calculated. A constant relaxation method has been also implemented for measuring the self diffusion coefficient in the presence of strongly inhomogeneous magnetic fields generated by single-sided NMR devices [26]. To investigate porous media, the time-dependent self-diffusion coefficient, which is linked with the mean squared displacement (MSD) of liquid molecules in a restricted pore volume, is an important value, as it can help, along with T_1 and T_2 relaxation times, to unambiguously characterize the pore size. The strong magnetic field gradient which characterizes single sided NMR devices was exploited to measure the MSD of liquid molecules without using a gradient pulse-coil in the probe. The experimentally obtained time dependence of the diffusion coefficient was used to determine the surface-to-volume ratio, the formation factor, and the permeability of porous media [27].

The inhomogeneous field associated with unilateral NMR devices, causes problems in accurate measurements of transverse relaxation times, nevertheless, provided that samples are compared under identical experimental conditions, very reliable data may be obtained. It was also demonstrated that if the spatial inhomogeneities of the static and radio frequency fields are matched, then even spectroscopy is possible with unilateral NMR devices [28,29]. More recently [30], it was shown that the field of an open magnet can be shimmed to high homogeneity over a large volume external to the sensor, making it possible to measure localized high-resolution proton spectra outside a portable open magnet with a spectral resolution of 0.25 part per million.

A recent development of single-sided NMR devices, is the availability of sensors to produce depth profiles with microscopic spatial resolution. The simple magnet geometry of this sensor, generates a magnetic field with a uniform gradient to resolve the near surface structure of arbitrarily large samples [31]. The use of these sensors to investigate Cultural Heritage has already opened a number of new possibilities [32–37].

2. Porous stones

Water plays an important role in the degradation of ancient and modern inorganic porous materials such as stone, concrete, brick, and mortar. The formation of deep holes with loss of granular material is commonly observed in calcarenite where rainwater dissolves and weakens the bonds among granules, and wetting/drying cycles favoured by the action of wind and solar radiation cause solubilization and recrystallization of salts inside the porous structure inducing the breaking down of the structure itself. The capillary rise of rainwater is a common cause of weathering of the stone material constituting the base of urban monuments. Also water supplied by condensation may cause dissolution of the stone matrix. Condensation/evaporation cycles favour migration of solubilized salts and, consequently, the occurrence of efflorescence and subflorescence, therefore causing the weakening of the material and the loss of the aesthetic value. Wet materials may have their mechanical resistance diminished. When the temperature of the stone drops below the freezing point the pressure exerted by the ice crystals may have destructive effects. In some cases, such as clay minerals, water may alter the structure of the material, causing expansion, stress, and fractures. Dampness favours biological life and biological weathering, the longer the duration and/or the frequency of the wetness, the heavier the damage. Besides, in wet stones, chemical reactions may occur between the pollutant deposited on the surface and the stone. Condensation may also increase the deposition rate of airborne pollutants, in fact the particles and the hydrophilic gases that impact on a wet surface stick to it rather than bouncing off, so that the capture efficiency of the surface is increased. The condensation occurring near the wet surface causes the transport of gases and particles towards the surface. Capillary rise of water from the ground or collected rainfall is even more efficient than condensation in causing dampness, as it occurs with the progressive displacement of water and cannot be stopped by pockets of air entrapped in pores and capillary systems [38].

The formation of crusts on monuments is also related to the presence of water. The visual feature of the deterioration pattern depends on the way the water wets or washes the surface. Run-off is associated with the presence of white areas characterized by crystals of reprecipitated calcite formed when water evaporates. Condensation is associated with grey areas where the stone has been previously covered by a layer of dust and particles. Damping due to percolation near zones where run-off has previously occurred, is associated with the presence of black gypsum crusts with embedded carbonaceous particles. These particles originate from combustion products containing sulphur compounds and catalysts which, when wet, nucleate gypsum crystals [38].

The weathering of a stone also depends on the pore characteristics. In fact stones are characterized by a wide variety of pores differently interconnected, with different shape and size. In subsurface layers, where migration of salts, leaching, dissolution, erosion, chemical and biological attack occur, the porosity may change with the time.

An important field of research in Cultural Heritage is obviously focused on the weathering of porous stones. Hydrophobic, protective and consolidating treatments are often mandatory to prevent more extended damage to monuments and stone artifacts, however the choice of the treatment to be applied is not trivial as application of unsuitable treatment may cause further damage to stone

material. The pore size distribution of the stone, the variation occurring in the pore size distribution with the ageing, the variation induced in the open porosity by an applied treatment, the depth of penetration of a treatment inside a stone, the quantitative evaluation of the dampness inside a stone, are all important and difficult tasks to be assessed. In this framework NMR plays a major role as this technique provides a powerful non-destructive and, more recently, non-invasive tool for investigating porous materials. Among porous media, our interest is focused on lapideous materials largely employed in historical buildings, statues, monuments and works of art.

It is well known that the hydrophobic treatment is one of the most important interventions usually carried out in the conservation of stone artifacts and monuments. The choice of a hydrophobic product and the method of application should be aimed at preventing the penetration of liquid water, allowing vapour leakage, delaying degradation process, and avoiding modification in the optical properties of the material. As a consequence, the study of water ingress and diffusion inside a stone, before and after a hydrophobic treatment, is a very important task in stone preservation.

Conventional MRI gives the possibility of monitoring and visualizing water infiltration in porous material specimens. In fact, one of the most straightforward MRI applications is the measurement of spin density maps of nuclear spins in fluids, provided that the spin relaxation effects on the signal amplitude are taken into account. However, while relaxation effects complicate the quantitative interpretation of the signal amplitude, the sensitivity of NMR signals to the molecular environment provides many opportunities. The availability of various contrast schemes enables the use of methods to study fluids in porous media with MRI. Based on spin relaxation contrasts arising from differences in molecular mobility in different material environments, structural heterogeneities can be mapped. The sensitivity of NMR signals to molecular translational motion may be exploited as a contrast to measure molecular diffusion and fluid velocity. By imaging fluids introduced in pores, the properties of porous systems can be spatially resolved. In the literature, MRI applications to water-saturated porous stones before and after applying hydrophobic, protective, and consolidating treatments, have been reported. MRI has been applied to investigate the evolution of the hydrophobic activity of Paraloid B72 and Silirain 50 when a treated biocalcarenite, namely Lecce stone, is exposed to liquid water [39,40]. It was shown that, by following the height of the imbibition front by MRI, relevant parameters characterizing the effect of the treatment and different methods of application, can be obtained [41]. The efficacy of hydrophobic treatments in preventing water absorption in Carrara and Condoglia marble, and in travertine, was monitored by MRI [42,43], furthermore images showing water distribution at short absorption times were reported to show the suitability of this technique for monitoring the water absorption rate and diffusion within the porous matrix. The pore filling process of a porous carbonate stone widely used in monuments, sculptures and artifacts in the Veneto district (Italy), has been studied during different absorption phases by capillary rise [44]. Longitudinal magnetization decays were measured at different absorption steps and, based on the Brownstein and Tarr model [45], the magnetization decay was related to the pore geometry and dimension.

As is well known, ^{1}H low resolution NMR has been also widely used to characterize different types of water-saturated porous stones, as relaxation times of the liquid phase are sensitive to the pores size and to changes occurring in the porous structure after a treatment. With the aim of better understanding the properties of untreated and treated porous stones, combined MRI and ^{1}H low resolution NMR studies, have sometimes been carried out.

The effect of hydrophobic treatments with Wacker Polysiloxane 290 on travertine and pudding stone has been investigated by T_1 and T_2 relaxation time distributions measured in a homogeneous low magnetic field [46]. In the case of travertine samples, after the treatment, the amplitude of an intermediate component was found to be greatly reduced whereas the amplitude of the longest one remained almost unaffected. In the case of pudding stone samples, a loss of the amplitude of the long and intermediate components, was observed.

MRI and ^{1}H relaxometry were used for monitoring the effectiveness of calcium hydroxide nanoparticles to consolidate dolostone, a stone which was typically used in historic buildings of Madrid (Spain) [47].

It must be noted that, conventional unmovable NMR instrumentation requires taking a sample from the object. The development of portable unilateral NMR devices allows one to overcome this difficulty, for instance porous stones may be investigated non-invasively *in situ*, the only drawback being the inhomogeneous field generated by these devices. With unilateral NMR, relevant parameters, such as the proton spin density, longitudinal and transverse relaxation times, and diffusion coefficients can be measured [20].

The apparent NMR relaxation time distribution is affected in different ways by wall relaxation and internal field gradients in porous materials. Provided that the material is saturated by low-viscosity fluids and the exponential signal decay is dominated by wall relaxation, the decay curve associated with a single pore size shows a single exponential trend, the decay constant (T_1 or T_2) is proportional to the pore size, with small pores characterized by relaxation times shorter than those measured in large pores. Therefore the ^{1}H NMR signal of water in porous media can be related to the porosity and the pore size distribution of the investigated material.

In a homogeneous field the longitudinal and transverse relaxation rates in saturated porous media may be written as follows:

$$\frac{1}{T_1} = \frac{1}{T_{1b}} + \rho_1 \frac{S}{V}, \tag{1}$$

$$\frac{1}{T_2} = \frac{1}{T_{2b}} + \rho_2 \frac{S}{V}, \tag{2}$$

where T_{1b} and T_{2b} are the bulk relaxation times, $\rho \frac{S}{V}$ originates from the molecules in contact with the pore surface, ρ_1 and ρ_2 are the relaxivities of the surface, and $\frac{S}{V}$ is the surface to volume ratio. Bulk contributions are often much smaller than those of surfaces and in many cases may be neglected [10]. However, in the case of transverse magnetization, in the presence of a magnetic field gradient of strength G, attenuation due to molecular diffusion must be accounted for. The gradient may originate from variations in the magnetic susceptibility associated with pore geometry or from inhomogeneity in the applied magnetic field B_0. As a consequence, in strongly inhomogeneous polarization and RF fields such as the case of unilateral NMR, the transverse spin–spin relaxation rate also depends on the G strength:

$$\frac{1}{T_2} = \frac{1}{T_{2b}} + \rho_2 \frac{S}{V} + \frac{D(\gamma G t_E)^2}{12}, \tag{3}$$

where D is the diffusion coefficient, γ is the gyromagnetic ratio of the nucleus observed, and t_E is the echo time. The effect of diffusion may be markedly reduced provided that CPMG sequence uses an echo time as short as possible to measure T_2 [23].

In the fast diffusion limit, in a porous material with a distribution of N different pore sizes, the transient variation of the transverse magnetization $M_{x,y}(t)$ is a sum of exponentials:

$$M_{xy}(t) = \sum_{i=1}^{N} M_{xy,i}(0) \cdot \exp\left(-\frac{T}{T_{2,i}}\right), \tag{4}$$

In a homogeneous field the distribution of transverse relaxation times is a map of the pore size distribution, whereas in an inhomogeneous

field the magnetic field gradient does not vanish and the decay of the echo envelope is affected by diffusion. As a consequence, T_2 distributions measured in a strongly inhomogeneous field cannot be directly related to pore size distributions. Nevertheless, a T_2 distribution may give a better resolving power than T_1, although, in a strongly inhomogeneous field, it is affected by diffusion.

A Halbach magnet has been designed for measuring porosity and pore size distributions of water-saturated cylindrical geological cores with diameters up to 60 mm [48,49]. The main advantage of an NMR scanner with Halbach geometry compared to conventional NMR equipment is its small size, weight and mobility. A Halbach magnet consists of a suitable number of identical rectangular bar magnets. It provides a strong and sufficiently homogeneous magnetic field in a large and accessible cylindrical volume, the field direction is transverse to the cylinder axis, and solenoidal or surface RF coils can be used. To built long cylinders with such field characteristics, magnet rings are assembled and stacked using threaded rods. The average flux and the inhomogeneity inside the volume increases as the number of bar magnets decreases [48,49]. In particular the Halbach magnet array used to investigate water-saturated cylindrical geological cores, consists of 16 bar magnets assembled to produce a ring with 70 mm inner diameter and 155 mm outer diameter. Six rings have been stacked resulting in a 165-mm tall magnet weighting about 8 kg [49]. Compared to T_2 distributions obtained with a Halbach core-scanner, distributions obtained with a unilateral NMR device, due to diffusion, were found to be compressed towards shorter relaxation times [49]. However, in the case of the Halbach core-scanner, which generates a homogeneous low magnetic field, full cylindrical and split semicylindrical cores of porous stone to be investigated must fit within the coil, whereas, with unilateral NMR, no particular geometry as well as no sampling of the stone is required.

T_2 relaxation times distribution in a series of water-saturated limestone and sandstone specimens were obtained using unilateral NMR [50]. Even though the relaxation time distributions at long relaxation times were found to be compressed with respect to distributions measured in a homogeneous field, the amplitude of the signals and the values of the corresponding distribution integrals were directly related to the spin density in the sensitive volume probed by the instrument. Absolute values of porosity were obtained by calibrating the NMR measurements on pure water which corresponds to 100% porosity, and the apparent relaxation time distribution varied along the specimen so that porosity profiles were mapped along the specimen.

In another paper [51], sandstone specimens untreated, partially and fully consolidated with stone strengtheners, and also historical brick materials, were analyzed by transverse NMR relaxometry and MIP. To understand the relevance of unilateral NMR as a non-invasive tool for investigating porous materials, transverse relaxation time distributions of water in water-saturated specimens were measured by low field NMR using both homogeneous and inhomogeneous fields. Measurements in inhomogeneous field were performed with two different sensors, one with a field gradient of 2 T/m and the other one with an average field gradient of about 20 T/m. The T_2 relaxation time distributions of water-saturated untreated sandstone specimens measured with the two inhomogeneous fields were found to be similar, albeit those measured with the grossly inhomogeneous field showed a loss of signal at long relaxation times. In all cases untreated specimens showed a considerable signal at long relaxation times indicating the presence of large pores. Specimens partially and fully consolidated with Tegovacon V100 and Funcosils 100 and 300, showed an overall attenuation of relaxation time distributions, in particular for the longest relaxation times. The attenuation was found to be stronger in fully consolidated specimens, in a good agreement with filling and size reduction of the pores by deposition of stone strengthener. In comparison to untreated samples, the number of large pores was reduced up to a depth of a few millimeters into the specimen. However, in the case of specimens consolidated with Funcosil 300, the shape of the relaxation time distribution was found to be very similar to the one measured in untreated specimens. In contrast with sandstone, the historical brick materials contain different amount of paramagnetic impurities. Surprisingly, for these materials the distributions measured by an unilateral NMR device with a grossly inhomogeneous field, showed a better match with the pore size distributions obtained by MIP, than those measured in a homogeneous field. The hypothesized explanation is in the role possibly played by the distribution of para- and ferromagnetic impurities in bricks. A few, large agglomerates may be less likely to be found in the thin sensitive volume of the unilateral NMR sensor with a strong field gradient, than in the homogeneous field of a conventional low-field NMR device where the signal is detected from the entire sample [51].

In another paper, the distribution of relaxation times measured *in situ* in a cryptoporticus at Colle Oppio in Rome, was reported [52]. An ancient Roman fresco which appeared very wet, as well as bricks in the surrounding wall, were investigated. Although some signal loss occurred due to the translational diffusion in the highly inhomogeneous field, the T_2 distribution in the wet fresco showed strong signals both at short and long T_2 values, indicating that small and large pores were filled with water. The brick wall supporting the fresco gave similar results, whereas bricks in another, apparently dryer part of a different wall of the cryptoporticus showed a very attenuated signal at long T_2, indicating the presence of a very low amount of water in large pores [52].

The effect of consolidation treatments of Pale Finale stone, widely used in the Liguria district (Italy), was monitored by unilateral NMR [53]. Different slices of the specimens at different depths were investigated. In order to consolidate the stone, a mixture of butyl methacrylate and ethyl acrylate (BMA/EA), or a pure monomer 1,6-hexanediole diacrylate (HDDA), was introduced into the stone by capillarity, and thereafter it was frontally or *in situ* polymerized. The small size of the monomer molecule was expected to produce a deeper penetration into the stone. A specimen treated applying Paraloid B72 by brush was also investigated. Decays obtained by applying saturation recovery and Carr–Purcell–Meiboom–Gill (CPMG) sequences to measure T_1 and T_2 respectively, on water-saturated untreated and consolidated specimens, showed a trend which clearly matched the trend of the capillary water absorption curves at the longest time of water uptake. As an example, CPMG decays measured at a depth of 3 mm inside specimens are shown in Fig. 1a. The slowest decays were observed in the untreated specimen and in the specimen treated with Paraloid B72, the fastest one being observed in the specimen after polymerization *in situ*, whereas the specimen frontally polymerized showed an intermediate behaviour. The transverse relaxation times in porous media decrease as the fluid saturation is lowered [54] so that these data clearly indicate that the specimen treated by *in situ* polymerization had the highest hydrophobic efficiency, whereas the specimen treated with Paraloid B72 had no hydrophobic efficiency. In fact, in accordance with the trend of the capillary absorption curve, see Fig. 1b, the stone treated with Paraloid B72 for long hydration times, fully lost its hydrophobic efficiency. CPMG trends also clearly matched results obtained by the conventional MRI technique, see Fig. 1c–f. In the images, bright areas indicate areas filled with water, whereas dark areas indicate the absence of water. Images of the untreated specimen and of the specimen treated with Paraloid B72 (Fig. 1c and d respectively) showed the brighter areas, whereas the specimen treated by *in situ* polymerization (Fig. 1f) showed very few bright areas, and the specimen treated by frontal polymerization showed an intermediate behaviour (Fig. 1e). Unilateral NMR also allowed the

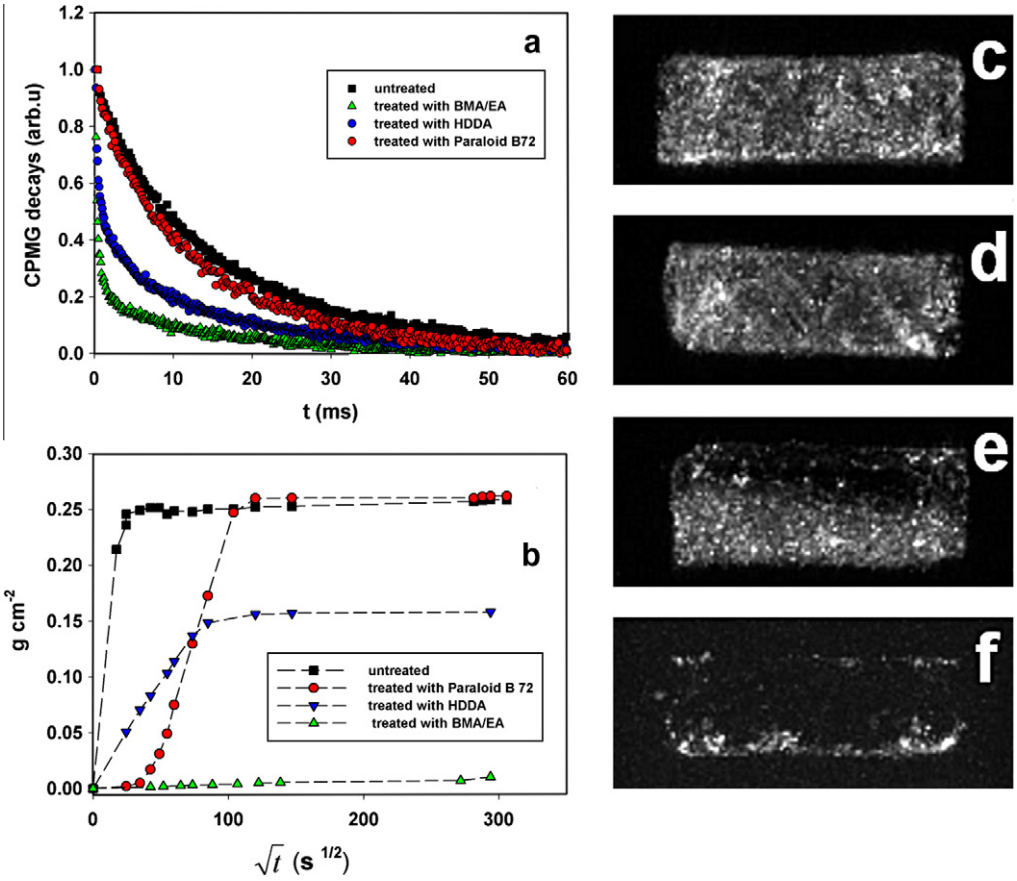

Fig. 1. (a) CPMG decays measured at a depth of 3 mm on untreated Pale Finale stone, stone treated with Paraloid B72, stone treated with HDDA frontally polymerized, and treated with BMA/EA polymerized *in situ*. (b) Capillary water absorption curves of untreated Pale Finale stone, stone treated with Paraloid B72, with HDDA frontally polymerized, and with BMA/EA polymerized *in situ*. MRI images (5 cm × 2 cm) of the untreated stone (c), treated with Paraloid (d), treated with HDDA (e), and treated with BMA/EA (f). (Adapted from [53].)

monitoring of the hydrophobic action as a function of the depth inside the specimen. As an example, in the case of the specimen polymerized *in situ*, the CPMG decay became faster with increasing the depth of measurements indicating that the fluid saturation lowered with the depth, see Fig. 2.

Bortolotti and coworkers studied the water absorption kinetics in Lecce stone untreated and treated with Paraloid B72, by a combined use of unilateral NMR and MRI [55]. The visualization of water and the quantitative data obtained by imaging at different absorption times, supported the interpretation of the changes of relaxation time distributions measured by unilateral NMR.

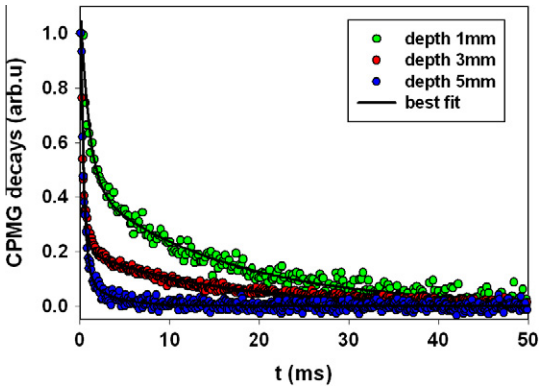

Fig. 2. CPMG decays measured at different depths on Pale Finale stone treated with BMA/EA. The solid lines were obtained by applying a best fit procedure to the experimental data. (Adapted from [53].)

NMR relaxation time distributions obtained both with laboratory and portable NMR devices have been used for characterizing the pore size distributions of building materials from the Roman remains of the Greek–Roman Theatre of Taormina (Italy) [56]. The distribution of relaxation times obtained were compared with pore size distributions measured by MIP. Whereas T_1 distributions measured both in homogeneous and inhomogeneous field, show a substantial match with the distributions obtained by MIP, T_2 distributions measured in inhomogeneous field are influenced by molecular diffusion.

The Profile NMR-MOUSE (Mobile Universal Surface Explorer) device was used to investigate non-invasively, the hydrophobic action of dimethylsiloxane on sandstone and calcarenite specimens, as a function of the time of application of the treatment [36]. As an example, depth profiles measured in water-saturated sandstone specimens untreated and treated with the hydrophobic agent for 5 s, 600 s, and 1800 s, are reported in Fig. 3a. These profiles describe water absorption throughout specimens as amplitude (proton spin density) variations with a resolution of 20 μm. To understand the meaning of depth profiles, it must be born in mind that the amplitude is directly proportional to the amount of absorbed water. By comparing the amplitude of depth profiles regarding untreated and treated specimens, it is possible to obtain information about the amount of water absorbed by specimens, and, consequently, to scale the hydrophobic action of treatments.

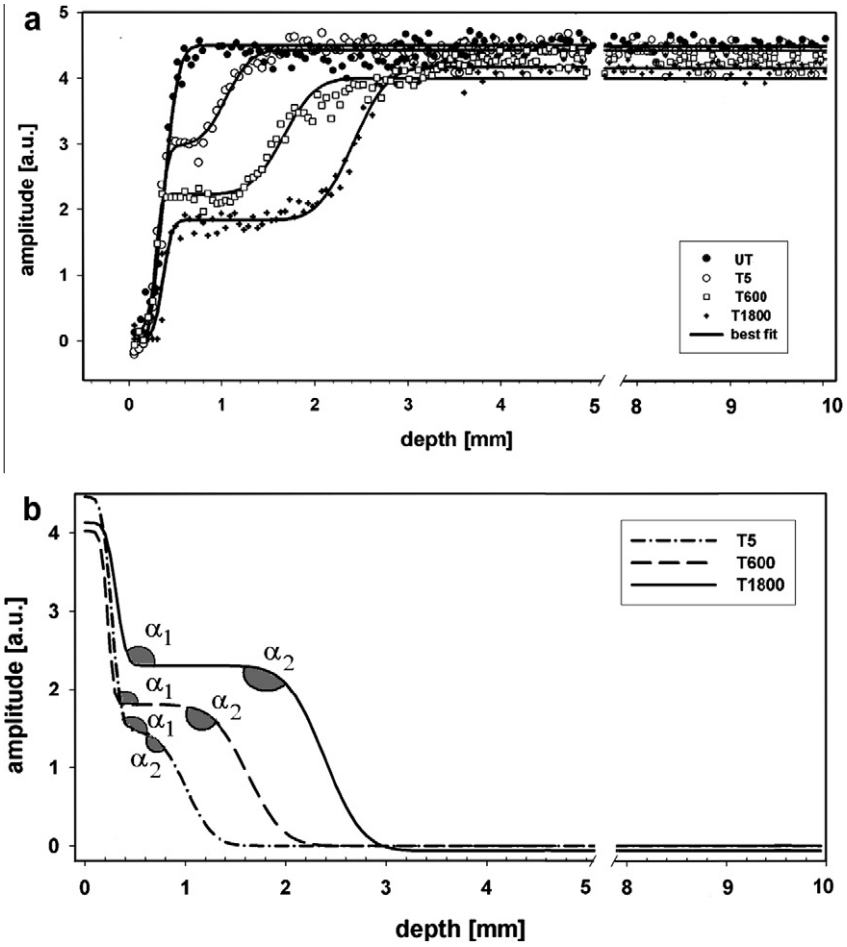

Fig. 3. (a) Depth profiles of proton spin density of sandstone untreated (UT) and treated with dimethylsiloxane for 5 s (T5), 600 s (T600), and 1800 s (T1800). Solid lines were obtained by applying a best fit procedure to experimental data. (b) Depth profiles of sandstone encoding the compound absorption throughout the specimen due to the hydrophobic treatment. Angle α_i are defined according to Eq. (11). Note that the lower the angle α_i the steeper the change in slope between the lines, on the contrary, the higher the angle α_i the smoother the change in slope. (Adapted from [36].)

It is worth noting that each profile of treated specimens shows two inflection points which are related to abrupt variations of the amount of absorbed water, see Fig. 3a. Each inflection point indicates the presence of a transition from a low to a high content of water absorbed by the specimen. The first inflection point which encodes the fast rising initial part of the profile, is affected by surface effects being very close to the water–air-specimen interface. The second inflection point encodes the penetration depth of the applied treatment, in fact, at greater depths, the hydrophobic action was found to be no longer effective because of the absence of dimethylsiloxane at those depths [36].

To evaluate the penetration depth of treatments, the experimental depth profiles $f(x)$ were fitted [36] to the following equation:

$$f(x) = \sum_{k=1}^{N} \frac{w_k}{2} erf\left[\frac{x_k - x}{\sqrt{2}\Delta_k}\right] + q_0, \tag{5}$$

where N is the number of inflection points, x_k is the depth at which the inflection point occurs, Δ_k is the half width of the transition of the amplitude from low to high value of the spin density, w_k is the spin density, and q_0 is the lowest spin density. The value of the inflection point is the penetration depth of the treatment, as a consequence a low x_k value corresponds to a shallow penetration depth of the treatment, and a high x_k value corresponds to a great penetration depth of the treatment.

Slopes at inflection points were calculated according to the following equation:

$$b_k = \frac{f(x_k + \Delta_k) - f(x_k - \Delta_k)}{2\Delta_k} \quad k = 1, \ldots, N, \tag{6}$$

where x_k and Δ_k are the parameters obtained applying the best fit procedure to Eq. (5). The parameter b_k encodes the fastness of the variation of the amplitude of the profile, therefore a high b_k value indicates a sharp variation of the amount of the absorbed water, whereas a low b_k value indicates a gradual variation of the amount of the absorbed water.

Profiles of treated specimens reported in Fig. 3a showed an amplitude reduced as a function of the duration of the treatment, and the penetration depth of the treatment x_2 increased with the duration of the time of application of the hydrophobic agent. In fact the greatest x_2 value, i.e. 2.39 mm, was found in the specimen treated for 1800 s, and the smallest one, i.e. 1 mm, was found in the specimen treated for 5 s, whereas an intermediate value of 1.63 mm, was found in the specimen treated for 600 s. In all treated specimens, at depths greater than x_2, the amplitude of the profile progressively increased up to values as high as those measured in the untreated specimen, see Fig. 3a.

These profiles determine the penetration depth of the treatment agent by showing that the amount of absorbed water is modulated by the presence of the agent inside the specimen. In this case, the

depth profile encoding water absorption may be thought of as a sort of negative image of the profile regarding the absorption of the hydrophobic compound that penetrated the specimen. As a consequence, the profile of the absorbed compound can be easily calculated point by point [36]:

$$F(x_i) = Q - f(x_i) \quad i = 1, \ldots, L, \tag{7}$$

where L is the number of experimental points constituting the profile, $f(x_i)$ is the value of function $f(x)$ calculated at the point x_i, and

$$Q = q_0 + \sum_{k=1}^{N} w_k \tag{8}$$

is the highest spin density.

Slopes at inflection points were also calculated:

$$B_k = -b_k \quad k = 1, \ldots, N, \tag{9}$$

where N is the number of inflection points, and used to define an angle θ as:

$$\theta = \text{arctg}\left|\frac{B_k - B_{k+1}}{1 + B_k B_{k+1}}\right|. \tag{10}$$

The absolute value in Eq. (10) was used to calculate the acute angle θ between the two lines, and the supplementary angle α between the two straight lines was obtained as:

$$\alpha = 180^{\circ} - \theta. \tag{11}$$

Note that the lower the angle α_i the steeper the change in slope between two straight lines, on the contrary, the higher the angle α_i the smoother the change in slope. Changes in slope are closely related to the occurrence of inhomogeneities in a treated stone, the steeper the change in slope the sharper the inhomogeneity [36]. In the case of two straight lines perpendicular to each other the denominator of Eq. (10) is equal to zero, therefore the angle α must be directly set at 90°.

The depth profiles of the hydrophobic agent absorbed for 5 s, 600 s, and 1800 s were calculated from Eq. (7), see Fig. 3b. Slopes at the inflection points give important information regarding the dispersion of the treatment agent inside the specimen, as changes in slope indicate a variation of the amount of the absorbed agent inside the specimen. In particular, angles α_i were found to be suitable analytical parameters which account for inhomogeneities occurring inside a stone after a treatment. It is worth noting that an important requirement in stone conservation is that the compound absorbed in the stone should not give rise to regions where sharp variations of the amount of the absorbed product occur. In fact, under these circumstances, chemical and physical inhomogeneity occurs between the impregnated layers and the layers underneath. These layers might respond differently to changes in thermo-hygrometric conditions, for instance the volume expansivities of adjacent layers might be different causing mechanical damage to the porous structure of the stone [57]. Actually, the depth profile along with the parameters obtained by the best fit procedure of experimental data, constitute a fingerprinting of the action of the hydrophobic treatment and of the porous network which underwent the treatment. Fig. 4 shows T_2 relaxation time distributions measured at depths of 1 mm and 4 mm in a sandstone treated for 1800 s. The distributions clearly show that, at a depth of 1 mm, the greatest amount of water was confined in small pores and the remaining water was confined in medium pores, whereas at 4 mm three T_2 peaks corresponding to water in small, medium, and large pores, were observed [36]. These results match those of depth profiles which show that, at a depth of 1 mm the amount of absorbed water is reduced due to the hydrophobic action, whereas at 4 mm the hydrophobic action is no longer effective, see Fig. 3a.

The Profile NMR-MOUSE has been used to monitor the penetration and the sublimation process of cyclododecane in Carrara marble, Lecce stone, and mortar [33]. Depending on the porous structure and on the method of application, cyclododecane can act as a suitable temporary consolidant and protective compound. It can be used in cases of emergency or during transportation of objects to the restoration site. The suitable time of application of the treatment may be chosen if its sublimation kinetics is known. The kinetics can be monitored only by non-invasive techniques that do not interfere with the sublimation process and that can be applied *in situ*. Depth profiles clearly showed the different sublimation kinetics and penetration occurring in the three selected materials. In the same paper [33], the Profile NMR-MOUSE with 2.5 cm depth access was used to investigate the moisture content of the world Cultural Heritage mosaic of Neptune and Amphitrite at Herculaneum. Depth profiles measured at two positions through the mosaic, detected a large difference in moisture content of the two different types of tesserae (ocre and blue tesserae), whereas the same moisture profiles were detected for the mortar embedding the mosaic stones.

3. Salts in porous stones

Although salt damage to buildings, monuments and stone artifacts has been extensively investigated, there is a scarcity of adequate and reliable experimental data about the mechanism responsible of the formation of salt crystals and the development of damage by crystal growth.

To shed light on this task, Pel et al. [58,59] investigated salt transport during the drying of NaCl contaminated fired clay bricks, as this process induces salt crystallization at the surface of the material. For this purpose, a home-built MRI device [60] was used which allowed the investigation of cylindrical samples. With this device a one-dimensional resolution of 1 mm was obtained. Samples were saturated with solutions at different NaCl concentrations. The probehead detected ^{23}Na signals as well as ^{1}H making possible the study of salt transport in the material. The duration of the echo time used in the experiment was purposely chosen to detect Na nuclei only in solution, excluding signals from NaCl crystals. At initial drying times, the Na concentration profile clearly showed that Na ions were advected at the top of the sample up to a local concentration equal to the saturation value. Obviously, at this point, additional advection would have caused white efflorescence at the top of the sample. At longer times of drying, the NaCl concentration profile of the sample, started levelling off until the concentration in the whole sample was equal to the saturation

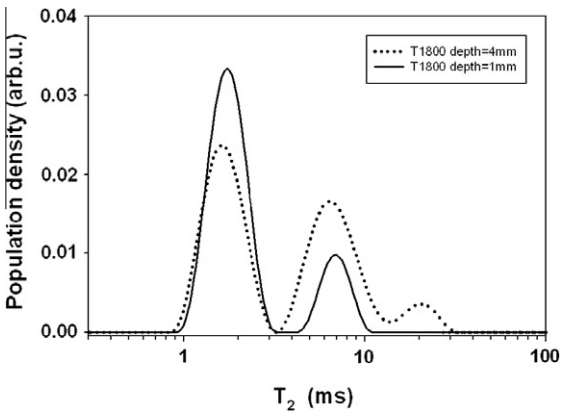

Fig. 4. Transverse relation time distributions in sandstone treated for 1800 s, measured at depths of 1 and 4 mm. (Adapted from [36].)

value. Actually, the measured NaCl concentration profiles described the competition between advection which transports Na ions to the surface of the sample causing salt accumulation, and diffusion which levels off any accumulation. To account also for the crystallization process, Kopinga and Pel [60] represented the measured moisture and NaCl concentration profiles in an efflorescence pathway diagram (EPD) where the amount of NaCl measured by NMR, was plotted against the average saturation. Diagrams indicated that crystallization at the surface usually cannot be avoided, however the drying rate is a key parameter in the salt crystallization process. It was suggested [60] that, in the case of historical objects preserved indoors, where the environmental conditions can be controlled, the relative humidity should be kept as constant as possible and airflow in the proximity of the object should be prevented to avoid wetting/drying cycles. In the case of outdoor monuments which are frequently exposed to wind and variations of the relative humidity, to attenuate the problem of salt crystallization the source of salts should be eliminated by avoiding flooding and rising damp, or partly prevented by the use of a salt inhibitor [59].

Crystallization pressure of salt in porous materials is one of the mechanisms that may induce serious damage to buildings and monuments of interest for Cultural Heritage. Because this pressure also causes the solubility of the salt inside a porous material to differ from the bulk solubility, it can be assessed experimentally by measuring the solubility inside the pores. The size of a salt crystal is limited in porous materials by the size of pores, and as a consequence, the salt solubility is predicted to increase with decreasing pore size. This increase is believed to be related to the stress generated by the crystallization process on the pore wall. Rijniers et al. investigated the crystallization of salts in porous materials with well defined pore sizes [61,62]. Samples were saturated with Na_2SO_4 and Na_2CO_3 solutions, and then cooled and, after the nucleation had occurred, they were heated slowly to guarantee thermodynamic equilibrium. During the heating both ^1H and ^{23}Na intensity profiles and relaxation times were measured. In the case of sodium carbonate, the solubility inside the 30 nm pores was found to be the same as that found for the bulk solution, with a phase transition from the decahydrated phase to the monohydrated phase at 32 °C. The solubility inside smaller pore sizes, namely 10 and 7 nm, was found to be definitely higher than that for the bulk solution, with a large temperature shift of the phase transition to lower values, see Fig. 5. Furthermore these authors used the increase of solubility determined by NMR measurements to calculate the excess of pressure p in a crystal [62]:

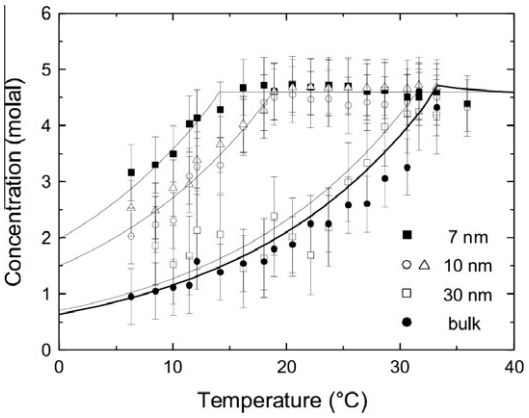

Fig. 5. Solubility of Na_2CO_3 in bulk and inside the pores of various dried silica gels (Nucleosils) with a well known pores dimension. (Reproduced with permission from [62].)

$$p = nRT\left[\frac{1}{v_s^c}\ln\left(\frac{C}{C_0}\right) - \frac{\chi v_w^l}{v_w^c}(C - C_0)\right], \quad (12)$$

where n is the number of ion moles in the salt, R is the gas constant, T is the absolute temperature, v_s^c is the molar volume of salt in the crystal (m^3/mol), v_w^l is the molar volume of water in the liquid (l/mol), v_w^c is the molar volume of water in the crystal (l/mol), C is the saturation concentration in the pore, C_0 is the saturation concentration in the bulk solution. The factor χ (=1000) accounts for the fact that the concentration C is given in mol/l instead of mol/m^3. It was found that crystallization pressures of about 9 and 13 MPa were actually developed in 10 and 7 nm pores respectively. NMR intensity profiles collected for Na_2SO_4 bulk solution as well as for solutions in pores with different sizes, showed that in all cases, the solubility of this salt coincided with the solubility of a Na_2SO_4 heptahydrated metastable crystal phase known from the literature. The solubility of this metastable phase was found to be independent of the pore size, which means that the surface tension of this phase is very small. Therefore no crystallization pressure is developed, and consequently, no damage is induced in the porous structure [62].

The possibility of applying the Brownstein–Tarr model [63] to the relaxation of Na nuclei of NaCl solutions in porous materials, has been investigated by Rijniers et al. [64]. According to this model, the relaxation rate of the ^1H NMR signal is inversely proportional to the pore size. Results obtained on porous materials with a well defined pore size and on porous building materials such as calcium silicate brick and mortar, indicated that the ion distribution over the pores can be obtained from the analysis of the ^{23}Na NMR signal decay, provided that the pore sizes are approximately below 1 μm.

Gombia and coworkers [65] investigated the kinetics of water condensation and salt deliquescence inside the pore space of three different lithotypes with a similar composition (carbonate rocks) and a different pore space architecture, untreated and polluted with calcium nitrate. Calcium nitrate is a deliquescent salt found as a pollutant even in porous substrata not directly exposed to acid rain, such as stone artifacts, wall paintings, and statues. Experiments were performed in a homogeneous field following in time the formation of liquid water inside pores by T_1 and T_2 relaxation time distributions [66,67]. The distributions allowed the observation of the effects of both the salt concentration and pore space structure on the amount of water vapour condensed and its kinetics. It was found that, for a given lithotype, even with different amounts of pollutant, the rate-average relaxation time (i.e. the reciprocal of the average relaxation rate $1/T_1$) tends to increase monotonically with the intensity of the NMR signal which is proportional to the amount of liquid water. The authors found that the rate-average relaxation time behaviour suggests a trend toward the filling of larger pores as the amount of liquid water increases, even if it does not indicate a strict sequential filling of pores in order of size. Increased amounts of salt lead to both markedly increased rates and markedly increased amounts of adsorbed water [65].

MRI was used to monitor the drying process of water-saturated unpainted and painted Portuguese calcitic calcareous stones, with the aim of reaching a better understanding how paints influence the drying of porous materials [68]. NMR images and 1D moisture profiles showed that unpainted specimens dried faster than painted ones. The difference was particularly significant during a first step of drying when a lower drying rate was observed for the painted than for the unpainted specimen. As a consequence, the drying front receded earlier into the unpainted specimen, and, therefore the surface of the painted specimen remained wet for a longer time, and a higher amount of moisture was eliminated by surface evaporation from the painted specimen. The monitoring of the drying process may give important information about the

evaporative crystallization processes, as soluble salts crystallize at the drying front. The distribution of salts across the material depends on the position of the drying front throughout the drying. At the beginning of the drying, the wet front is located at the outer surface and, therefore, efflorescence takes place. As the drying proceeds, the front recedes inside the material, and, therefore, subflorescence occurs. Consequently, the authors found that worsening of dampness problems and of surface damage by salt crystallization may arise from the use of paints that reduce the evaporation rate [68].

4. Wall paintings

The conservation of wall paintings requires specific methodologies and treatments that are related to their specific physical nature [69]. In fact wall paintings are constituted of materials having a high and open porosity, resulting in an easy accessibility of liquids and gases such as salt solutions, atmospheric pollutants, dampness, and solutions of materials used for conservation treatments. Wall paintings are part of an essentially open physical system due to contact with contiguous structures (walls, ground, roofs) that are dynamically involved in a series of physical and chemical events. Additionally, in many cases the surrounding microclimate cannot be controlled. Recently, the development of portable NMR devices has allowed the investigation of these artworks. These studies have been focused on the detection of the dampness which affects wall painting causing heavy damage to the surface and the porous structure of these precious and unmovable artworks. Other investigations have been devoted to detecting the occurrence of detachment of the pictorial film from the plaster and to monitor the effect of cleansing and consolidating treatments.

4.1. Moisture in wall paintings

Water is a very widespread cause of decay to masonry materials, and, in particular, to building masonry belonging to Cultural Heritage [70]. When soluble salts are present in the soil or in the mortar, they are drawn in solution into the porous network constituting the wall. As a consequence, salts crystallize causing fretting and crumbling of the wall when the product of the salt concentration activities is greater than the equilibrium constant and/or when the ambient relative humidity becomes lower than the equilibrium relative humidity of the saturated solution of the particular salt phase. An accurate diagnosis of the causes and extent of the moisture, and an understanding of water transportation and distribution throughout the wall, is essential for determining the mechanism by which water triggers and accelerates the damage [71]. This is particularly true for wall paintings, where a number of factors must be taken into account, such as the vulnerability with respect to the thin painted surface, the surrounding environment, the difficulty in controlling moisture and pollution, and the proximity of crowded areas. With respect to other painted artifacts, wall paintings show a special behaviour because of their high and open porosity and because the pores may easily intercommunicate among themselves, with the plaster and with the external environment. The amount and the distribution of the moisture in the plaster underneath the wall painting should be known before performing any conservation and/or restoration treatment. However, the amount and the distribution of moisture within a wall painting is difficult to determine: the methods currently used are Infrared Thermography (IRT), electrical conductivity and gravimetric tests. IRT does not allow a quantitative evaluation of the moisture content and in some cases the use of IRT is impaired by the environmental conditions [72]. Electrical conductivity may be affected by the presence of salts, and gravimetric tests require the drilling of solid cores, which is strictly forbidden in the case of ancient and precious wall paintings.

More recently, unilateral NMR has been used for quantitatively mapping the moisture distribution in wall paintings in a fully non-invasive way [73]. The intensity of the signal detected by unilateral NMR is directly proportional to the water content and by performing a suitable number of measurements and processing the experimental data in a proper way, it is possible to obtain a precise map of the moisture distribution in the wall painting under investigation. This method has been applied to monitor the moisture in the 16th century wall paintings of Serra Chapel in the "Chiesa di Nostra Signora del Sacro Cuore", Piazza Navona, Rome [73]. Wall paintings on the left side of the Chapel, were affected by a marked degradation with a loss of pictorial film, which had been ascribed to the effects of moisture rising from the ground. Because the field generated by unilateral NMR is inhomogeneous, the signal decays very quickly and must be recovered stroboscopically [52]. As a consequence, the moisture signal was collected after applying a Hahn echo pulse sequence. To detect the moisture inside the wall paintings, measurements were carried out choosing a matrix of points on the painted surface. Each experimental point covered an area of about 2×5 cm^2 that corresponded to the area of the probehead. Afterwards a contour plot was created after applying an algorithm for smoothing sharp variations of the dependent variable values within the 3D data set. As an example, the moisture distribution map obtained in an area of the wall paintings of the Chapel, is reported in Fig. 6. In this map the moisture distribution is shown as a colour gradient, where red indicates a very low water content, while dark blue indicates the highest water content. The map clearly shows the dampness throughout the wall painting. Although the map differentiates areas as a function of the moisture content, a further step was necessary to establish the precise amount of moisture in each area of the map. Thus, the calibration of the integral of the NMR echo signal was carried out using four specimens purposely made by restorers according to the ancient original recipe to reproduce the same type of plaster and bricks of the wall painting under investigation. The specimens were dried until they reached a constant weight Ps_d and the integrals of the NMR echo signal As_d were measured. Then the specimens were fully saturated with water by capillary water absorption up to constant weight Ps_w and the integrals of the NMR echo signal As_w were measured.

The average values of the weights of the dry ($\overline{Ps}_d$) and of the water-saturated ($\overline{Ps}_w$) specimens as well as the average values of

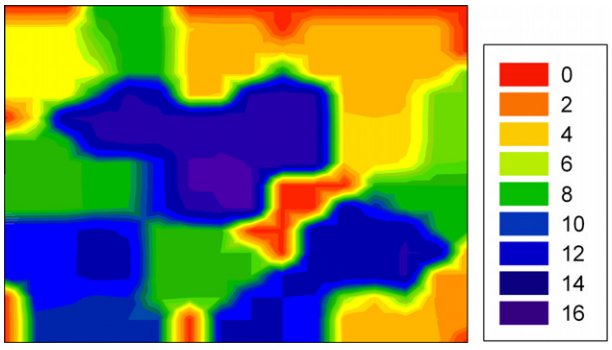

Fig. 6. Quantitative moisture distribution map (125 cm × 100 cm) obtained for a wall painting of Serra Chapel (Chiesa di Nostra Signora del Sacro Cuore, Piazza Navona, Rome, Italy). The moisture distribution is shown as a colour gradient, where red indicates a very low water content, while dark blue indicates the highest water content. The scale of values of the moisture content in percentage measured for the wall painting, is also reported. (Adapted from [73].)

the integrals of the NMR echo signal of the dry ($\overline{As}_d$) and of the water-saturated ($\overline{As}_w$) specimens, were calculated.

The average values $\overline{Ps}_w$ and $\overline{Ps}_d$ were used to calculate the imbibition coefficient (absorption), *ic*, which depends on the type of porous material. It was calculated from the maximum amount of water adsorbed by the specimen compared to its dry weight:

$$ic = \frac{\overline{Ps}_w - \overline{Ps}_d}{\overline{Ps}_d} \cdot 100. \quad (13)$$

For instance, in this study case *ic* was found to be 25%. Accordingly, a scale ranging from 0% to 25% was used to calibrate the level of moisture content in the wall painting. The relationship between the integral of the NMR signal and the weight of the adsorbed water is given by:

$$MC_i(NMR) = (A_i - A_{\min})\left(\frac{ic}{\overline{As}_w - \overline{As}_d}\right), \quad (14)$$

where $MC_i(NMR)$ is the moisture content measured by NMR in each area of the wall painting, A_i is the integral of the NMR signal measured on the wall painting, A_{min} is the lowest value of the integral measured on the wall painting. According to this calibration procedure, each area of the map corresponds to an accurate amount of moisture with a maximum amount of water of 16% in the dark blue areas, see Fig. 6.

A multi-techniques study of microclimate monitoring, IRT, gravimetric tests and portable unilateral NMR was applied in the framework of planning an emergency intervention on a very deteriorated wall painting in San Rocco church, Cornaredo (Milan, Italy) [74,75]. The IRT investigation showed that the worst damage, due to water infiltration, was localized on the wall painting of the northern wall of the church. Unilateral NMR allowed a detailed moisture distribution map at a depth of 0.5 cm in the plaster underlying the wall painting, to be obtained. The map revealed the presence of two wet areas separated by a dry area. The moisture found in the lower area of the wall painting was ascribed to the occurrence of rising damp from the bottom of the wall due to the slope of the garden soil towards the northern exterior. The moisture found in the upper area was ascribed to condensation phenomena associated with the presence of considerable amounts of soluble, hygroscopic salts. Most importantly, the moisture content measured by gravimetric tests performed on an unpainted area of the northern wall, was found to be in very good agreement with the moisture content measured on the same area by unilateral NMR. These results of gravimetric tests validated portable NMR as a new analytical tool for measuring, *in situ* and without any sampling, the distribution and the amount of moisture in wall paintings.

Fig. 7. Unilateral NMR instrument measuring the moisture content in the *St. Clement at mass and the legend of Sisinnius* wall painting, St. Clement Basilica, Rome.

Unilateral NMR was also used to map the moisture distribution in a medieval, very precious and markedly deteriorated wall painting located in the second hypogeous level of St. Clement Basilica, Rome at a depth of about 6 m below the road level [76]. *St. Clement at mass and the legend of Sisinnius* wall painting is one of the earliest examples of the passage from Latin to the Italian language. Fig. 7 shows the unilateral NMR instrument in use while measuring moisture in this wall painting that is rapidly deteriorating due to the capillary rise of water from the ground below. The presence of a watercourse flowing under the foundation of the Basilica is the most important cause of the rising damp in the walls of this archaeological site. The critical environmental conditions, i.e. very high relative humidity and a low temperature during the whole year, impaired the use of IRT, and, because of the preciousness of the artifact, the drilling of solid cores for gravimetric tests, was absolutely forbidden. The quantitative moisture distribution map obtained by NMR, at a depth of about 0.1 cm showed a moisture content up to 13%, see Fig. 8a. This map obtained for the first layer of the wall painting was affected by the peculiar environmental condition of the second hypogeous level of the Basilica and by the presence of salt efflorescence and encrustations on the surface of the wall painting. In contrast, the moisture distribution map obtained at a depth of 0.5 cm, clearly showed the path of the capillary rise from the ground and indicated a maximum moisture content of 8%, see Fig. 8b [76].

In another step of work, unilateral NMR was used to monitor the evolution of the level of the moisture in *St. Clement at mass and the legend of Sisinnius* wall painting, after an intervention to reduce the capillary rise of water through the walls [77]. In fact, to reduce the rising damp in the masonry, a horizontal cut was carried out through the bricks of the wall just above the floor level, and a hydrophobic mixture of polyester resin and marble powder was introduced in the holes drilled into the wall. The moisture distribution maps at a depth of 0.5 cm obtained 4 and 7 months after the intervention, clearly showed a lowering of the path of the rising damp and a net reduction of wet areas. The maps at a depth of 0.1 cm were found to be heavily affected by the environmental conditions of the hypogeum. In fact it was found that the map with the lowest moisture content and the highest number of dry areas was obtained after the intervention in presence of a scaffolding site covered with plastic sheets in the proximity of the wall painting, when the relative humidity measured inside the structure was, on average, about 10% lower than outside the structure. After removing the scaffolding site, the moisture distribution map at a depth of 0.1 cm was found to be similar to that obtained before the intervention [77].

Recently, a Profile NMR-MOUSE was employed in the non-destructive characterization of the layer structure of historic walls and wall paintings [78]. Different paint and mortar layers were studied *in situ* in Villa Palagione built under the Medici dynasty in 1598, and in the Seminario Vescovile di Sant'Andrea in Volterra, Italy dated 1170. In the detached and restored fresco "*La Madonna della Carcere*" from the Fortezza Medicea in Volterra, NMR depth profiles allowed one to differentiate between paint and mortar layers. Also, differences in the moisture content of the adhesive that fix the detached wall painting to its support, were evidenced by measuring depth profiles in both restored and original sections [78].

4.2. Detection of detachment in wall paintings by unilateral NMR

Unilateral NMR has been used to monitor the state of conservation of wall paintings in Vasari's house in Florence [79,80]. Hahn echo measurements were performed in areas chosen by the

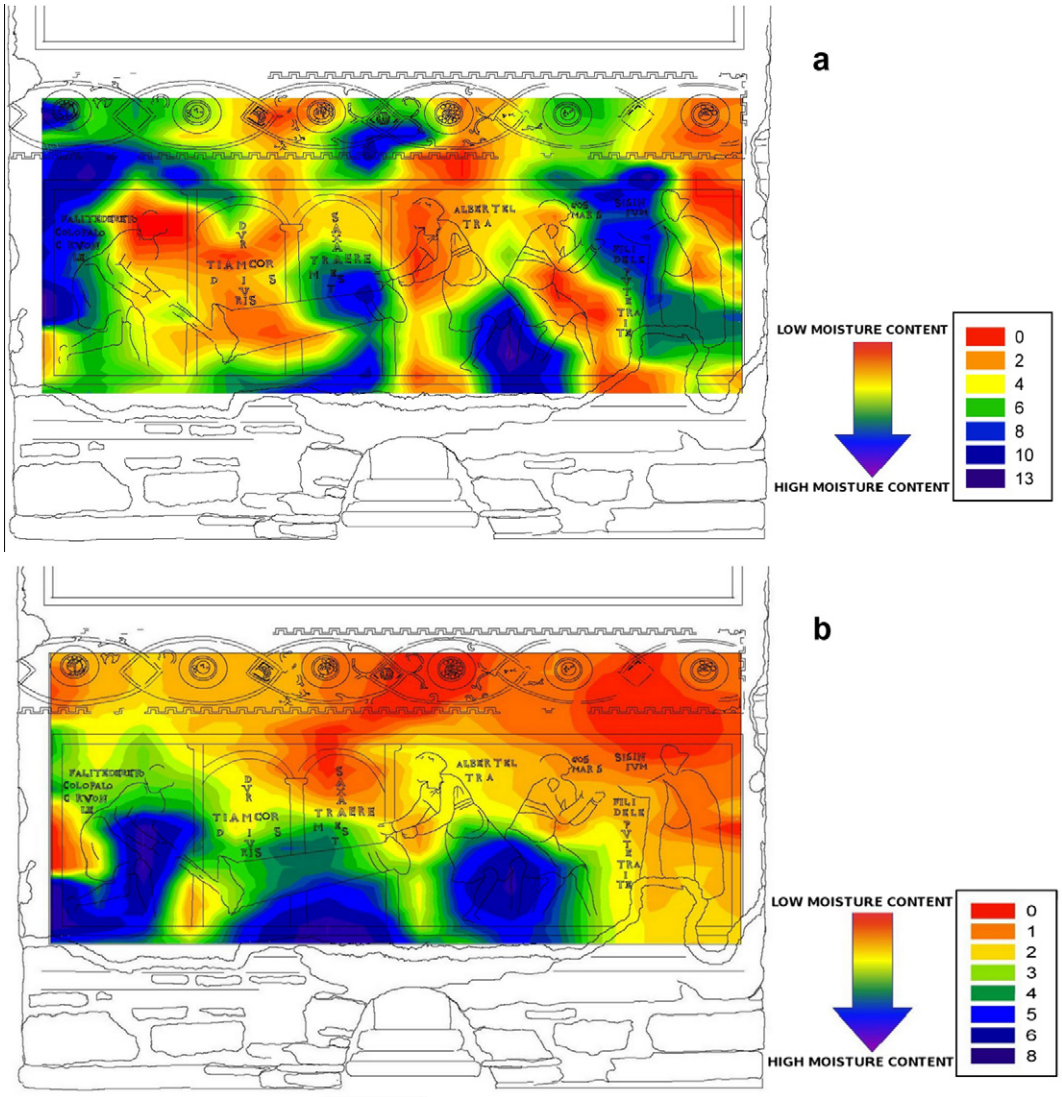

Fig. 8. Moisture distribution maps measured at depths of 0.1 cm (a) and 0.5 cm (b) in the *St. Clement at mass and the legend of Sisinnius* wall painting. (Reproduced with permission from [76].)

restorer on the basis of his knowledge of the different extent of detachment observed with raking light or softly knocking on the wall. In Fig. 9a regions are indicated where Hahn echo experiments were performed. In Fig. 9b results obtained on the selected regions in the first layers of the artifact (0.1 cm), are reported. A net decrease of the intensity of the Hahn echo was found in regions 3 and 4 where detachment occurred. A detectable decrease of the intensity of the echo was also observed in region 2, which was located near a detachment region, whereas in region 1, where no detachment occurred, the highest NMR signal was observed. In a well conserved fresco an exchange equilibrium between the wall and air humidity is established. When detachment occurs this balance is no longer maintained and the cohesion strength between the plaster and the painting layer weakens. Therefore, the weaker the signal, the stronger the detachment. Hahn echo measurements were also performed on the same regions at a depth of 0.3 cm, disregarding the signal from the first layers, see Fig. 9c. In this case the signal from the deeper layers of lime mortar (the inner part behind the fresco), was detected. Obviously, in this case, in the presence or in the absence of detachment of the pictorial film from the plaster, no difference in the intensity of the signal, was expected. Accordingly, the measured areas did not show any difference in the echo intensity. In fact, the simple measurement of a Hahn echo gave direct information about the possible occurrence of detachment of the pictorial film.

4.3. Monitoring of the effect of cleansing treatments in wall paintings by unilateral NMR

In the past, a common procedure used to fix pigments and to prevent crumbling of wall paintings consisted in the application of a mixture of organic substances such as egg yolk, animal glue, wax, or linseed oil. The degradation affecting these materials sometimes even changed the appearance of the surface of the artworks and constituted an optimum substrate for promoting biological colonization. These materials are usually removed with water and successively, when necessary, with a water solution containing ammonium carbonate. An important piece of information useful to the restorer, is the knowledge of the degree of moisture in the pictorial film after different cleansing treatments. The effect of the cleansing procedure has been investigated by unilateral NMR [79,80]. Note that the investigation has been carried out after

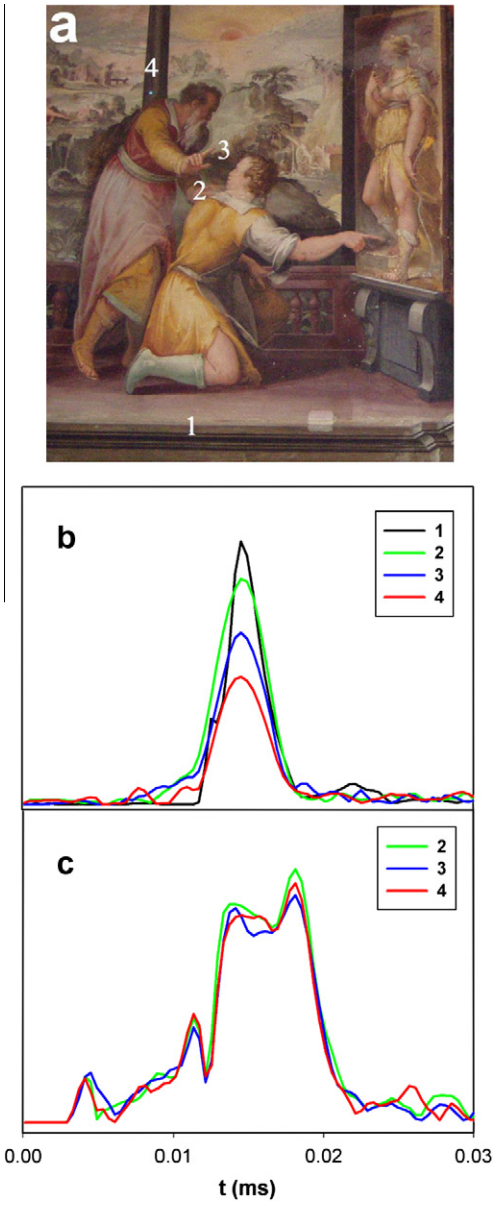

Fig. 9. (a) The wall painting where measurements were carried out: the numbers indicate the measured regions. In regions 3 and 4 detachment has occurred, region 2 is near a detached region, whereas no detachment is present in region 1. Intensity of NMR signal measured in the selected regions at depths of 0.1 cm (b) and 0.3 cm (c). (Adapted from [80].)

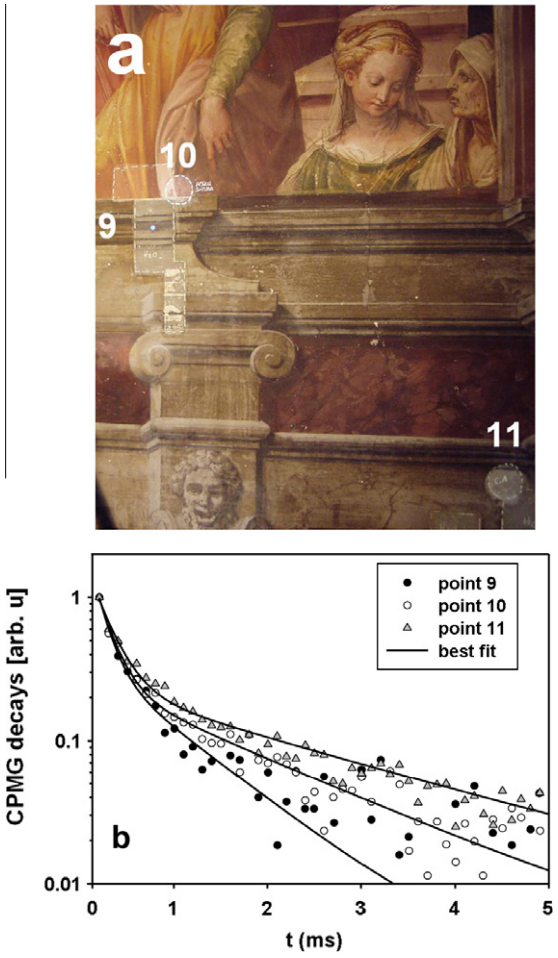

Fig. 10. (a) The wall painting on which measurements were carried out: the numbers indicate the measured regions. Region 9 was uncleaned, region 10 was washed with water, and region 11 was washed with water and, successively, with an ammonium carbonate solution. (b) CPMG decays measured on the selected regions. (Adapted from [80].)

1 year the cleansing had been performed. Fig. 10a shows regions on which T_2 measurements were performed. In Fig. 10b, the CPMG decays measured in the regions indicated in Fig. 10a, are shown. The shortest T_2 value was obtained for the uncleaned region 9. In this region the proteic substances used in a previous restoration did not allow a proper exchange of moisture between the wall painting and its environment, as a consequence that region was rather dry. The longest T_2 value was obtained for region 11 cleaned with ammonium carbonate. This treatment removed the layer of proteic substances allowing a good exchange of moisture between the wall painting and its environment. Region 10, washed only with water showed a T_2 value which is intermediate between values measured in regions 9 and 11. Actually, T_2 measurements allowed one to observe the differentiation among uncleaned areas and areas cleaned with different procedures.

5. Clays and fired clays

Investigations on clays used for manufacturing ceramic artifacts in antiquity, either building materials or pottery, and on the possible areas of provenance of their supply, are of great interest for archaeologists and art historians, in particular when no historical witness is available. Therefore scientific effort is devoted to characterizing ancient ceramic artifacts and to investigating the possible sources of prime matter and the technology of production. To improve the knowledge of the trade pathways and manufacturing activities of ancient civilizations, many studies of ancient ceramics concern the composition and firing, methods of manufacturing, and technological variability. The firing process involves the breaking down of some phases and the formation of new ones. Consequently clay artifacts are considered as artificial rocks formed in a kiln. The growth of new phases, during and after firing, is related both to the firing temperature and to the composition of microsites in which the phases grow.

A multi-technique study of the firing process of an illite-rich clay from Deruta was performed to study the modification induced by firing as a preliminary step to obtain information about ancient ceramic technology in this area [81]. Deruta has been for many centuries one of the most important centers for the production of ceramics in Italy, one of the reasons being the availability of suitable earth from which to form a clay. In particular, the hills around

Deruta are rich in a pure strain of clay which also washes up along the shores of the nearby Tiber river. In the framework of this study, an Electron Spin Resonance (ESR) investigation was preliminary to the NMR analysis with the aim of characterizing paramagnetic centers in the raw and fired clays. ^{29}Si and ^{27}Al MAS spectra revealed the structural features of the raw material and structural modifications due to the firing. As an example, Fig. 11 shows the ^{27}Al and ^{29}Si spectra of the raw clay, (a) and (c) respectively, and of the clay fired at 1100 °C, (b) and (d) respectively. ^{27}Al Triple Quantum Magic Angle Spinning (3Q MAS) NMR experiments [81] were carried out to gain a better spectral resolution, as these experiments refocus second order quadrupolar effects that broaden ^{27}Al MAS spectra [82,83]. The 2D maps of the raw clay and clay fired at 1100 °C are shown in Fig. 11e and f respectively. In these maps the dotted lines represent different orientations of the signals, "*A*" denotes the anisotropic axis, "Q_{IS}" is the axis representing the direction of the induced quadrupolar shift, and "C_{IS}" axis gives the direction of isotropic chemical shifts. The centers of gravity δ_{G1} and δ_{G2} of the two-dimensional spectral ridges in the F1 and F2 frequency domains, were used for estimating the isotropic chemical shift δ_{iso} and the second order quadrupolar effect P_q using:

$$\delta_{iso} = \frac{\xi\delta_{G2} - \delta_{G1}}{\xi - |p|}, \tag{15}$$

$$P_Q = \nu_0\sqrt{\frac{9}{10}\frac{[4I(2I-1)]^2}{p^2-1}\cdot\frac{\left(\frac{\delta_{G1}}{|p|} - \delta_{G2}\right)}{10^6}}, \tag{16}$$

where ξ is the slope of the quadrupolar axis Q_{IS}.

The parameters obtained were used as initial guesses in a spectral deconvolution procedure [84] from which the isotropic chemical shift and the Al quadrupolar coupling constants of each sample, were obtained. The improved resolution obtained by multiple quantum MAS allowed the observation of three distinct sites in the spectrum of the raw clay, two sites typical of Al in a tetrahedral environment, and one site typical of Al in an octahedral environment, see Fig. 11e and a. As the firing temperature is increased, the illite structure breaks down and the signal due to ^{27}Al in octahedral environment is no longer observable, see Fig. 11f and b. After the break down at about 850 °C, new phases were observed containing only Al in tetrahedral environments. ^{29}Si spectra of the raw clay and of the clay fired at 1100 °C are also indicative of marked structural modifications due to the firing process, see Fig. 11c and d. The ^{29}Si chemical shifts and relative peak intensities were obtained by deconvoluting the spectra. Actually, a careful ^{29}Si and ^{27}Al MAS and 3Q MAS analysis along with spectral deconvolution, allowed several parameters to be obtained which characterize each sample. Furthermore, a careful analysis of the shape and orientation of spectral ridges in 3Q MAS maps with respect to significant orientations, such as CIS, A, and QIS, might possibly contribute to work out a fingerprinting of clays and fired clays. Obtaining a large set of experimental data on clays and fired clays from different areas of provenance and different firing technologies, along with the use of suitable methods of statistical analysis, is mandatory in order to find criteria based on NMR analysis, for possibly determining a fingerprints of the raw materials and artifacts.

The water absorption process in fired clay bricks was investigated by Pel et al. [85]. In these materials, a serious complication arises because of the presence of considerable amounts of paramagnetic ions which impair the use of the standard NMR imaging

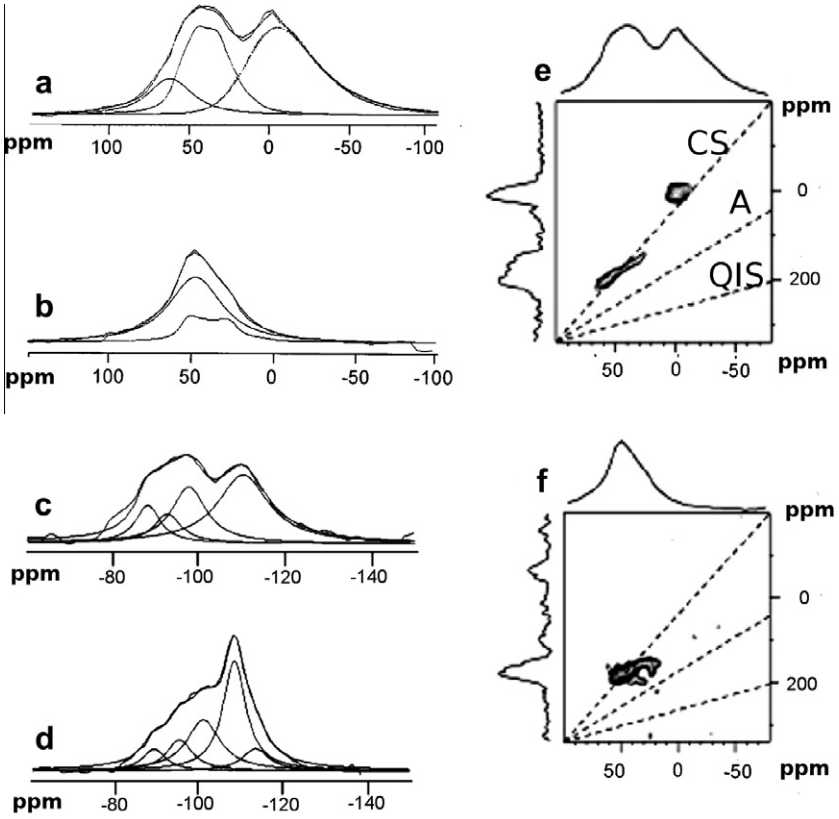

Fig. 11. ^{27}Al MAS NMR spectra at 52.15 MHz of (a) a raw clay, and (b) a clay fired at 1100 °C. (c) ^{29}Si MAS NMR spectra at 39.76 MHz of a raw clay, and (d) a clay fired at 1100 °C. The spectral deconvolutions are also reported for each spectrum. (e) Unsheared ^{27}Al 3Q MAS NMR spectra of a raw clay, and (f) a clay fired at 1100 °C. (Adapted from [81].)

technique. The study was carried out with a home-built NMR imaging. The instrument allowed quantitative one dimensional moisture concentration profiles in the brick to be obtained [60]. The transport of moisture was monitored during water absorption, and modelled by a diffusion equation. The moisture diffusivity for absorption was approximated by an exponential function for the various types of fired-clay brick investigated.

A further development in the study of fluids confined in porous materials, was the possibility to acquire T_1–T_2 correlation maps, in homogeneous, as well as in inhomogeneous magnetic fields of portable NMR devices [86–88]. A constant T_1/T_2 ratio in relaxation time distributions of porous media indicates a uniform pore environment for small and large pores [89]. The measurement of T_1, unlike that of T_2, is not affected by an error due to signal attenuation from diffusion, and so the correlation maps reveal the effect of diffusion on T_2 distributions even in the presence of the internal gradient rising from para- and ferromagnetic attributes of the pore walls. Diffusion–relaxation correlation maps provide a direct tool to study magnetic susceptibility in porous media.

T_1–T_2 correlation maps have been reported for water saturated sandstone measured with a mobile Halbach scanner. The constant T_1/T_2 ratio for all values of relaxation times revealed an uniform pore environment for small and large pores [88].

T_1–T_2 correlation maps were employed to study water-saturated archaeological ceramics from archaeological sites of Miseno and Cuma (Naples, Italy) [90,91]. These studies investigated the paramagnetic composition and the pore-size evolution with thermal treatment. T_1–T_2 correlation maps [15,16] were analyzed in terms of signal displacement and shape over the (T_1, T_2) plane. Basically, these two-dimensional relaxation maps correlate the distribution of longitudinal and transverse relaxation times of a spin system, or, in other words, generate maps of the spin populations distribution on the basis of their relaxation times coordinates. It was suggested that the obtained T_1–T_2 maps might represent a sort of NMR fingerprinting of the composition and manufacturing technology of ceramic objects, as the maps summarized the correlation between the pore size distribution and the magnetic composition of the matrix. In further work [92], T_1–T_2 correlation maps were collected on pottery objects found at the ancient Latin city of Praeneste, dated between third and second century BC and attributed to two different Roman families. The authors identified a marker which possibly distinguishes with respect the different firing techniques of these two families.

6. Characterization of volcanic tuffs from ancient monuments

Volcanic tuffs are rocks composed of a consolidated ash matrix made of small particles containing lithic, vitric, and crystal clasts in different amounts [93]. In addition to the relative content of clasts, the nature of the matrix is also different and a broad distinction is made between welded and lithified tuffs. The term "welded tuffs" identifies rocks bonded by sintering and compaction of glass in the matrix. The welding process occurs when the deposit is still hot and plastic which leads to large vitric scoriae being often present in these tuffs. The term "lithified tuffs" identifies rocks whose original ash matrix has undergone chemical alteration so that authigenic minerals, mainly composed of zeolites, act as binding agents for the material.

Both welded and lithified tuffs have been extensively used as building materials since BC times, mainly because they are light, easy to cut and shape and have a good resistance to fire. Their wide use is testified by the large number of ancient monuments, sculptures, and artifacts that have been accumulated in some countries rich in volcanic deposits, such as Italy, Turkey, Mexico, Germany, and Japan.

Recently, a multi-technique study was carried out to characterize five tuffs from different sources [94]. Two of these tuffs were sampled from monument structures dated between the 4th and 2nd century BC belonging to the Etruscan Necropolis of Norchia, Viterbo, Italy. Samples were investigated by ^{29}Si, ^{27}Al, and ^{1}H MAS NMR. The relative content of Al in the crystal and amorphous phase was determined from the relative integrals of the two phases by deconvoluting ^{27}Al MAS spectra [84]. 3Q MAS maps allowed the isotropic chemical shift and the second order quadrupolar effect to be obtained, which were used as initial guesses in the procedure used to deconvolute experimental MAS spectra. As an example, ^{27}Al MAS spectra of two different tuffs from the Necropolis, one lithified (cemented with chabazite) [95] and another one welded [96], are shown in Fig. 12a and b, the corresponding 3Q MAS maps are also shown in Fig. 12c and d. The MAS spectra of the two materials are very different to each other: that from the lithified tuff has a rather sharp resonance centred about 50 ppm, which is from chabazite, and a definitely broader resonance due to Al in a disordered, amorphous environment, whereas the spectrum of the welded tuff has only one broad resonance of Al in an amorphous phase, as expected in a welded tuff. The shapes of the spectral ridges in the 3Q MAS maps are also very different from each other. Particularly, the shape observed in the map of the welded tuff is characteristic of a distribution of chemical shift and quadrupolar coupling constant as expected for a very disordered material. The prevalent zeolitic or glassy nature of the matrix can be assessed by ^{29}Si MAS NMR: in the zeolite cemented tuff the intense peaks of zeolite are prominent in the spectrum, see Fig. 13a, whereas broad and unresolved peaks are observed in that of the welded tuff,

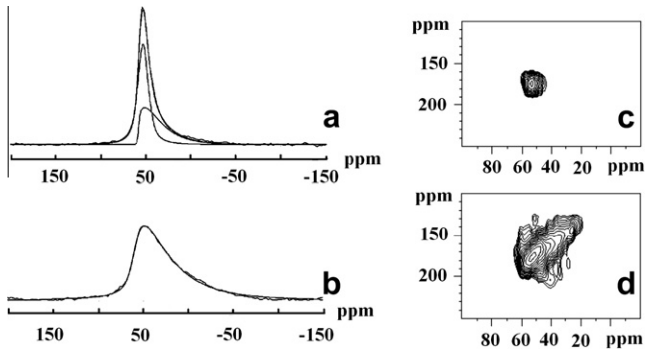

Fig. 12. Volcanic tuffs from the Etruscan Necropolis of Norchia. Experimental and deconvoluted ^{27}Al MAS NMR spectra at 52.15 MHz of (a) a lithified tuff, and (b) a welded tuff. ^{27}Al 3Q MAS NMR spectra of the same volcanic tuffs are reported in (c) and (d) respectively. (Adapted from [94].)

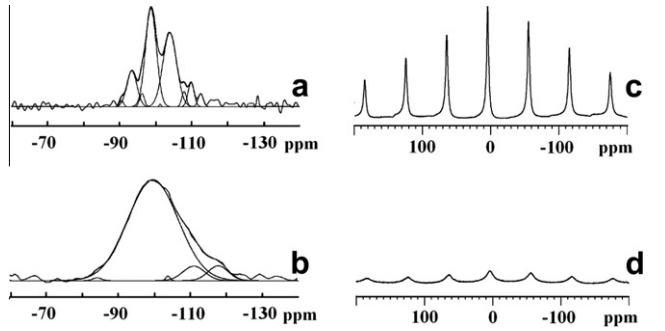

Fig. 13. Volcanic tuffs from Necropolis of Norchia. Experimental and deconvoluted ^{29}Si MAS NMR spectra at 39.76 MHz of (a) a lithified tuff, and (b) a welded tuff. ^{1}H NMR spectra at 200.13 MHz of the same tuffs are reported in (c) and (d) respectively. (Adapted from [94].)

see Fig. 13b. Furthermore the deconvolution of the spectra allowed relative integrals of all peaks to be obtained. In zeolite cemented tuffs the Si/Al ratio [97] was determined from:

$$\frac{\mathrm{Si}}{\mathrm{Al}} = \frac{\sum_{n=1}^{4} n I_{\mathrm{Si}(n\mathrm{Al})}}{0.25 \times \sum_{n=1}^{4} n I_{\mathrm{Si}(n\mathrm{Al})}}, \quad (17)$$

where Si(nAl) indicates all the bands generated by Si-tetrahedral sites (SiO_4) linked to a different number of Al atoms, and $I_{\mathrm{Si}(n\mathrm{Al})}$ indicates the integral of each resonance. Si/Al is a very important parameter, as it differentiates between well preserved tuffs and tuffs in which natural weathering occurred. For instance in the lithified tuff, Si/Al was found to be 2.42, whereas a definitely lower value of 1.98 was found for the naturally weathered lithified tuff, showing that Si–Al substitutions had occurred in the zeolithic component of the weathered tuff.

^{1}H MAS spectra give a direct measurement of the mobile and adsorbed water in the lithified and in the welded tuff, see Fig. 13c and d respectively. The total amount of adsorbed water measured by NMR was found to correlate well with Thermo Gravimetric Analysis (TGA)–Differential Thermal Gravimetry (DTG) analysis, however the NMR determination is a direct measurement of the mobile and adsorbed water, and, unlikely TGA–DTG, is not affected by phase transitions other than dehydration of glass and zeolites.

To summarize, despite the presence of paramagnetic ions up to 3–3.5% w/w, satisfactory results were obtained by applying multinuclear solid state NMR to characterize tuffs from ancient monuments and to differentiate between unaffected material and material which has experienced natural weathering.

7. Solid state NMR of building material from historical monuments

Solid state ^{29}Si and ^{27}Al MAS NMR has been applied to investigate building stones [98] from Guanajuato City Main Church, (Central Mexico), designated a "World Heritage Site" by UNESCO, to obtain information about the degradation and to observe the changes in the consolidated material after consolidating treatment with tetraethoxysilane (TEOS). Guanajuato historical monuments are built with quartz and feldspar-based materials, called pink quarry. These materials have been extensively used since the 17th century to construct the main buildings of the city. ^{29}Si and ^{27}Al MAS NMR spectra of non degraded pink quarry stone were also collected for comparison [98]. The ^{29}Si MAS spectrum of the non degraded material shows a rather broad signal between −80 and −100 ppm indicating the presence of albite and other silicates. A weak peak due to quartz is present at −107 ppm from tetramethylsilane (TMS). The ^{27}Al MAS spectrum has a rather sharp signal at about 59 ppm from $Al(NO_3)_3$ indicative of aluminium in a tetrahedral environment, possibly accounting for the presence of feldspar, in particular albite, as also revealed by X-ray Diffraction Analysis (XRD). Another weak peak is present at about 0 ppm indicative of aluminium in an octahedral environment and ascribed to the presence of clays. The ^{29}Si spectrum of degraded material clearly shows a very marked loss of the feldspar signal possibly due to albite degradation, whereas the ^{27}Al NMR spectrum shows intense signals representative of Al in tetrahedral and octahedral environments [98]. These data are in accordance with the known mechanism of degradation of these materials, as feldspars are usually degraded to clay materials by kaolinization. A very marked change was observed in the spectra from the stones after they were treated with TEOS when compared with those of untreated, degraded material. After the treatment, samples tended to recover the original ^{29}Si and ^{27}Al spectral pattern of the non degraded material, the degree of recovery depending on the state of degradation of the material before the treatment [98].

^{27}Al and ^{29}Si MAS NMR have also been applied to characterize the masonry of the pyramid of Cheops at Giza (Egypt) [99]. The NMR spectra of the modern synthetic materials used as a reference were compared with spectra of several samples from the pyramid. A small amount of Al in a tetrahedral environment was found in the spectra of ancient samples.

8. Paints

A paint consists of pigments in the form of a fine powder of inorganic or organic coloured material dispersed in a matrix which is usually called the binding medium and enables the pigment to be dispersed and applied with a paint-brush. The binder may be a vegetable gum, a drying oil, a proteinaceous material such as egg or casein, a natural wax, a synthetic polymer or a mixture of these materials. The surface on which the paint must be applied needs to be prepared with a ground layer. For instance, paintings were often coated with a varnish containing oils and/or plant resins, a mixture of animal glue and gypsum was used over centuries as a ground for canvas and wooden panels [100]. The chemical characterization of organic components is obviously of great interest to gain information on the painting techniques employed. Furthermore, the organic component of the paint layer undergoes degradation, and a knowledge of its composition is mandatory in order to assess the suitable conservation and display conditions, to prevent or slow the decay process, and to plan the restoration. Macroscopic degradation, such as yellowing and loss of cohesion, is related to chemical alteration of the organic media, namely oxidation, hydrolysis, crosslinking, depolymerization and biological colonization. In addition, chemical reactions between pigments and organic materials may cause the occurrence of colour alteration or, even, discolouration [100].

8.1. Drying oils

Since ancient times, drying oils of natural origin such as poppyseed, walnut and linseed oil, have been largely used as the binding media of oil paints. During drying, the trygliceride unsaturated fatty acids crosslink solidifying the paint and, therefore, trapping and stabilizing the pigments. The mobile phase of an oil paint may be easily separated by solvent extraction from the insoluble highly crosslinked solid phase and pigment grains. High field NMR spectroscopy in solution is a very powerful analytical tool for obtaining information on the levels of hydrolysis and oxidation resulting from the ageing of an oil painting. As an example, the ^{1}H NMR spectrum of a sample of linseed oil which is used as a reference, is reported in Fig. 14a, along with the assignment [101,102] of some resonances, and the spectrum of an oil painting extract is reported in Fig. 14b. By comparing the spectra, it was deduced that there is a net reduction of polyunsaturated fatty chains in the oil painting extract. In fact, a marked reduction of intensity of all resonances related to linolenic and linoleic fatty chains occurs in the spectrum of the extract, see for instance signals D and H (diallylic protons of linolenic and linoleic chains), signal A (allylic protons bonded to carbon C8 of linolenic and linoleic chains), signal Y (methyl of linolenic fatty chains), see Fig. 14. In Fig. 15a and b, the regions between 3 and 5 ppm of the ^{1}H spectra of the two samples, are shown. Resonances due to monoglycerides (MG) and diglyceride (DG) moieties and to other degradation products are present in the spectra. It is worth noting that in the reference sample the amount of these compounds does not exceed 2.5%, whereas in the extract these compounds are present in a considerable amount, about 16%. Furthermore, DOSY maps of the reference

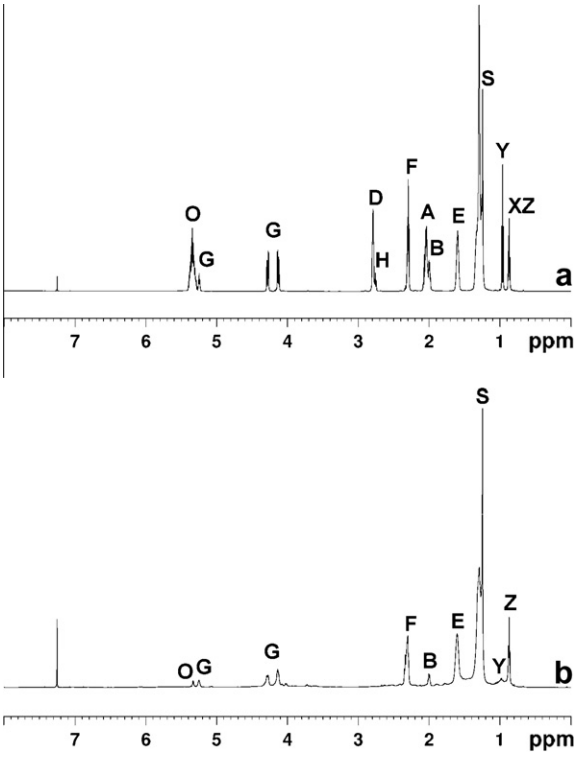

Fig. 14. ^{1}H NMR spectra at 600.13 MHz of (a) linseed oil and (b) an oil painting extract. Y = methyl of linolenic fatty chains; X = part of the triplet of linoleic fatty chain; Z = methyl of saturated and oleic fatty chains; S = methylenic protons of saturated chains; E = methylenic protons bonded to C3 of all fatty chains; A = allylic protons bonded to C8 of linolenic fatty chain and allylic protons of linoleic chain; B = allylic protons of oleic fatty chain; D = diallylic proton of linolenic fatty chain; H = diallylic proton of linoleic fatty chain; F = methylenic protons bonded to C2 of all fatty chains; G = glycerol moiety; O = double bonds. (Assignement from [101,102], L Mannina, F. Presciutti, N. Proietti, D. Capitani, A. Sgamellotti, B.B. Brunetti, unpublished data.)

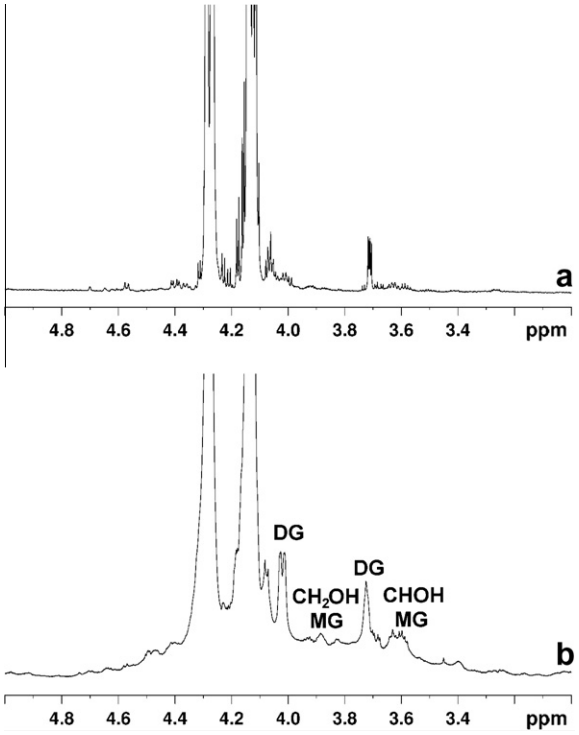

Fig. 15. Expanded spectral regions (3–5 ppm) of the 600.13 MHz ^{1}H NMR spectra shown in Fig. 14 of (a) linseed oil and (b) an oil painting extract. (Assignement from [101,102], L Mannina, F. Presciutti, N. Proietti, D. Capitani, A. Sgamellotti, B.B. Brunetti, unpublished data.)

and extract showed that the diffusion coefficient of the extract is definitely smaller than that of the reference sample, clearly evidencing an increase in the molecular weight of the extract due to crosslinking [103].

Spyros and Anglos applied high resolution 1D and gradient enhanced 2D NMR spectroscopy to investigate the binding medium from two original oil paintings dated from the early 20th (*Portrait of Young Men*) and the late 17th century (*The Duhe*) [104]. The binding medium was collected by carefully removing a small quantity of paint from the side of the painted canvas to avoid intervention with the top surface of the painting and to minimize the sampling. The collected material was dissolved in deuterated acetone and extracted by sonication. Before analyzing the two original paintings, a systematic study of the solvent-extractable component from model samples of drying oils, namely raw oil paints, and aged oil paints, was carried out. The authors reported the ^{1}H and ^{13}C NMR chemical shift assignments of the main resonances of trygliceride (TG), diglyceride (DG) and monoglyceride (MG), free fatty acids (FA), diacids (DA), and hydroxy (or oxo) acid (HA) moieties that contribute to the spectra of the aged paint, whereas in the spectra of the fresh paint the signals mainly of TG and few 1,3-diglycerides were observed. Most importantly, molecular markers based on the ratios of signal integrals of chemical species in proton and carbon spectra, were defined. In accordance with the notation reported in the paper, the authors found relevant molecular markers such as B_f/B, the ratio of free to total carboxyl groups, HFA (HFA = (2DG + 4MG)/6(TG + DG + MG) where TG, DG, MG are the molar ratios of each type of glyceride) indicating the extent of triglyceride hydrolysis, and HA/FA which measures the amount of hydroxyacids. The marker that best differentiates the two old original paintings from the younger ones appeared to be the ratio TG/FA, which has a much smaller value in the old paintings. The low TG/FA values, combined with high values of B_f/B and HFA appear to be indicative of oil paintings of significant age. Furthermore, the marker that best differentiates the two original paintings was found to be TG/FA. Moreover, during the ageing, the TG content of a paint extract decreases. However, the concentration of DG and MG components reached a maximum in the extract, followed by a slow decrease with further ageing, as these compounds suffer further hydrolysis to glycerol and free fatty acids.

In another paper Spyros and Anglos [105] investigated aged binding media used in painting, namely egg tempera, linseed oil, and an acrylic medium. The previously defined set of markers [104] was used to establish the state of hydrolysis and oxidation of the linseed and egg tempera binders after 5 years of ageing. Acetone extracts of lipid-containing binders were found to contain molecules characteristic of the ongoing processes of TG hydrolysis and oxidation, such as MG and DG, FA and DA. For similar ageing conditions, the linseed binder seems to suffer greater lipid hydrolysis and degradation than the egg tempera binder. Furthermore, 1D and gradient enhanced 2D NMR were successfully applied to identify both the polymeric constituents of the acrylic medium, and a surfactant used to prevent association of acrylic particles before drying.

Cipriani et al. investigated samples of aged films obtained from three drying oils, namely linseed, walnut, and poppyseed oil [106]. The soluble fraction of aged films used as reference samples, was studied by high resolution ^{1}H NMR spectroscopy, whereas the insoluble fraction was swollen in $CDCl_3$ and investigated by ^{1}H High Resolution Magic Angle Spinning (HRMAS) NMR using a nanoprobe which allowed the collection of spectra from a very

low amount of material. However, the spectra of the soluble and insoluble fractions were not found to be substantially different. In all cases the intensity of signals for protons involved with double bonds and in the groups adjacent to them, were found to decrease with respect to that intensity recorded for oils which had not been aged. However, whereas in the HRMAS spectrum this decrease can be attributed to polymerization and oxidation reactions involving double bonds, the spectra of the soluble fraction show the presence of unreacted, saturated, and partially mono-unsaturated triglycerides. After studying the reference films, both the soluble and insoluble swollen fractions of real painting films containing drying oils as binders, were analyzed using the same NMR technique, and the signals of the drying oils were identified separately from those from other organic compounds acting as binding agents, such as waxes or egg-yolk media. In fact, triglycerides contained in egg-yolk are completely soluble and no fatty components can remain after swelling. Besides, if waxes are used, no glyceride signals are expected in the ^{1}H NMR spectrum.

8.2. NMR depth profiles of painting layers

Paintings are constituted of multiple layers, such as preparation, underdrawing, paint, varnish, and so on. The knowledge of the layer structure, or stratigraphy, allows information on the working practices and techniques of the artist to be obtained, and, even more importantly, helps in selecting correct and suitable conservation and restoration procedures. Nowadays, the common practice to get information about the stratigraphy, is to cut small cross-sections from the painting, which can then be analyzed by Optical Microscopy, Scanning Electron Microscopy, micro-Raman, micro Fourier Transform Infrared Spectroscopy, and other techniques. These techniques allow the visualization of the sequence of layers in the paint under investigation and the possible identification of binders and pigments, the primer, repaintings if any, and also the detection of the presence of *incamottatura*, a textile used to cover and join the wood panels of the support as a base for the primer.

Presciutti et al. [32] used the Profile NMR-MOUSE to reveal the stratigraphy of paintings and other non transparent objects spanning several millimeters in depth with a resolution of 50 μm. With this method, the thickness of proton-rich layers in paintings was measured non-invasively and *in situ*, and the binder ageing was also investigated. In particular, two depth profiles were measured in different regions of an ancient oil painting, the "*Adorazione dei Magi*", by Pietro Vannucci "Il Perugino", dated about 1470, and are shown in Fig. 16. The profiles revealed four different layers ascribed to the wood, the *incamottatura*, the primer and the paint layer. It was also possible to measure the thickness of each layer with an accuracy of 10–15 μm.

Contemporary art employs a wide variety of materials of different vulnerability and complexity that challenge the NMR analysis. NMR depth profiles [33] were collected on a contemporary painting "*Bianco e Nero*" dated 1971, by Alberto Burri who used synthetic poly(vinyl acetate) as binder instead of conventional oil or tempera. The NMR depth profile through the painting revealed that the same binder was used for both the paint and the primer.

9. Paper

Paper is one of the oldest, and sometimes precious of man-made materials. For many centuries paper was the support for recording cultural achievements all over the world. Historical paper differs in many ways from contemporary paper. In fact the quality of ancient paper was particularly good, as it was manufactured from carefully selected cotton rags with only a few impurities. After 1850, the quality of paper changed for the worse as a consequence of being produced by industrial manufacturing processes. Low quality modern paper is derived from the stem of wood or wood pulp and, in addition to cellulose, it contains a considerable amount of hemicelluloses, lignin, and non-fibrous components including various colouring agents, fillers, coatings. The amount of these components varies according to the papermaking process, the type of paper and the period of production. Originally animal glue was used for sizing, subsequently the animal glue was substituted by rosin and alum, and, more recently, by other synthetic products. Therefore, modern paper is usually more vulnerable to degradation than the older one.

The degradation of paper is a complex phenomenon with different causes among which the more common ones include biological, physical and chemical processes. Moreover, a common risk factor is inadequate storage and careless handling which can accelerate the degradation process. Generally, the protection and preservation of paper-based artworks poses a serious problem for numerous libraries, archives, and museums. This is the reason why in recent years several studies have been focused on the monitoring of paper weathering and the development of appropriate and long-term resistance treatments to protect valuable documents.

High quality paper may be considered as a bi-components material consisting of cellulose and water in an almost equimolar amount, plus a small amount of impurities. Cellulose, is a linear polysaccharide of β-D-anhydroglucopyranose units linked by 1-4-glycosidic bonds. Paper may also be considered as a porous material with water pools embedded into the rigid cellulose matrix. The removal of even a small amount of water may cause an irreversible destruction of the material.

In order to understand and explain the degradation processes occurring in paper, several NMR studies aimed at clarifying the paper

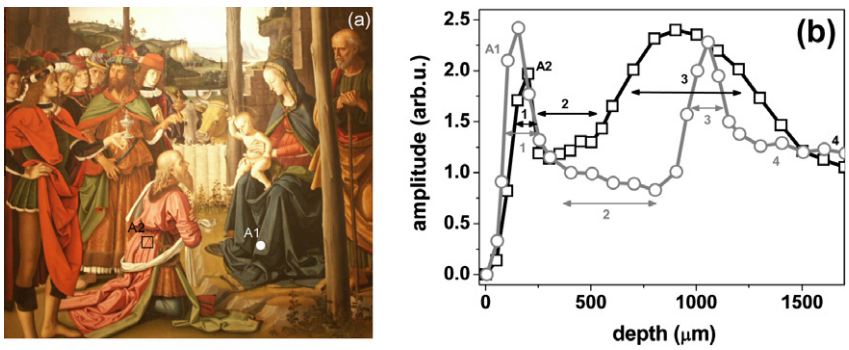

Fig. 16. (a) The position A1 and A2 in the painting the *Adorazione dei Magi* by il Perugino (≈1470) used to obtain the depth profiles with a spatial resolution of 50 μm shown in (b). The labels in (b) refer to 1: paint layer; 2: primer; 3: canvas and glue; 4: the wood of the panel. (Reproduced with permission from [32].)

structure and morphology were carried out in recent decades. These studies were mainly focused on the water–cellulose interaction in paper and on the monitoring of degradation processes.

The cellulose component of paper was studied by ^{13}C CPMAS NMR spectroscopy [107], whereas the water–cellulose interaction in paper was investigated using low field ^{1}H NMR relaxometry [108,109]. ESR was applied to identify the type and the stereochemical environment of paramagnetic impurities present in paper [110,111].

The ^{13}C CPMAS spectrum may be considered as the "fingerprint" of the solid component of the paper. As an example, the spectrum of Linters paper is reported in Fig. 17a. The sharp resonances are due to the long fibres of cellulose in crystalline domains, while the broad ones are due to cellulose in amorphous domains. In particular the resonance at 106.3 ppm is that of the anomeric carbon atom C_1, resonances at 90.3 and 66.8 ppm are respectively from C_{4c} and C_{6c} in crystalline domains, while resonances at 85.4 and 64.5 ppm are respectively due to C_{4a} and C_{6a} in amorphous domains. The shape of resonance C_1 clearly indicates the presence of amounts of microcrystalline polymorphous forms of type I_α and I_β [112,113].

The Free Induction Decay (FID) of paper shows always two components, see Fig. 17b: a fast decaying component from the polymeric matrix, and a slow decaying one from the confined water. After a Fourier transformation, see Fig. 17c, the cellulose component appears as a broad hump on top of which a rather sharp resonance due to water is observed. A best fit procedure may be applied to the FID of a piece of paper to obtain the molar ratio between the water component and the polymeric component [108]. The function used to fit the FID intensity, Y, is a sum of a gaussian function $G(t)$, accounting for the cellulose component, and an exponential function $E(t)$, accounting for the water component:

$$Y = C_0 + \left[W_{\text{cell}} \exp\left(-\frac{t^2}{G_{\text{cell}}^2}\right)\right] + \left[W_w \exp\left(-\frac{t}{E_w}\right)\right], \tag{18}$$

where W_{cell} is the cellulose signal intensity, and W_w is that of water, C_0 is the average value of the noise, and $E_w = T_2^*$. In the case of the gaussian function $G(t)$, a characteristic decay time can be defined as the time T_2 required for $G(t)$ to decay to $1/e$ of its starting value $G(0)$, as a consequence $G_{\text{cell}} = T_2$. The water/cellulose molar ratio was found to be characteristic of different types of well preserved paper [108]. As an example, in good quality paper this ratio was found to be about 0.9, whereas in low quality paper this ratio was about 1.7.

Pulsed low resolution ^{1}H T_1 measurements on high and low quality modern paper, were performed separately on the cellulose and on the water component [108,109]. The spin–lattice relaxation time of both components shows a multi-exponential behaviour. The faster relaxation times measured on cellulose and water components, do not show any correlation. This component is possibly related to the presence of domains rich in paramagnetic impurities as detected by ESR analysis. In contrast, the longest T_1 relaxation times of water and cellulose were found to be equal, which corresponds to their being dominated by spin-diffusion. The longest T_1 relaxation times measured as a function of the temperature, allowed the calculation of the activation energy (Arrhenius term) which is related to motions of the cellulose–water system. In this system many motions may contribute to the relaxation. In cellulose the chain motion is dominated by rotations around the glycosidic bonds. It may be reasonably assumed that the higher the energy, the higher the order and the orientation of macromolecules in cellulose fibres. The other factor which affects the relaxation of the system is the water motion, the water being in spin-diffusion with the cellulose. Again, a high activation energy of the water indicates a water tightly bound to the cellulose, whereas a low

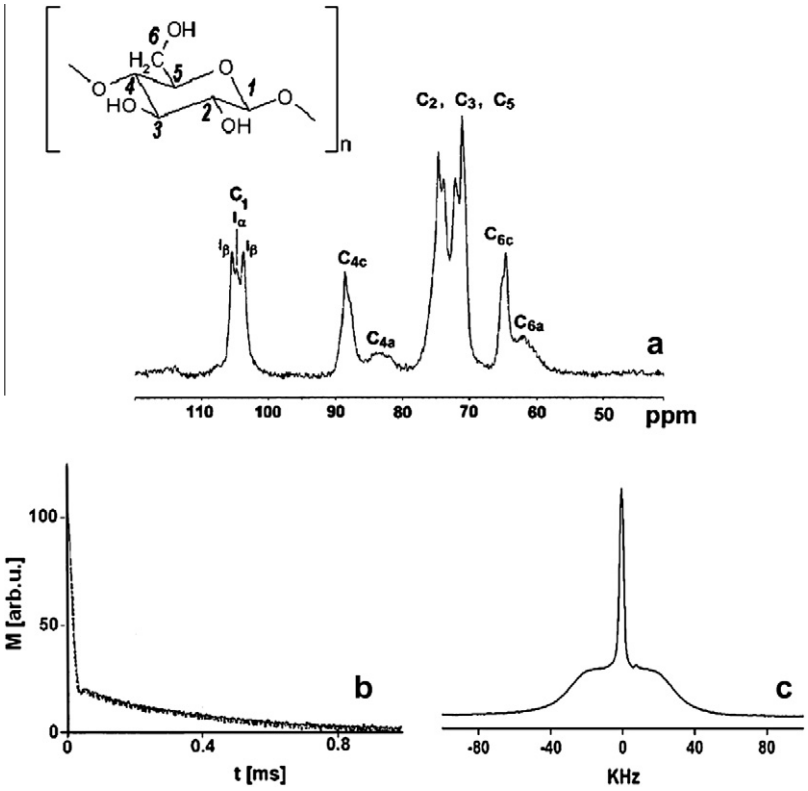

Fig. 17. Linters paper. (a) ^{13}C CPMAS NMR spectrum at 50.13 MHz along with resonance assignments. (b) Free Induction Decay, the fast decaying component is from cellulose, the slow decaying one is due to water. (c) ^{1}H proton wide line spectrum, the broad line is from cellulose (line width at half height about 64 kHz), and the sharp line is due to bound water (line width at half height about 1.5 kHz). (Adapted from [115].)

energy may indicate a water loosely bound the cellulose. To summarize, it was hypothesized that the higher the activation energy, the higher the physical "quality" of the paper. Accordingly, in the case of high quality modern paper (Linter paper), the activation energy was found to be about 31 kJ/mole, in Kraft pulp it was found to be about 27 kJ/mole, and in the lowest quality modern paper the activation energy was 22 kJ/mole [108].

At room temperature, the water resonance in paper is a sharp peak on the top of the broad cellulose component. By lowering the temperature, the water resonance progressively broadens, however, at 213 K the water resonance is still observable, see Fig. 18. Therefore, the freezing point of the bound water, or confined water, was found to be lower than 213 K [108,109]. Obviously the freezing point is related to the nature of hydrogen bonds existing between the water and the cellulose. In general, the physical properties of a liquid confined within pores are different than those for the bulk liquid, in particular the melting temperature of the confined liquid is depressed by an amount related to the pore size [114]. Therefore paper was treated as a porous system with a mobile species, the water, embedded into a rigid polymeric matrix [115]. The intensity of the water resonance was measured as a function of the temperature. The curve obtained, known as an Intensity–Temperature Plot (IT plot), was modelled by assuming that paper is a porous network without requiring any model of the shape of the pores, but with a pore size distribution which was obtained to be strongly asymmetric with a well-defined maximum at about 1.4 nm. This method did not give any information about the type of cellulose surrounding the water pools, and the question arose about the water pools proximity to the crystalline or to the amorphous polymeric domains. Since the line width of an ^{1}H wide line spectrum characterizes the strength of dipolar couplings among protons, and, therefore, the molecular mobility, the marked difference previously observed in the line width of cellulose and water suggested the use of the dipolar filter technique for ^{13}C CPMAS [116]. By applying the dipolar filter sequence, the selection of the ^{13}C magnetization of the mobile component of the paper, was achieved. At very short mixing times τ, the carbon signals corresponding to the broad component in the ^{1}H spectrum of the cellulose are partly removed. At long mixing times, when the spin diffusion process is complete, the conventional ^{13}C CPMAS spectrum is obtained. Fig. 19 shows the dipolar filtered ^{13}C CPMAS spectra obtained at increasing mixing times. Note that at the shortest mixing time (τ = 0.5 ms) the resonance at 66.8 ppm from C6c is very weak, while the resonance at 64.5 ppm due to C6a is well observable. The same trend was observed for the intensity of resonances of C4c and C4a. At the longest mixing time (τ = 40 ms), when the spin diffusion process is complete, the conventional ^{13}C CPMAS spectrum is obtained, with C4c and C6c resonances being very intense and sharp with respect to the resonances of their amorphous counterpart. Therefore, at very short mixing times, a polarization transfer from the ^{1}H signal of the water pool to the ^{13}C signals of the cellulose domains has occurred, allowing an indirect selection of the amorphous domain in the cellulose matrix. Given the marked difference in mobility between water and cellulose, also WIdeline SEparation (WISE) [8,117] experiments were carried out to study the water–cellulose interaction. With a series of these experiments, the build-up of the intensity of the water resonance from the ^{1}H projection corresponding in the ^{13}C dimension to the resonances due to C6c and C6a, was obtained. The build-up of the intensity of the water resonance observed for crystalline and amorphous cellulose domains, led to the space relationship between these domains and the water pools. It was found that the build-up of the magnetization of the water resonance was complete after different times for C6a and C6c respectively. Water pool dimensions were calculated from results obtained by dipolar filtered and WISE experiments. Calculation was carried out according to the theory developed by Spiess et al. [118]. Based on this theory, a model was obtained in which water pools, with an

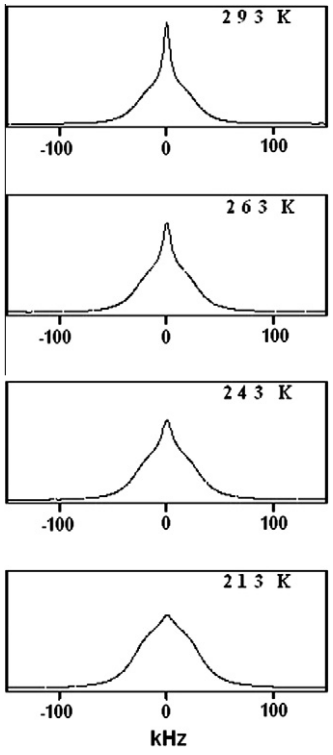

Fig. 18. ^{1}H wide line NMR spectra at 80 MHz of paper collected at different temperatures. The sharp water peak progressively broadens as the temperature decreases. (Adapted from [109].)

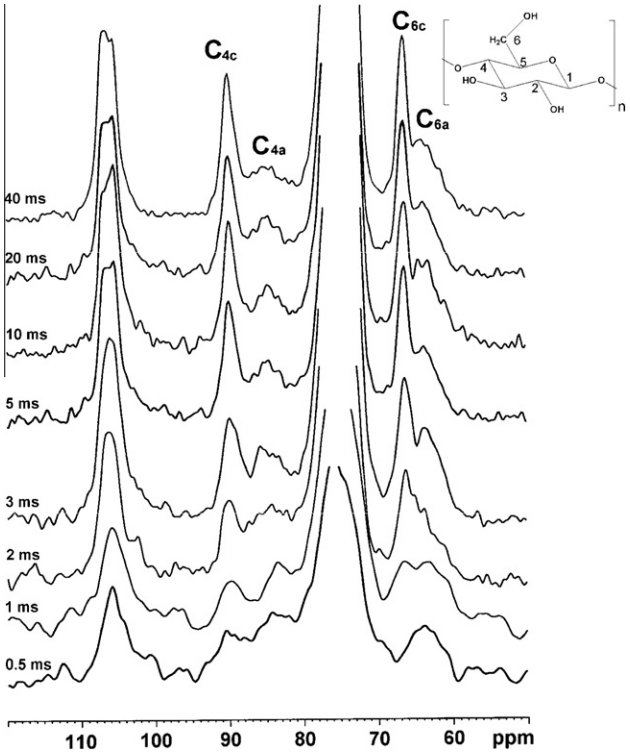

Fig. 19. Linters paper: dipolar filtered ^{13}C CPMAS NMR spectra at 50.13 MHz obtained at various mixing times. (Reproduced with permission from [115].)

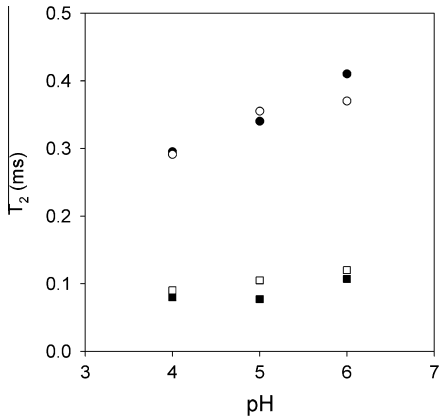

Fig. 20. T_2 intermediate component measured in Linters paper used as a control (circles) and treated with the enzyme (squares). (Adapted from [120].)

average dimension of about 1.5 nm, are surrounded by amorphous cellulose domains, and the crystalline domains are surrounded by amorphous domains which included the water pools [115].

Several other researches have focused on the study of paper deterioration. In chemical terms, the degradation of paper is essentially the conversion of fibrous and highly crystalline cellulose into a largely amorphous degraded material. Besides, in ancient and modern paper, a measurable loss of bound water is always found in degraded paper [111]. Also paramagnetic impurities play an important role in the degradation of paper, as they may act as catalysts and initiators of hydrolytic and/or oxidation reactions. Furthermore paramagnetic centers undergo profound changes upon thermal or photochemical ageing of paper [108,111].

The fungal growth on paper is one among the causes responsible for paper deterioration often occurring in archives and libraries. It is well known that many fungi active on paper produce different hydrolytic enzymes such as cellulases and ligninases [119]. This enzymatic activity has different operating mechanisms in the solubilization of different paper components. Thus cellulose degradation arising from different types of fungi, involves the synergic action of enzymes such as esoglucanases, endoglucanases, and β-glucosidases. However, the biodeterioration of lignin, which is present in most papers manufactured after 1850, needs a complex of enzyme activities such as lignin peroxidases, Mn-peroxidase and laccase. Ligninase and cellulase act in synergism to achieve a complete solubilization of paper components. In order to study the effect of fungal attack on historical documents, a purified enzyme, namely endoglucanase, with a well defined activity, was used on model samples of paper. ^{1}H pulsed low resolution relaxometry proved valuable in assessing the paper degradation with regard to the detection of an early enzymatic attack not observable with any other methods [120]. Three series of samples were incubated with 5 and 10 units of cellulase of Aspergillus niger in citrate–phosphate buffer pH 4.0, 5.0, and 6.0 solutions. Three paper strips were also soaked in the buffered solutions without the enzyme and used as a control. After soaking, all samples were dried at 60 °C for 24 h.

Before submitting the paper to the enzymatic attack by *Aspergillus Niger*, the enzymatic activity of this enzyme was tested on carboxymethylcellulose (CMC). It was found that 1 unit of enzyme releases 1.0 mol of glucose from CMC in 1 h at pH 5 and 37 °C. Generally the activity of this enzyme decreases as pH increases, and, at pH greater than 6, the enzyme tends to be no longer effective. The most sensitive parameter to monitor the effect of the enzymatic attack by NMR was found to be the transverse relaxation time T_2. Before and after the enzymatic attack of paper (Linters and woodpulp), three T_2 components contribute to the CPMG decay, namely a slow, an intermediate and a fast relaxing one. The slow relaxing component was found to be (9.0 ± 0.5) ms, the intermediate one ranged between 0.1 and 0.5 ms and the fast relaxing one ranged between 0.05 and 0.1 ms. The fastest component is due to tightly bound water, this water is either involved in a spin-diffusion process with the polymers (cellulose, hemicellulose and lignin) or is close to paramagnetic centers [108]. The slowest component found in all samples, is never present in samples not soaked [108]. Thus this component was ascribed to a very small amount of residual free water after soaking. Both the fastest and the slowest components are not affected by the enzymatic attack. The intermediate component is the only one markedly shortened after the enzymatic attack, see Fig. 20. In fact T_2 values were found to be about 0.3–0.4 ms in control samples, whereas they shortened to about 0.1 ms in paper attacked by the enzyme. Additionally, whereas in samples used as a control, the intermediate component clearly lengthens with increasing pH, in samples incubated with the enzyme, this component was found to be not affected by pH, see Fig. 20.

Recently, research has been focused on developing appropriate and long term resistance treatments to protect valuable documents. The protective efficacy of commercial waterborne polyurethanes against enzymatic attack has been tested on several types of paper [121]. The evolution of structural and physical–chemical characteristics of both uncoated and coated paper samples before and after biodegradation, was monitored by several techniques, including ^{13}C CPMAS NMR spectroscopy. ^{13}C solid state NMR allowed the detection of the structural modification occurring in the cellulose matrix at different times of incubation with the enzymatic complexes (cellulosomes), both in uncoated paper and in paper coated with polyurethanes. In the uncoated paper, after 2 and 5 days of incubation, the cellulose structure was found to be essentially unchanged, however, after 10 days of incubation, evident damage in the cellulose matrix occurred, see Fig. 21, left side. In fact all resonances are markedly broadened, with the ratio between the intensity of C4a and C4c clearly increased, thus indicating a net increase of the amorphous cellulose fraction. Moreover, broad shoulders between 93 and 100 ppm possibly due to cellulose oligomers, were observed. After 15 days of incubation, the uncoated paper was fully destroyed and no solid sample could be recovered from the aqueous solution where the paper had been soaked during the enzymatic treatment. However, the paper coated with polyurethane showed a prolonged resistance to the biodegradation. In fact the ^{13}C CPMAS spectrum of coated paper incubated for 10 days showed only a slight increase of the amorphous fraction. This effect was more evident after 15 and 30 days of incubation, see Fig. 21, right side. Actually, the NMR spectra show that after 30 days of incubation, even if affected by a loss of crystallinity, the cellulose matrix of coated paper still exists, whereas in the case of uncoated paper, at incubation times longer than 10 days, the cellulose structure is fully destroyed [121]. It is evident that the use of waterborne polyurethanes in the protection of paper-based materials, when submitted to the enzymatic attack, is able to delay the destruction of cellulose matrix.

Another cause of paper deterioration in archives and libraries is because oxidation occurs in the cellulose matrix. As an example, the ^{13}C CPMAS spectrum of a sample of paper from a book dated 1665, is shown in Fig. 22. The paper appeared browned and fragile. In the 60–110 ppm range the resonances characteristic of cellulose with a good degree of crystallinity are observed, however, the broad signal at about 175 ppm shows that there are a number of different sites for the carboxyl carbons which indicates the occurrence of oxidation in the cellulose matrix [122]. Oxidation reactions in cellulose involve the primary and secondary hydroxyl groups of the pyranose ring leading to carbonyl and carboxyl groups which are able to absorb UV and visible radiation. Both

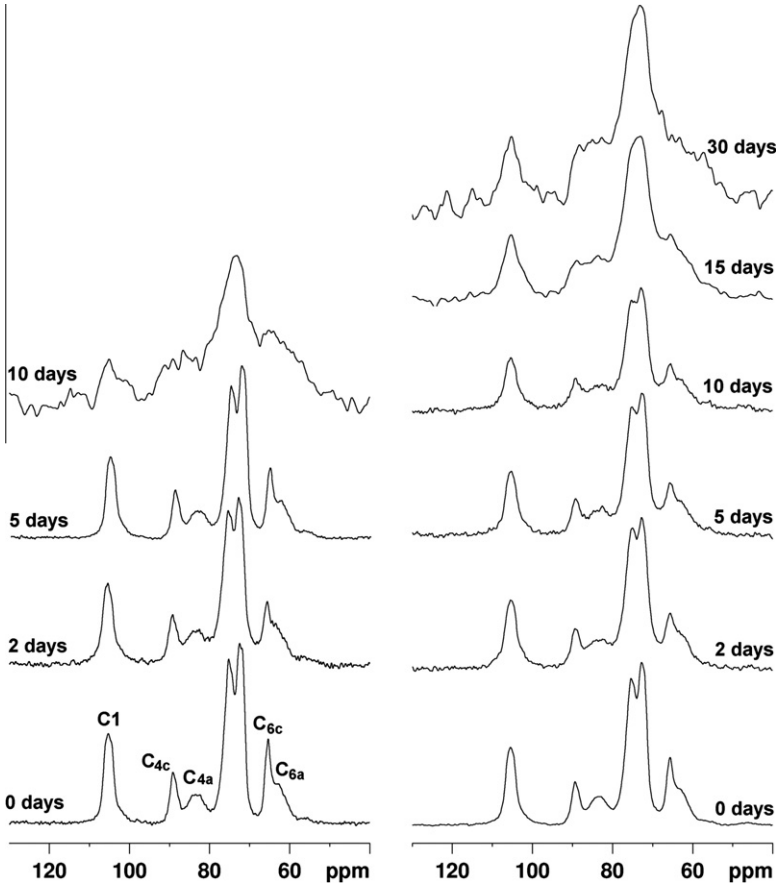

Fig. 21. ^{13}C CPMAS NMR spectra at 50.13 MHz of, on the left, uncoated paper before (0 days) and after 2, 5, and 10 days of enzymatic attack, and on the right, spectra of paper coated with polyurethane before (0 days) and after 2, 5, 10, 15, and 30 days of enzymatic attack. (Adapted from [121].)

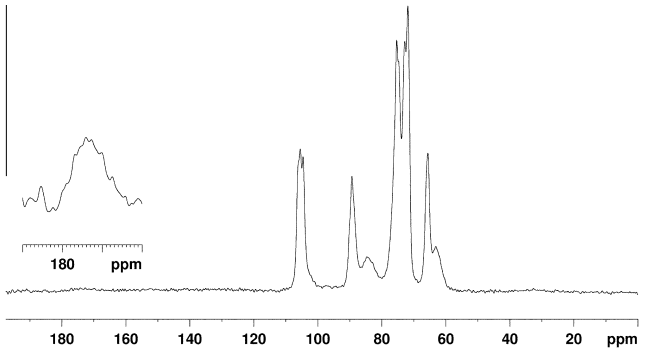

Fig. 22. ^{13}C CPMAS NMR spectrum at 100.13 MHz of a sample of ancient deteriorated paper from a book dated 1662. In the insert the resonance of carboxyl carbons is shown with a vertical multiplication. (D. Capitani, N. Proietti, V. Di Tullio, unpublished data.)

carbonyl and carboxyl groups are chromophores and their formation is responsible for the yellowing of paper [122]. The oxidation reaction may also be accompanied by the opening of the pyranose ring. In both cases, the glycosidic bond becomes weaker and the eventual formation of the carboxylic acids increases the acidity of the paper. Therefore, the depolymerization of cellulose occurs along with a general worsening of physical and mechanical properties.

Studies have been carried out on the use of polymeric materials to consolidate and protect oxidized paper [123]. In particular, a grafting reaction was carried out on paper using vapourised acrylic monomers, namely ethylacrylate (EA), methylacrylate (MA) and methylmethacrylate (MMA). In order to simulate the ageing of paper, before the grafting, chemical oxidation was performed with $NaIO_4$, a specific oxidizing agent. The oxidation process was needed to obtain dialdehydic groups where acrylic monomers could be grafted. ^{13}C CPMAS NMR spectroscopy was used to follow the oxidation process in paper and also to confirm the occurrence of the grafting reaction on the oxidized paper. At short times of oxidation, the ^{13}C CPMAS spectra show the presence of a weak resonance at about 202 ppm which is attributed to dialdehydic groups [123]. After prolonged oxidation, the spectrum shows a general broadening of all resonances of cellulose, along with a consistent increase of resonances due to oligomers. By spectral deconvolution it was possible to evaluate the relative amount of oligomers and the crystalline/amorphous ratio as a function of the oxidation time.

^{13}C CPMAS spectra also allow one to demonstrate the grafting of EA, MA and MMA on oxidized cellulose chains. As an example, the spectrum of paper grafted with MMA is reported in Fig. 23. It is worth noting that the monomer insertion did not alter the appearance of the grafted paper, as this aspect is very important in Cultural Heritage material. A semi-quantitative evaluation of the grafting was performed by studying the cross-polarization dynamic process [124]. Parameters obtained from the best fit of the equation describing the kinetics of the cross-polarization process, allowed the evaluation of the grafting yield. It was found that the grafting with MMA gave the best result with the highest number of acrylic monomers grafted on cellulose chains.

The cross polarization dynamics also give information on the morphology of grafted chains with respect to the bulk cellulose. As an example, Fig. 24 shows the correlation between the intensity of C1 (cellulose) and C3′ (grafted monomer) with the contact time t

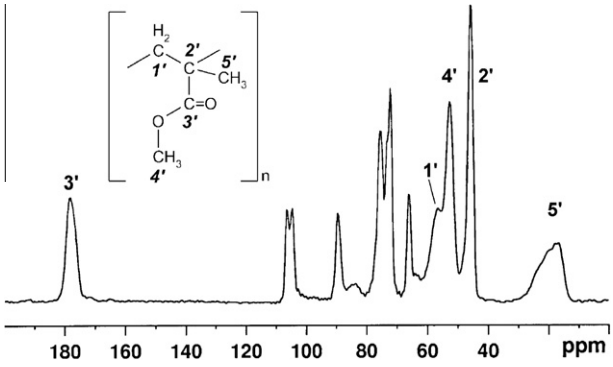

Fig. 23. ^{13}C CPMAS NMR spectrum at 50.13 MHz of oxidized paper grafted with MMA along with resonances assignment. (Adapted from [123].)

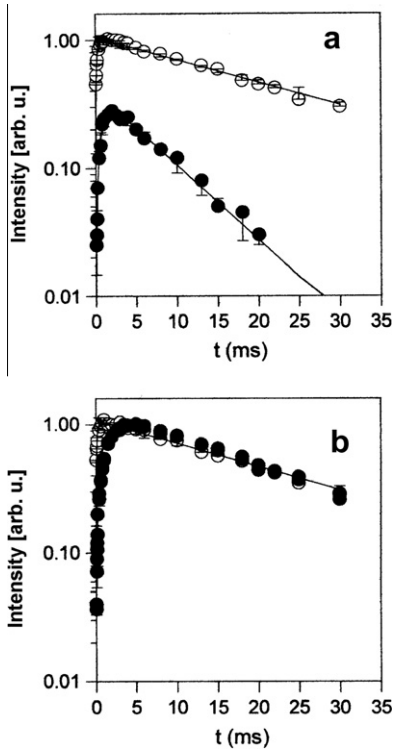

Fig. 24. The intensity as a function of contact time, t, of the anomeric carbon resonance C1 (empty circles), and the carbonyl carbon 3′ of MMA (filled circles) in the 50.13 MHz ^{13}C CPMAS spectra from (a) methyl acrylate and (b) methyl metacrylate. (Adapted from [123].)

in paper grafted with (a) MA and (b) MMA. A value for $T_{1\rho H}$ may be evaluated from the slope of the downward part of curves shown in Fig. 24a and b [123]. The spin diffusion process is fully active in equalising $T_{1\rho H}$ values of cellulose and of the grafted monomer in paper grafted with MMA, but in paper grafted with MA the spin diffusion process from cellulose to the grafted monomer is interrupted. Thus it was hypothesized [123] that in paper grafted with MMA the grafted chains possibly lie on the cellulose surface or inside, whereas in paper grafted with MA, the grafted chains might lie outside the cellulose surface.

Recently, the development of non-invasive mobile NMR equipment has allowed the non-invasive study of historical documents for which the sampling of an even small amount of paper must be strictly avoided. The first application of unilateral NMR to investigate non-invasively the degradation of historical documents and books was reported by Blümich et al. [125]. Historical books dating from the 17th century were measured by positioning the probehead directly on pages showing a different degree of deterioration. The values obtained for transverse relaxation times can be used to discriminate among pages of the same book showing degradation to different extents, as the longest T_2 values were obtained in the case of paper with a low degradation, and the shortest for increased levels of degradation. Although the magnetic field generated by the unilateral NMR device is strongly inhomogeneous, it was shown that the quality of the experimental data is sufficient for discriminating among different states of paper degradation in the investigated books [125].

A further advance was made by a systematic study of paper artificially aged by oxidation to reproduce one of the common causes of paper degradation [126]. The artificial ageing was monitored invasively by ^{13}C solid state NMR and conventional ^{1}H NMR relaxometry, and non-invasively by using the unilateral NMR technique. Both conventional and unilateral NMR devices operated at approximately the same ^{1}H carrier frequency (about 18 MHz). It is worth noting that the use of artificially oxidized paper samples allowed a direct comparison between transverse T_2 relaxation times measured by unilateral NMR and those obtained in a homogeneous field. Results from both devices showed that increasing exposure to the oxidising agent resulted in an increased shortening of the T_2 relaxation time of the confined water. Even very low concentrations of oxidizing agent ($NaIO_4$) and short exposure times provided a noticeably reduced relaxation time, even when the damage was not visible, and not detectable by ^{13}C CPMAS NMR analysis, suggesting that T_2 values are extremely sensitive to paper degradation. The T_2 values obtained by conventional and unilateral NMR were found to be equal within the experimental error, as is clearly observable in Fig. 25 where T_2 distributions obtained from CMPG decays measured with both devices, are compared. Also, in both cases, the centre of the distributions shifts down to shorter T_2 values as the degradation of samples increases. A strong field gradient is applied in the unilateral NMR experiment and if molecular diffusion is present this will affect the T_2 values obtained. The absence of this effect shows that diffusion is weak, which reflects the small average size (≈1.4 nm) of water filled pools [115].

A study has been made on Papyrus, Whatman, and Newsprint paper before and after physical and/or chemical ageing [127]. Analytical techniques were applied to characterize the samples and to monitor the damage, including ^{13}C CPMAS NMR spectroscopy, and conventional and unilateral NMR. Fig. 26a shows the ^{13}C CPMAS spectrum of papyrus which is an early type of writing material, produced from the *Cyperus* papyrus plant. In newsprint and papyrus a considerable amount of lignin is present in addition to cellulose. Note that in these materials, the presence of lignin enhances the effect of weathering processes. It was found that the chemical ageing mostly affects the cellulose matrix, whereas physical ageing in a solar box mostly affects the lignin matrix. The deconvolution of spectra collected before and after ageing, allowed a quantitative evaluation of the modifications occurring in the cellulose and lignin matrix to be made, such as the amount of oligomers, the variation of the crystalline to amorphous ratio, the increase of carboxyl carbons, and variation in the aromatic and methoxyl regions [127]. The ^{13}C CPMAS spectra of papyrus before and after ageing in a solar box, reveal modifications in the aromatic region, and also that the intensity of the resonance of OCH_3 groups of lignin has decreased, see Fig. 26b and c. In Fig. 26d, the spectrum of an ancient papyrus from the archaeological site of Antinoe, Egypt, is also reported. In this ancient sample, the degradation of the lignin is evident, with all resonances markedly broadened, whereas the cellulose component is in a rather good state of conservation. The effect of physical and chemical ageing processes was also monitored by ^{1}H low resolution relaxometry, with both conventional and unilateral

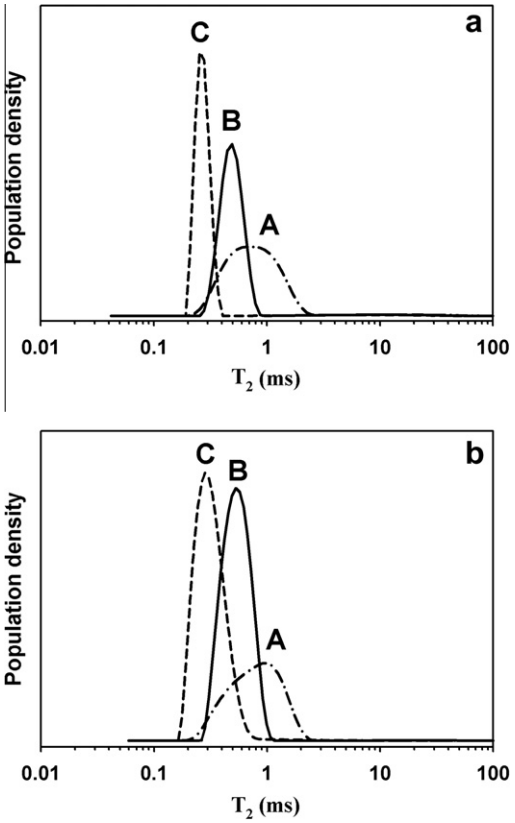

Fig. 25. T_2 distributions obtained (a) in a homogeneous magnetic field with a conventional relaxometer, and with (b) unilateral NMR. A: Untreated paper. B: Paper oxidized with $NaIO_4$ 0.1 M. C: Paper oxidized with $NaIO_4$ 0.4 M. (Adapted from [126].)

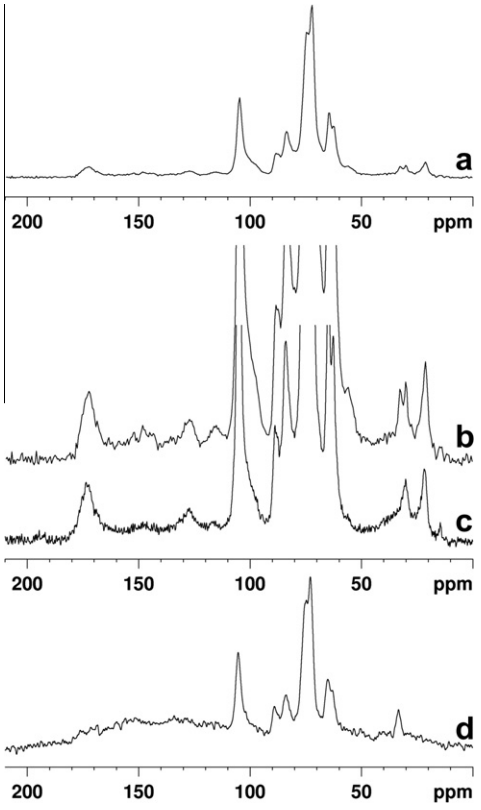

Fig. 26. ^{13}C CPMAS NMR spectra of papyrus at 50.13 MHz. (a) Modern papyrus, and (b and c) before and after treatment in a solar box reported on a vertical expanded scale. (d) Ancient papyrus from the archaeological site of Antinoe, Egypt, the sample was a kind gift from the Antiquity Science Department, Sapienza University of Rome. (Adapted from [127].)

devices. In all samples, as the degradation occurred, the maximum in the T_2 distributions shifted to shorter values, further confirming that the T_2 relaxation time is a suitable index of degradation in cellulose based materials. As an example, T_2 distributions of untreated and aged papyrus obtained by conventional relaxometry, and therefore with a homogeneous field as well as with an unilateral device, which has an inhomogeneous field, are reported in Fig. 27a and b respectively. The most pronounced shift to short values was found in the sample weathered in a solar box. Once again, the results obtained with conventional and unilateral devices, were found to be in accordance.

Based on these results, unilateral NMR has been employed to study precious old books and ancient documents. The state of conservation of ancient maps from the 17th and 18th century [128,129] was investigated by a non-destructive and non-invasive multi-analytical approach. In particular, unilateral NMR was used to measure T_1 and T_2 relaxation times in different areas of the maps. T_1 measurements discriminated between areas showing foxing (discolouration with brown spots) and areas in a good state of conservation, as shorter T_1 values being found for areas with foxing. T_1 also detected the presence of paramagnetic ions in areas with green ink where shorter T_1 values were measured. This result was confirmed by non-invasive X-ray Fluorescence (XRF) analysis which revealed the presence of Cu and Fe ions in these areas. T_2 transverse relaxation times detected the presence of organic substances used in a previous undocumented restoration: T_2 values in unrestored areas were found to be very similar to those of ~0.3 ms measured for well preserved paper, whereas the T_2 values were definitely longer, 0.6/0.8 ms, in restored areas, see Fig. 28, bottom.

Recently, a novel application of unilateral NMR to paper, was reported in which micrometer thick oil stains on paper were differentiated and characterized [130]. Oils can stain works of art on paper such as manuscripts, photographs, drawings and so on. When the stains are visually disruptive and the damage is not considered part of the history of the object, art conservators remove them by applying a suitable conservation treatment that ideally reduces the stain without affecting the paper support, the pigment, or other media present. The degree of cross-linking of the oil is a good guide for determining the choice of the treatment, but is not the sole identifying factor of the type of oil. The degree of cross-linking of oils was assessed non-invasively by tracking changes in the T_2 transverse relaxation time: T_2 decreased as the degree of crosslinking of the oil increased. The value of the longest T_2 component measured on oil stains on paper can be used to determine whether an oil stain was caused by a drying, a semi-drying, or a non-drying oil, and to follow up the treatment to remove the stains, as, after removing the stain, the longest T_2 component converged to the T_2 value characteristic of the paper substrata [130].

Unilateral NMR has also been used to monitor the degradation of *Codex Major*, a 17th century musical anthology manuscript belonging to the library of the Palazzo Altaemps, Rome [131,132]. The analysis of different areas of the same document allowed information to be obtained about the state of preservation of the paper. NMR relaxation measurements indicated the good state of preservation of the pages of the Codex, as most of the investigated areas of the manuscript have relaxation properties similar to those found in well-preserved paper. Furthermore, the average dimension of water pools in the paper was estimated from T_2 values, and was found to be in a very good agreement with previously

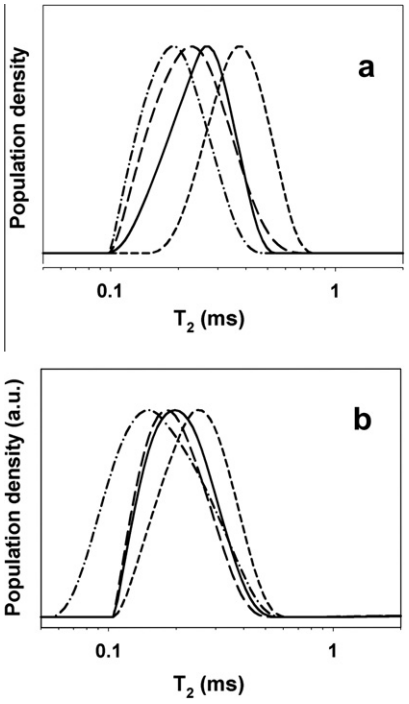

Fig. 27. (a) T_2 distributions of papyrus obtained with a conventional relaxometer, and (b) with unilateral NMR. Untreated papyrus (short dashed line), papyrus oxidized with $NaIO_4$ (solid line), papyrus weathered in oven (long dashed line), papyrus weathered in solar box (dash dotted line). (Adapted from [127].)

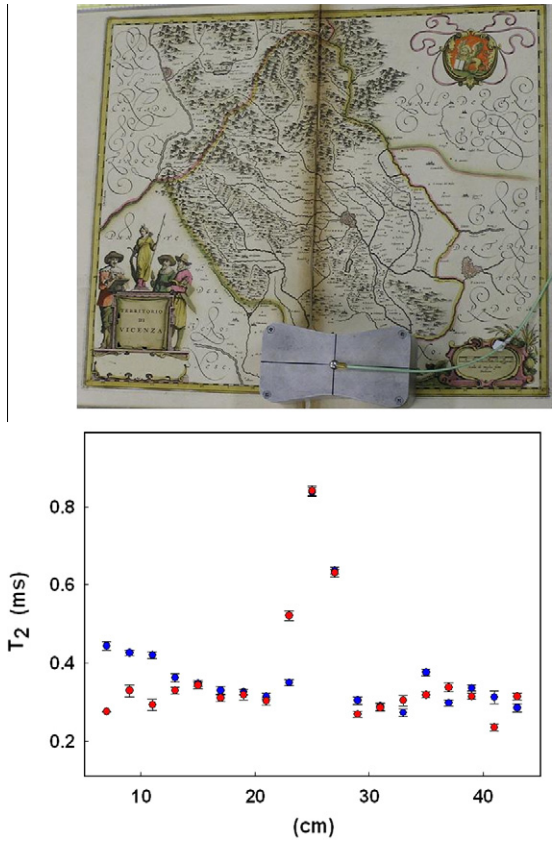

Fig. 28. Top: picture of an ancient map dated 17th century. Bottom: T_2 relaxation times vs the position of measurement on the map. The longest T_2 values were obtained for the middle of the map, where a previous undocumented restoration had been carried out. (Adapted from [128].)

published data [115], indicating a well-preserved paper structure. Damaged areas seem to be mostly related to the acid iron-gall ink action, in fact, the shortest relaxation times were measured for these areas, possibly indicating the presence of a considerable concentration of paramagnetic impurities from the ink.

10. Wood

Wood is a complex natural composite material made of cellulose, hemicelluloses, lignin and water. Hemicelluloses are relatively short-branched homo- and heteropolymers made up of pentose and hexose sugars and their uronic acid derivatives. Hemicelluloses constitute the alkali-soluble carbohydrate fraction of wood. Lignin is a complex three-dimensional amorphous polymer synthesized by enzymatic polymerization of p-coumaryl, coniferyl and synapyl alcohols being the respective precursors of p-hydroxyphenyl (H), guaiacyl (G) and syringyl (S) phenylpropanoid units linked by C–C and ether bonds. The most complex HGS lignins are typical of grasses, whereas hardwoods contain GS lignins, and G lignins are characteristic of softwoods.

Cellulose is present mainly in the secondary wall layer in the form of microfibrils, hemicelluloses are present in all cell wall layers, whereas lignin is primarily found in cell wall corners, middle lamella and primary cell walls. Hemicelluloses and lignin interact with cellulose microfibrils [133,134] creating a rigid structure that strengthens the cell wall. The structure and molecular organization of wood cells in a living plant modulate the mechanical strength, the action of the water-conducting elements and the function as storage cells. Cell wall structure gives rise to chemical and anatomical properties which are very variable and strongly dependent on the plant species and on the plant age as well.

Degradation of any of the components of wood decreases its mechanical strength and modifies its morphology. Degradation changes the properties of wood, and information on the original state of an ancient wood is obscured. Evaluation of the degree of deterioration of ancient wooden artifact belonging to Cultural Heritage is of interest for archaeology, archaeometry and conservation science. An assessment of the degree of deterioration of wood, characterized by its morphological, chemical and physical properties, is mandatory in order to design an appropriate conservation approach.

^{13}C CPMAS NMR spectroscopy is a very powerful technique for studying structural changes in wood [135,136]. The position and the integral of resonances in the carbon spectrum give valuable information on the type of wood, namely hardwood or softwood, and on its state of degradation. As an example, a marked degradation

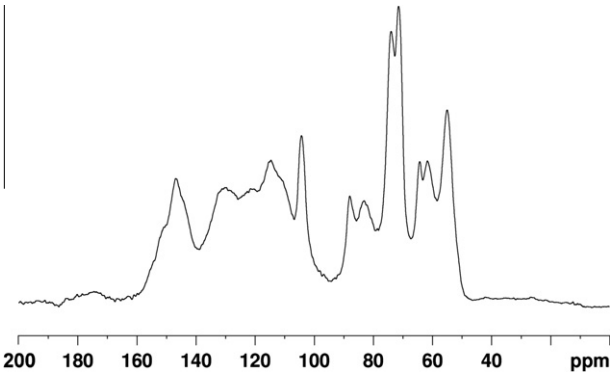

Fig. 29. ^{13}C CPMAS NMR spectrum at 100.13 MHz of wood from the Dunarobba Fossile Forest (Terni, Italy). In the spectrum, the carbohydrates depletion is particularly evident by comparing the relative amount of cellulose with respect to lignin. (D. Capitani, N. Proietti, V. Di Tullio, unpublished data.)

due to a significant carbohydrate depletion in wood, may be clearly observed in the ^{13}C CPMAS spectrum of a sample from the Dunarobba fossile forest (Terni, Italy), see Fig. 29. However the residual cellulose has rather sharp well resolved resonances characteristic of cellulose with a still good degree of crystallinity.

The ^{13}C CPMAS spectrum acts as a fingerprint of the wood, and a qualitative analysis of such a spectrum is the first step in the investigation of structural changes occurring in ancient wood. The most common strategy is to compare NMR spectra of ancient wood samples with a similar modern wood sample used as control. Obviously such a comparison is only meaningful provided that the spectrum of the reference sample has been already assigned. The assignment of carbon resonances is aided by the large amount of available data from previous, pioneering studies. These studies involved the NMR characterization of purposely synthesized compounds to model the different basic units of wood components and the inter-unit bonds in wood [137,138], the NMR characterization of compounds extracted from wood with different extractive procedures, and, finally, the application of basic and advanced mono e two-dimensional NMR experiments to assign the carbon resonances in wood [139,140].

^{13}C CPMAS NMR spectroscopy has been used to evaluate the state of conservation of an ancient wooden panel of an Egyptian sarcophagus (XXV–XXVI dynasty, Third Intermediate Period) [35]. In Fig. 30 the ^{13}C CPMAS spectra of samples from the outer and the inner sides of the sarcophagus are compared with a seasoned yew wood sample used as control. The assignment of the resonances is reported in the caption of Fig. 30. The weak signal at 21 ppm (1) is due to the CH_3 carbon of the acetyl group in hemicelluloses. The signal at 55.6 ppm (2) is assigned to methoxyl groups

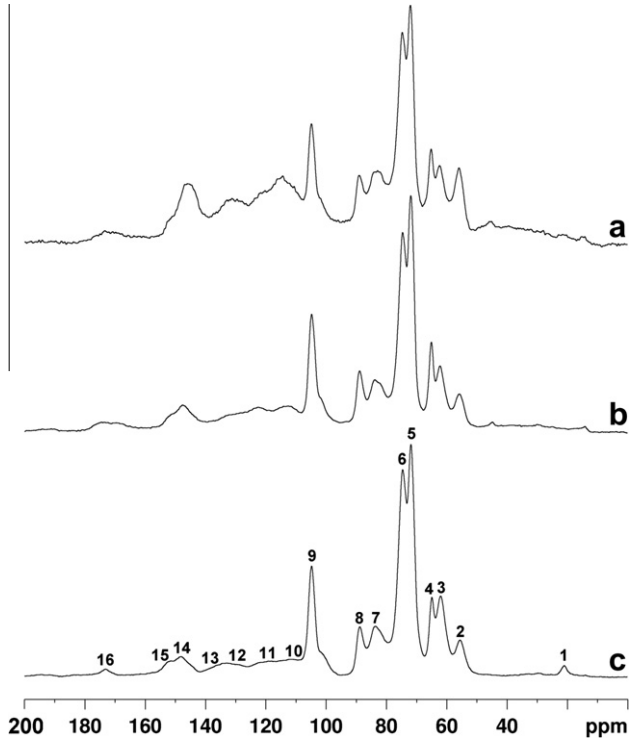

Fig. 30. ^{13}C CPMAS NMR spectra at 100.13 MHz of wood samples. (a) Sample from the outer side of the panel of an ancient Egyptian sarcophagus. (b) Sample from the inner side of the panel. (c) Seasoned yew wood. Assignment from [141]. 1:carbohydrates, $\underline{C}H_3COO–$; 2: lignin OCH_3; 3: lignin Cγ; 4: carbohydrates C6; 5: carbohydrates C2, C3, C5; 6: lignin Cα, carbohydrates C2, C3, C5; 7: lignin Cβ, carbohydrates C4; 8: carbohydrates C4; 9: carbohydrates C1; 10: lignin G5, G6, S2, S6; 11: lignin G6; 12: lignin S1(ne), S4(ne), G1(e); 13: lignin S1(e), S4(e), G1(e); 14: lignin S3(ne), S5(ne), G1, G4; 15: lignin S3(e), S5(e); 16: carbohydrates $\underline{C}OO–R–$, $CH_3–\underline{C}OO–$. (Adapted from [35].)

of aromatic units of lignin. The region between 60 and 105 ppm is dominated by signals mostly assigned to cellulose, whereas the region between 105 and 160 ppm is specific to the aromatic carbons of lignin. The signal at 172 ppm arises from carbonyls in acetoxy groups of hemicelluloses and to acid groups possibly present in wood. According to the literature [141], the resonance at 152.6 ppm (15) is assigned to carbon atoms C3 and C5 of S (syringyl) units in etherified arylglycerol β-aryl ethers, namely S3(e) and S5(e), and the resonance at 147 ppm (14) is assigned to carbon atoms C3 and C5 of S units in non-etherified arylglycerol β-aryl ethers, namely S3(ne) and S5(ne) and to carbon atoms C1 and C4 of G (guaiacyl) units, namely G1 and G4. The integrals of all resonances were obtained by applying a deconvolution procedure. It is worth noting that the resonance at 21 ppm (acetyl groups of hemicelluloses) which is clearly observed in seasoned yew wood is absent from the spectra of samples obtained from the sarcophagus, clearly indicating the occurrence of hemicelluloses depletion. According to the literature [141], the relative amount of carbohydrates and lignin was evaluated from the integral I(9) of resonance 9 at 104.8 ppm of the anomeric carbon of cellulose as a reference, and the integral I(2) of resonance 2 at 55.6 ppm of the methoxyl groups of lignin. The ratio between I(9) and I(2) is found to be 2.17 in seasoned yew wood, whereas it is 1.58 in the sample collected from the inner side and 0.87 in the sample from the outer side of the sarcophagus. These results clearly indicate that both samples from the inner and the outer side of the sarcophagus show a depletion of carbohydrates, however the depletion is definitely higher in the sample from the outer than in the sample from the inner side. The relative intensities of signals 15 and 14 allowed the evaluation of the depletion of the β-O-4 linkages in lignin. The ratio I(15)/I(14) is 0.51 in seasoned yew wood, 0.48 in the sample from the inner side and 0.25 in the sample from the outer side of the sarcophagus. These results indicate that the inner side is only slightly affected, whereas in the outer side a depletion of β-O-4 linkages inside lignin has occurred. However, in spectra of ancient samples the linewidths of carbon resonances are not significantly different from those observed in the spectrum of seasoned yew wood, indicating that, while ageing has induced a depletion of carbohydrates, no chemical rearrangements inside the bio-polymeric network have occurred. The effects of such rearrangements are commonly observed in carbon spectra of wood samples after pulping processes [141].

The state of conservation of the sarcophagus was also investigated by unilateral NMR [35], which allowed measurements to be performed *in situ* and in a fully non-invasive way. Transverse relaxation times measured on the inner and outer sides of the wooden panel of the sarcophagus were found to be shorter with respect to those measured in a sample of seasoned yew wood, indicating a loss of lumen water [142] because of the ageing. The shortening is more evident in areas on the outer side than in those on the inner side, indicating a more pronounced degradation in the outer than in the inner side of the panel of the sarcophagus, in accordance with results obtained by ^{13}C CPMAS NMR spectroscopy. In Fig. 31a, T_2 distributions obtained by inverting CPMG decays measured on seasoned yew wood, on the inner side and the outer side of the panel, are compared. In seasoned yew wood the distribution has three peaks resulting from cell water and lumen water in two different environments, whereas in the inner and in the outer side of the panel the peak centred at the longest T_2 value is missing. The longest T_2 component measured in the outer side is clearly shifted to a value shorter than that measured in the inner side. This result is in agreement with a previous observation indicating the transverse relaxation time as a suitable parameter for evaluating the state of degradation in cellulose based materials [120]. This study of the wooden Egyptian sarcophagus enabled an analytical protocol to be established for detecting, fully non-invasively, the

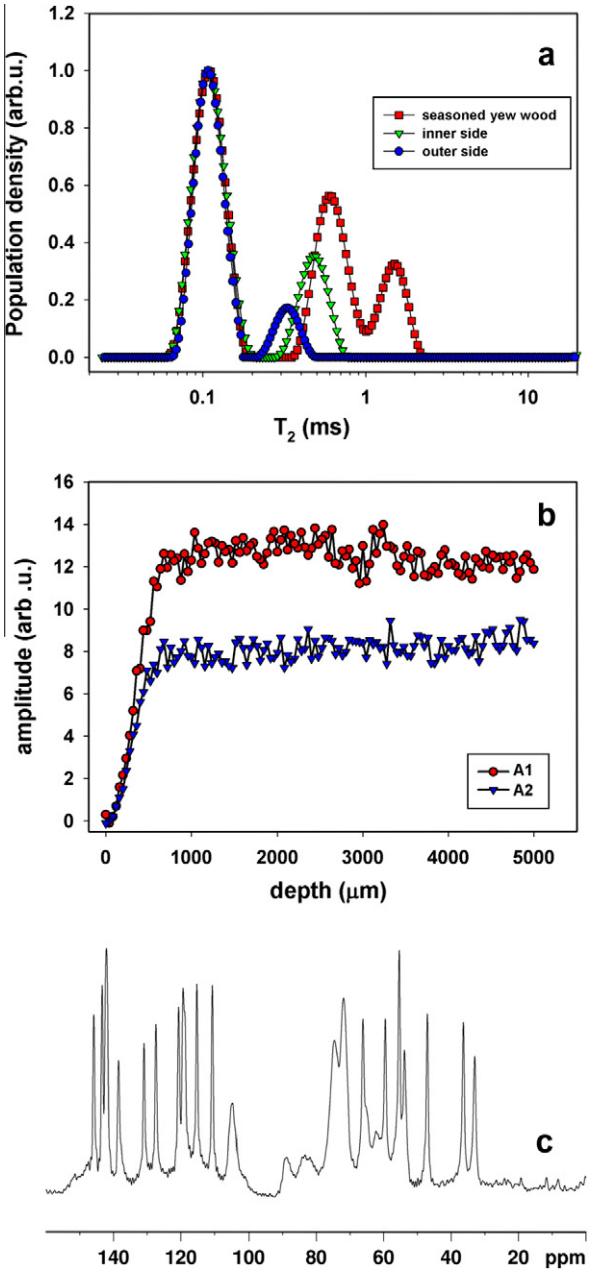

Fig. 31. (a) T_2 distributions obtained for seasoned yew wood (squares), for an area of the inner side of the panel of the sarcophagus (triangles), and for an area of the outer side of the panel (circles). (b) Comparison between NMR depth profiles measured in two different areas (A1, A2) of the outer side of the sarcophagus. (c) ^{13}C CPMAS NMR spectrum at 100.13 MHz, of a sample from an area of the outer side of the panel. (Adapted from [35].)

presence of organic substances on the surface and/or embedded into the wood matrix constituting the panel. According to this protocol, proton density maps of the outer side of the wooden panel were obtained in the first layers of the wood and at a depth of 0.5 cm inside the wood. In these maps, unexplained intense proton densities were found in many areas of the outer side of the panel of the sarcophagus. This finding was further confirmed after measuring NMR depth profiles spanning from 0 to 0.5 cm inside the wood. As an example, depth profiles measured in two areas of the outer side of the panel of the sarcophagus are shown in Fig. 31b. A net difference in the amplitude of the profiles, is observed. In order to clarify the source of the anomalous proton density, ^{13}C CPMAS spectra were recorded on samples taken from a few selected areas with the aim of investigating their structural composition. The carbon spectra of these samples, in addition to showing the typical resonances of wood, clearly feature 18 intense and very sharp resonances typical of molecules in a crystalline environment [35], see Fig. 31c. The analysis of these spectra also revealed the presence of an organic substance with a basically aromatic structure possibly used in an undocumented restoration.

Pournou has used ^{13}C CPMAS NMR spectroscopy to investigate the chemical composition of an archaeological oak wood found in a 16th century site in Zakynthos [143]. The most relevant feature found in the spectra of archaeological wood samples compared with a modern oak, is the absence of resonances at 21 and 172 ppm ascribed respectively to methyl carbons and carboxyl carbons of hemicelluloses. The preferential loss of hemicelluloses vs cellulose was reported to be mainly due to the hydrolysis of wood at a non advanced stage of decay. This is because the archaeological oak was recovered from a restricted-oxygen marine environment, where the presence of brown and white rot which cause decay was excluded. The disappearance of hemicellulose resonances in the carbon spectrum was interpreted as being caused by hydrolysis of the material rather than biodeterioration [143].

^{13}C CPMAS NMR spectroscopy has been employed to characterize archaeological beech wood samples from an 11th century site in Paladru lake at Chravines, France [144]. The aim was to investigate the degradation of wood after ageing in a water environment. To obtain the required quantitative intensities the polarization dynamics were carefully investigated. Thus, the intensity of each ^{13}C resonance was obtained vs the contact time t. The data were fitted to the equation:

$$M(t) = M_0\left[1 - \exp\left(-\frac{t}{T_{CH}}\right)\right]\exp\left(-\frac{t}{T_{1\rho H}}\right), \tag{19}$$

where $M(t)$ is the measured intensity for a contact time t, M_0 is the initial intensity of magnetization, T_{CH} is the cross-relaxation time between protons and carbons, and $T_{1\rho H}$ is the proton spin–lattice relaxation time in the rotating frame. It is worth noting that M_0, which is proportional to the spin density, may be used for quantitative analysis. In order to reduce the number of parameters in Eq. (19), $T_{1\rho H}$ may be measured with a separate experiment. Bardet et al. [144] showed that, at a spinning rate of 5 kHz, a contact time of 1 ms was a suitable time to obtain the maximum polarization for all the wood carbon resonances, with a maximum expected error for the signal intensities below 5%, and without applying any correction to the measured intensities. ^{13}C CPMAS spectra of archaeological beech wood samples showing a different degree of degradation were compared with a modern beech wood sample. It was found that, a marked carbohydrate depletion occurs in modern beech wood which has been aged in water, whereas the overall structure of lignin is not affected. Possibly, the presence of water favours the leaching of cellulose oligomers and hemicelluloses from the wood to the environment. Integrals measured from ^{13}C CPMAS spectra were used to calculate the percentages either in carbons or in weight of lignin and carbohydrates using the average empirical formula proposed for hardwood lignin [136], namely $C_9H_{7.72}O_{2.75}(OMe)_{01.53}$ with a molecular mass 207 g mol^{-1}, and using the average formula of sugars $C_6H_{10}O_5$ with a molecular mass of 183 g mol^{-1}.

^{13}C CPMAS NMR spectroscopy was also used to characterize archaeological oak wood samples from three Portuguese medieval dugout canoes [145], two of these were in a rather good state of conservation, whereas the third one appeared to be heavily degraded and fragile. A wood sample is considered to be slightly degraded if the water content obtained by weighing the wood sample before and after oven drying at 105 °C, ranges between 100% and 200%, whereas it is considered to be heavily degraded if the water

content is higher than 400%. The water content was found to be about 190% and 200% in the well preserved canoe samples, and 800% in the badly degraded sample. The NMR spectra of samples in a good state of conservation were found to be very similar to the spectrum of modern wood, as indicated by the presence of cellulose and lignin. However, the spectrum of the very degraded sample shows a strong decrease of carbohydrates, with a complete disappearance of hemicelluloses, whereas the lignin structure is unaffected. Furthermore, spectra of samples collected from bottom, medium, and internal parts of the same canoe clearly indicate some differences in the relative proportion of lignin and cellulose. All these results indicate that the marked degradation of hemicelluloses and the leaching out of their degradation products is the possible origin of the weakness of the dugout canoes. These results correlated well with the increase in the water content measured in the samples, as the water entered the wood in the free space previously occupied by cellulose fibrils [145].

Wooden archaeological samples from excavations in the Vesuvian area of Pompei have been studied by Alesiani et al. [146]. The wood samples belonged to a building in the Murecine countryside which was buried after the earthquake in 62 BC, and the samples were waterlogged until their discovery in 1999. All the samples were equilibrated in a moist environment for 1 month before the analysis. Spectra of archaeological samples were compared with modern wood samples obtained from poplar, oak, and silver fir. By considering the signal of methoxyl carbons of lignin as a reference, it was deduced that the relative amounts of carbohydrates and lignins differ in the archaeological wood compared with a modern wood. Again, archaeological waterlogged wood samples show a strong carbohydrate depletion.

Anaerobic bacteria are mostly responsible for the depletion of wood carbohydrates in an aquatic environment, leaving an unstable residual structure mainly made of lignin which easily collapses during drying. To reinforce the structure requires a specific consolidating treatment. The most commonly used conservation treatment for waterlogged wood is impregnation with polyethylene glycol (PEG) which relies on the formation of hydrogen bonds between PEG and the carbohydrates of wood. Bardet et al. [147] studied the molecular interactions between the wood and PEG in treated archaeological wood samples. Samples were obtained from a fragment of a halyard slade excavated from an Italian 17th century shipwreck "*La Lomellina*" in the Mediterranean sea. Because of strong degradation, the samples had almost lost their entire cellulose component and most of their initial volume had become occupied by water. Therefore a large volume inside the wood fibres was available for PEG polymers. In addition to signals characteristic of wood the ^{13}C CPMAS spectra of treated wood have new signals ascribed to PEG, i.e. an intense signal at 72 ppm due to carbons of CH_2O groups and a weak signal at 61.7 ppm assigned to terminal CH_2 bound to an hydroxyl group. Choosing a proper contact time (3–5 ms) for which the PEG component gives only a small residual NMR signal in the spectrum, it is possible to edit selectively the spectra of the wood components. Bardet et al. also showed that by editing the spectrum, the degradation extent of the archaeological wood is apparent from the NMR spectrum even after applying the conservation process with PEG. The cross-polarization dynamics in pure PEG and in the very deteriorated archaeological wood samples treated with PEG were carefully investigated by monitoring the build up of magnetization of different carbon signals. The slope of the downward part of these curves is proportional to $T_{1\rho H}$, whereas the slope of the rising part of the curve gives the cross relaxation time T_{CH}: both of these dynamic parameters give information on molecular motions. To obtain M_0, $T_{1\rho H}$ and T_{CH} in the case of a single component system, the experimental data were fitted to Eq. (19), whereas, in the case of a two-components system the experimental data were fitted to:

$$M(t) = \sum_{i=1}^{2} M_0^i \left[1 - \exp\left(-\frac{t}{T_{CH}^i}\right)\right] \exp\left(-\frac{t}{T_{1\rho H}^i}\right), \tag{20}$$

In particular the build up of the magnetization of the intense resonance of PEG, both in pure PEG and in PEG treated wood samples, was investigated. It was found that the PEG moiety, either inside wood or as pure product exists in two domains characterized by separate values $T_{1\rho H}^1$ and $T_{1\rho H}^2$. The relative size of the domains is given by M_0^1 and M_0^2, which reveal that, on average, in all samples, about 70% of protons in PEG are in a disordered domain, with short $T_{1\rho H}$ and long T_{CH}, and the remaining protons, about 30% are in a more ordered or even crystalline domain as indicated by long $T_{1\rho H}$ and short T_{CH} values. It was also found that, in the case of PEG in treated wood, $T_{1\rho H}$ values of the ordered phase are always longer than values assigned to crystalline domains in pure PEG, clearly indicating that the protons of the treated wood affected the dynamics of PEG protons. However, the $T_{1\rho H}$ values for the disordered phase are the same in pure PEG and in PEG treated wood. Furthermore, the $T_{1\rho H}$ values of some of the carbon signals in lignin match well the values measured for the slow relaxing component of PEG in treated wood. To summarize, by investigating the cross-polarization dynamics in PEG treated wood, it was found that only about 30% of PEG is in close molecular interaction with wood components, whereas about 70% of PEG does not interact. This may explain the weakness of the PEG treated wood, particularly when the wood is heavily degraded. It is worth noting that most intense PEG resonance at 72 ppm overlaps with the resonances C2, C3 and C5 of cellulose, and spectral deconvolution was mandatory in order to measure the integrals of the various carbon signals. With the deconvolution the integrals of resonances of woods and those of CH_2 assigned to PEG were measured in untreated wood and in wood impregnated by PEG aqueous solutions with increasing concentration of PEG, and this enabled the carbon ratio between PEG and wood components to be obtained [147].

High and low resolution NMR methods were applied to investigate ancient and very degraded larch and fir wood samples from the trussed rafter of the *Valentino Castle*, 15th century, Turin (Italy) [148]. ^1H wideline NMR spectra at 300 K show the presence of a broad and a sharp line. The former, arising from the polymeric matrix of wood (cellulose, hemicelluloses and lignin) is as broad as 50 kHz, whereas the latter, arising from bound water, has a line width of about 1.5 kHz. On lowering the temperature, the water resonance progressively broadens, and fully collapses into a broad resonance at about 200 K, indicating that, at this temperature, the water confined into the polymeric wood structure is fully frozen. This lowering of the melting point is associated with confinement in small cavities or pores. Bearing this in mind, wood may be treated as a porous system containing a mobile species, the water, embedded into a rigid polymeric matrix, and the pore size distribution was obtained by measuring the intensity of the water resonance as a function of the temperature. The marked difference in the line widths observed in the ^1H wideline spectrum allowed the use of the ^{13}C CPMAS Dipolar Filter technique [115]. At a very short mixing time, the carbon signals corresponding to the broad ^1H component were filtered, whereas, at long mixing times, when the spin diffusion process is complete, the conventional ^{13}C CP MAS spectrum was obtained. ^1H dipolar filtered ^{13}C CPMAS spectra obtained on deteriorated wood samples show that, at very short mixing times, an indirect selection of the amorphous phase can be achieved. Even at very short mixing times the ^{13}C resonances of lignin have intensities which are very similar to those observed for long mixing times. To explain this result, a model was proposed [148] in which water pools are surrounded by thin layers of amorphous cellulose and lignin, while the crystalline domains of cellulose surround layers of amorphous cellulose. The degraded wood

samples were also analysed by non-invasive unilateral NMR. In particular T_2 relaxation times were measured and compared with values measured for seasoned modern larch and fir samples. In accordance with results obtained for other cellulose-based materials [35,120,126,127], the T_2 relaxation times were found to be markedly shorter in degraded than in modern seasoned wood, as, due to degradation, the T_2 shortening reflects a net loss of bound water, or a loss of water confined in pores.

1D and 2D high resolution NMR spectroscopy in solution was applied in order to investigate in detail changes occurring in lignin structure of archaeological wood samples. Salanti et al. [149] characterized waterlogged wood from the site of the Ancient Ships of San Rossore (Pisa, Italy), where many shipwrecks dating from 2nd century BC to 5th century AD, have been discovered. This study was focused on obtaining a detailed picture of lignin chemical features in the archaeological wood samples and in modern samples used as a reference, and involved examining lignin extracted from archaeological and from reference samples by using high resolution NMR spectroscopy in solution. Quantitative ^{13}C spectra and inverse detected $^{1}H–^{13}C$ correlation 2D maps (HSQC) [4] were used to evaluate any significant changes in the polyphenol chemical structure, and to identify the principal inter-monomeric bonds. All the investigated samples were found to be rich in arylglycerol-β-arylether units (β-O-4). Cross peaks due to other principal inter-monomeric bonds (β-5, β–β) were also observed. It is worth noting that the results obtained confirmed that in ancient waterlogged woods the chemical structure of lignin has not been heavily modified by the ageing process, and the principal inter-monomeric linkages are still present [144].

Crestini et al. [150] applied high resolution NMR in solution to study lignin degradation processes in a sample extracted from an ancient Egyptian cypress coffin. A qualitative evaluation of the kind of lignin inter-unit bonding of soluble samples was obtained from 2D homo-correlated NMR spectroscopy (HOHAHA) [151,152] In the HOHAHA map of the aliphatic region of the lignin it was possible to identify some substructures. The lignin backbone was found to be still intact with the presence of signals representative of partially oxidized β-O-4 inter-unit bondings as the main binding pattern. A ^{31}P NMR analysis of the ancient lignin sample and of a recent reference wood after phosphytylation, allowed the characterization of the modifications induced by ageing on the distribution of the aliphatic and phenolic OH groups. The lower amount of aliphatic OH groups found in the decayed wood with respect to that found in modern wood, was ascribed [150] to the occurrence of side-chain oxidation reactions, oxidative coupling processes, and/or to the occurrence of reduction steps during overall lignin oxidations (disproportionation processes). Furthermore, the lower amount of phenolic guaiacyl and p-OH groups found in the decayed wood compared to that found in the reference sample, was ascribed to the occurrence of oxidative coupling reactions, and/or aromatic ring cleavage processes. To summarize, it was suggested that the degradation of the original lignin structure led to a residual lignin with a substantial lower content of phenolic and aliphatic OH groups, and that side-chain oxidation occurred, yielding the formation of diphenylmethane and aliphatic subunits.

An important step in the treatment of archaeological wood is the period of time necessary to impregnate the artefact with consolidating solutions, as the permeability of wood is extensively modified by degradation processes. Robertson and Packer investigated the diffusion of deuterated water in plugs obtained from archaeological wood by determining 1-D profile images [153]. Plugs were sampled at different depths, reflecting different degrees of degradation and orientation with respect to the wood structure of an oak timber from the *Mary Rose Trust*, Portsmouth, UK. The profiles were recorded as a function of diffusion times to sample the ingress of D_2O to its completion. The diffusion was found to be highest in the longitudinal orientation with respect to the wood structure and successively smaller in the tangential and radial directions, however these differences became less pronounced as the wood decay increased. The more porous outer layer has larger diffusion coefficients and fluid contents than the core. The authors developed a mathematical model capable of reproducing experimental data and able to predict the ingress of D_2O into a full-sized archaeological timber.

The ability of MRI to obtain non-destructive images from waterlogged wood samples, both prior to conservation and during consolidation, has been assessed by Cole-Hamilton et al. [154]. Good quality T_2-contrasted images were obtained in the case of an ash sample free from iron salts from an Armada warship *La Trinidad Valencera* which was excavated in the 1970s. In contrast, the ingress of paramagnetic iron salts into wooden artifacts from the water in the burial environment made the images of samples of waterlogged birch wood poorly resolved, and the presence of iron salts was found to be associated with the most degraded portion of the wood. Unfortunately, iron is a rather common contaminant in waterlogged conditions as it is often associated with organic remains and/or with the dissolution of nails buried with artifacts. Although the presence of iron salts may prevent obtaining of high quality images, these authors suggested that this drawback might be turned to advantage as a diagnostic probe for the presence of iron in a sample to be conserved, and to monitor the effectiveness of processes aimed at removing iron from the artifact. Cole-Hamilton and coworkers also followed the ingress of consolidating polymers in balsawood [154], using selective proton imaging after masking the protons of water by isotopic substitution with deuterated water. Using this strategy, it was shown that the conductive vessels which constitute the channels available to water movement in wood, are the preferred access route for PEGs with molecular weights up to 1500 Da. By inspecting polymer selective NMR images it was noted that the polymers do not penetrate the wood uniformly: the image appeared as blotchy, with high concentration patches around the most easily accessible routes.

An interesting application of portable Profile NMR-MOUSE to investigate *Stradivari* violins, in a fully non invasive way, was recently published by Blümich et al. [33]. The interest of this study lies in that part of the sound quality of these violins is ascribed both to the selection of wood and to the wood treatment. The depth profiles collected on a selection of violins detected the signal from the wood and the presence of one or more varnish layers as well. The signal shown in these depth profiles derives mostly from the wood density. Plots of the signal amplitude measured at 0.7 mm depth against the reported fabrication year of the violins showed that there is an increase of the wood density with the age of the violin for most of the violins investigated.

Nagyvary et al. [155] have used ^{13}C CPMAS NMR and infrared spectroscopy to analyze wood taken from antique instruments made by Stradivari and Guarneri. They compared ^{13}C CPMAS NMR spectra of maple wood samples, obtained as thin shavings during the repair of cracks in ancient violins, with samples of recent woods from Bosnia and central Europe. Differences observed in the spectra concern the weak peaks at 18 and 170 ppm of hemicelluloses, the weak peak due to methoxyl carbons, and the main lignin peaks at 135 and 155 ppm. In particular, in samples from *Guarneri* violins, a net decrease of these peaks was observed, and in samples from *Stradivari* violins, the decrease also occurred at a minor extent. In contrast, spectra of modern maple wood were found to be very similar to spectra of wood samples obtained from old French and English instruments. The authors hypothesized that these results, along with results obtained by infrared spectroscopy, support the idea that chemical treatments, such as oxidation or hydrolysis might have been used in the past in making *Guarneri* and also, to a lesser extent, *Stradivari* violins.

11. Textiles

Historical textiles represent a source of information about the history and development of science and technology of people over time. Textiles made with natural fibres and vegetables or animal dyes, tend to easily degrade.

A study has been carried out by ^{13}C CPMAS NMR spectroscopy on three silk pieces from the 12th century sampled from three coffins in north-eastern Japan [156]. The analysis focused on the carbonyl carbon resonances in the region 170–174 ppm assigned to C=O of the peptide bonds in fibroin molecules and ascribed to the differences in constituent amino acid residues, such as alanine and glycine as well as those of secondary structure. In particular, resonances were ascribed to alanine in Silk I, alanine in Silk II, glycine in Silk I and glycine in Silk II respectively for fibroin from Bombyx Mori. Silk I is close to being in random coil whereas Silk II is essentially anti-parallel ß sheet [157]. As a first approximation, the C=O peaks observed were deconvoluted in two peaks, one resonating at lower and one at higher field. In each sample, the fraction of glycine residues was calculated from the intensity ratio of the higher field peak to the sum of the intensity of both peaks.

As an example of such an analysis, Fig. 32 shows the ^{13}C CPMAS spectrum of a sample of Bombyx Mori silk, the reported assignment being obtained from the literature [158].

Chûiô and co-workers have made [159] a detailed study of archaeological and contemporary silk in which the values of T_1 spin–lattice relaxation times were correlated with the mechanical properties of the samples. These correlations were used to estimate the physical properties of archaeological silk samples. The effect of degradation and paramagnetic impurities was also addressed in this paper.

Other studies have focused on the strengthening of the cellulose matrix in degraded textiles [160,161] by using *in situ* polymerization as a method for protecting and consolidating cellulose based textiles. The method was tested both on modern linen and cotton samples previously oxidized to induce the formation of carboxyl and carbonyl groups used as photosensitive agents. ^{13}C CPMAS NMR spectra clearly show that the oxidation process affects linen more than cotton. Then, using low energy ultraviolet radiation for a short time, the grafting of EA or MMA, was carried out. The grafting was also performed on a naturally aged historical cotton sample. In this case, carboxyl and carbonyl groups due to the natural ageing, were used as photosensitive agents. A semi-quantitative evaluation of the degree of grafting was performed either by studying the cross-polarization dynamic process, or by direct integration of resonances in ^{13}C single pulse excitation spectra. As an example, in Fig. 33 the ^{13}C CPMAS spectrum of the naturally aged historical cotton sample grafted with MMA along with resonance

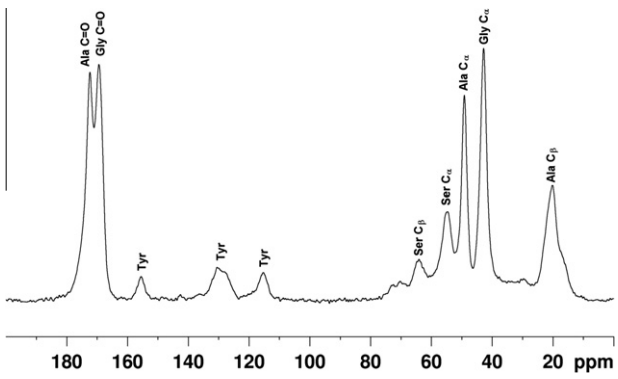

Fig. 32. ^{13}C CPMAS NMR spectrum at 100.13 MHz of Bombyx Mori silk, assignment from [158]. (D. Capitani, N. Proietti, V. Di Tullio, unpublished data.)

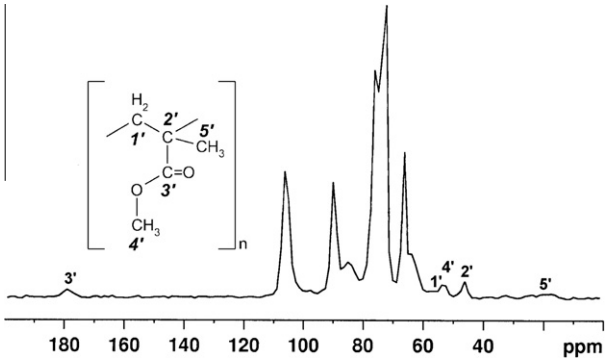

Fig. 33. ^{13}C CPMAS NMR spectrum at 50.13 MHz of naturally aged historical cotton reinforced with MMA. (Adapted from [160].)

assignments, is reported. In this case, the degree of grafting determined by NMR, was found to be about 7%.

12. Parchment and leather artifacts

Parchment was used for bookbindings, manuscripts, codices, scrolls and maps. The Dead Sea Scrolls found in Qumran dated between 250 BC and 65 AD, are, until now, the oldest known parchments. The heyday of parchment use was during the medieval period. Although parchment never stopped being used, primarily for official documents, it ceased to be a primary choice for artists by the end of the 15th century when it was largely replaced by paper. Parchment is made from goatskin, sheepskin or calfskin. It is prepared from wet, unhaired, and limed skin by drying on a stretching frame. After being flayed, the skin is soaked in water to remove blood and grime. Powders and pastes based on calcium compounds are also used to remove grease. It is distinct from leather in that parchment is limed but not tanned. As a consequence, parchment is very sensitive to changes in relative humidity. Because of its source and its method of preparation, parchment is mostly made of collagen. The structure of collagen contains a right-handed triple-helix with the three individual protein strands in the left-handed polyproline-II helix conformation [162]. The three strands of the helices are staggered by one residue, allowing for interchain hydrogen bonds. Gly–Pro–Hyp is the most common repeating sequence involved in the formation of the triple-helix conformation.

Gelatinization of parchment may occur spontaneously even during normal storage conditions, and this leads to the loss of the ordered triple-helix structure. Gelatin is considered to be a more disordered state of collagen as it is the product of collagen denaturation. Gelatine may further degrade because of hydrolysis of peptide bonds and crosslinks.

Aliev applied solid state NMR to characterize parchment and to evaluate the extent of degradation of historical parchments [163]. In this study wideline ^{1}H NMR was used to obtain information on the role of bound water in parchments and ^{13}C CPMAS NMR to evaluate the structure and dynamics of collagen in parchments. The ^{1}H wideline NMR spectrum of parchment was found to be the superposition of two peaks with very different linewidths, a broad component from collagen, and a narrow one due to bound water. The lineshape fitting was carried out assuming a pure Gaussian lineshape for the broad component and a mixed Lorentzian/Gaussian lineshape for the narrow component. Integrals obtained from the best fit procedure allowed the evaluation of the relative amount of collagen and water, P^W/P^C. This ratio was normalized to the number of protons of the water and of the collagen component respectively. In the case of the collagen component the average amount of protons was calculated from the amino acid

distribution obtained by High-Performance Liquid Chromatography (HPLC). In this way, the water content in each parchment sample, in gelatine, and in hydrolyzed collagen was evaluated. It was found that the water content in parchment decreases with the age of the sample and this was related to the partial hydrolysis of peptide bonds in collagen. The assignment of the ^{13}C CPMAS NMR spectra of historical and modern parchments was carried out on the basis of the assignments of amino acids, peptides and proteins reported in the literature [164,165]. It is worth noting that in the spectra of some historical parchments additional peaks assigned to calcite and aragonite were observed at 168.7 and 171 ppm (relative to TMS). In all samples a peak at 33 ppm assigned to Val C-3 was observed as a shoulder, however some samples showed an additional strong peak at the same chemical shift. This peak was assigned to chain carbons of fatty acids. The intensity ratio between the peaks at 33 ppm and 43 ppm, which were assigned to Gly C-2 and Arg C-5, was proposed for obtaining a semi-quantitative comparison of the lipid content in parchment samples. These peaks are the most intense signals of lipid and collagen respectively. It was found that chemical shifts are not affected by ageing, whereas a significant line broadening occurs on gelatinization. Most importantly, based on the linewidths, Aliev [163] introduced a disordered ranking parameter defined as:

$$R_d = \frac{\Delta\nu_{1/2} - \Delta\nu^C_{1/2}}{\Delta\nu^G_{1/2} - \Delta\nu^C_{1/2}}, \tag{21}$$

where $\Delta\nu_{1/2}$ is the linewidth of the peak at 71 ppm, ascribed to Hyp C-4, $\Delta\nu^C_{1/2}$ and $\Delta\nu^G_{1/2}$ are the line widths measured for collagen in new parchment and gelatin respectively. By definition R_d ranges between 0 and 1 in the case of historical parchments in their pre-gelation state, with higher R_d values corresponding to a higher level of degradation. Hydrolyzed collagen is a mixture of smaller molecular weight polypeptides than in gelatin and it can be considered as degraded gelatin. In this case values of $R_d > 1$ are possible depending on the extent of degradation of gelatin. The R_d parameter was proposed as an index for evaluating the extent of degradation in parchment. As an example, the ^{13}C CPMAS NMR spectrum of a 17th century parchment, is shown in Fig. 34. In this case R_d was found to be 0.4, indicating an intermediate state of degradation of the parchment. Furthermore, the intensity ratio between the peaks at 33 ppm and 43 ppm was found to be 0.59 indicating a detectable amount of lipids.

It was found [163] that $\Delta\nu_{1/2}$ increased as the relative water content decreased. To summarize, the decrease of water content, correlated with the broadening of the carbon linewidth which reflects the level of structural order in parchment.

Odlyha and coworkers [166] carried out a multi-technique study to characterize some modern and historical parchments. ^{13}C solid state NMR provided information on the amino and imino acid residues, and variations in their calculated ratios were measured in modern and naturally aged samples. These differences were compared with differences in glass transition temperatures and in shrinkage behaviour measured by Dynamic Mechanical Analysis (DMA).

Badea et al. [167] used unilateral NMR together with other techniques to investigate historical parchments in a fully non invasive way. In particular, proton spin–lattice relaxation times T_1 were measured, and were found to vary in accordance with deterioration pathways suggested by other techniques, such as Differential Scanning Calorimetry, Infrared analysis and Scanning Electron Microscopy. It was found that gelatinization produces disordered structures that can be associated with shorter T_1 values, whereas the occurrence of hydrolytic processes produces longer T_1 values.

Archaeological excavations in lake and seabeds, terrestrial levels and submerged areas in desert regions, often find a large number of leather artifacts, including harnesses, shoes and boots, clothes, and other objects of daily use. The preservation *in situ* critically depends on the environmental conditions at the excavation site, such as the depth of the layer and the dampness. Historical and archaeological leathers are a part of our Cultural Heritage, however their preservation is challenging, as it is a difficult material to conserve. The difficulty is due both to the nature of the raw hide and to the different processes applied for transforming it into leather. The macroscopic properties of the leather are mostly caused by the tanning process which may involve either organic compounds or mineral tannins. Oils or fats may be also introduced into the leather as tanning agents or at the end of the tanning process to increase the flexibility and the softness of the material, and to reduce water absorption.

^{13}C solid state NMR is a suitable technique for investigating both modern and archaeological leather samples. As an example, the ^{13}C CPMAS spectrum of a sample from an ancient leather shoe from the archaeological site of Antinoe, Egypt, is shown in Fig. 35.

^{13}C solid state NMR and ESR have been applied [168] to investigate the structural properties of waterlogged archaeological leathers and to follow their changes on ageing. Samples were collected from an excavation in Lyon, France. They were identified as being soles of shoes and dated from the 13th to 18th century. To facilitate the interpretation of archaeological samples, Bardet et al. [168] first characterized modern leathers tanned with vegetable tannins and

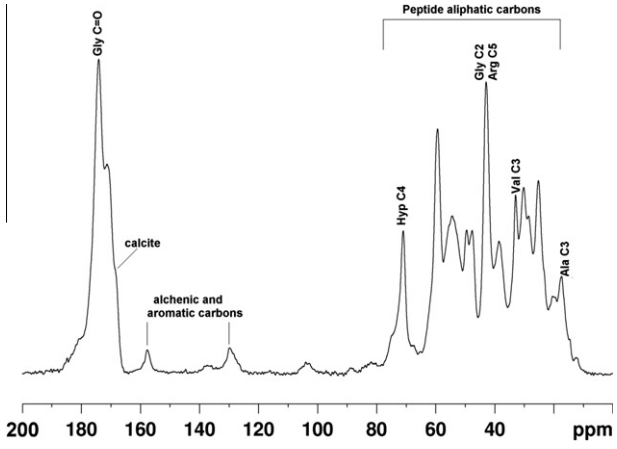

Fig. 34. ^{13}C CPMAS NMR spectrum at 100.13 MHz of a 17th century parchment from a private collection, assignment from [163]. (D. Capitani, N. Proietti, V. Di Tullio unpublished data.)

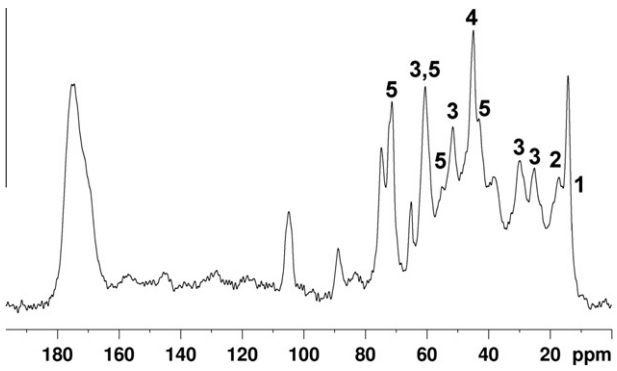

Fig. 35. ^{13}C CPMAS NMR spectrum at 100.13 MHz of a sample of an ancient leather shoe from the archaeological site of Antinoe, Egypt, the sample was a kind gift from Antiquity Science Department, Sapienza University of Rome. 1: Ala, Met; 2: Leu, Lys; 3: Pro; 4: Gly; 5: Hyp. Assignment from Ref. [168]. (D. Capitani, N. Proietti, V. Di Tullio unpublished data.)

to which lubricant has been applied. By comparing the ^{13}C CPMAS NMR spectra of leathers and tannins, it was possible to assign signals of tannin and collagen respectively. Tannins are aromatic compounds, and their ^{13}C spectra do not overlap with signals from collagen. The high degree of mobility of the molecules in the oils and fats in leather means that their ^{13}C resonances can be selectively edited by using direct carbon excitation with Magic Angle Spinning and a short recycle delay. The high mobility of the molecules in lubricants made it possible to apply the DEPT sequence [4] commonly used in solution NMR to discriminate methine, methylene and methyl carbon atoms of the lubricant in the leather. Despite a relatively broad range of ages, the ^{13}C CPMAS NMR spectra of archaeological samples were found to be similar to each other as all main peaks appear at the same chemical shift, however the intensity of some signals, in particular those at 70, 59, and 43 ppm from TMS, are slightly different in spectra of different samples. However all the leather artifacts were well conserved, showing ^{13}C CPMAS spectra typical of pure collagen. No traces of tannins or lubricants were found in the archaeological samples, possibly indicating that ageing in the water environment fully leached out both tannins and lubricants. ESR spectra detected a significant accumulation of iron and manganese oxides. To explain the surprising good state of conservation of the leather artifacts, the authors hypothesized a possible stabilization effect of the collagen moiety by metal oxides under those specific ageing conditions [168].

13. Archaeological bones and ancient mummies

Understanding the chemical and physical alteration in archaeological bones, which occurs after burial, is another subject of interest in Cultural Heritage.

Bones and dentine are composite materials made of inorganic and organic compounds. In particular, dentine is a calcified tissue of the body that, along with enamel, cementum, and pulp, is one of the four major components of teeth. The organic fraction consists of proteins (mainly collagen) and lipids, while the inorganic one is primarily semi-crystalline hydroxyapatite $Ca_{10}(PO_4)_6(OH)_2$. The crystallites of natural bone are extremely small (<50 nm) and for this reason X-ray information to date has been insufficient for a complete structural determination. Many researches have been carried out on the inorganic component of bone [169–171], however less is known about the mineral nature of the archaeological bone and changes occurring after burial (diagenesis). The term diagenesis describes the whole post-mortem chemical–physical process that produces alterations both in inorganic phases and in biological hard tissues after burial [172].

Solid-state NMR can be a helpful adjunct to other conventional techniques such as XRD in ascertaining the state of diagenesis of archaeological bones. An important advantage of solid state NMR is the ability to observe directly the environment of a phosphorus or carbon atom in a crystalline as well as in an amorphous phase, and to determine if the atom occupies a position in a hydroxyapatite lattice or a lattice type in which it is disordered around a lattice position [173]. Moreover solid-state NMR can give information about the presence and the mobility of hydrogen atoms which are not detectable by XRD. An example of the ^{13}C CPMAS spectrum of an archaeological bone is shown in Fig. 36, which is of a bone found during excavation in a site in Southern Italy.

Lee et al. [174] carried out one of the first studies in which ^{13}C solid state NMR results obtained on archaeological bones, were compared with XRD results. A single sample was examined described as a bovine knuckle aged about 15,000 years, from La Riera Cave in Asturias, Spain. XRD analysis suggested that the bone contained, in addition to hydroxyapatite, some calcium phosphate hydrate ($Ca_3(PO_4)_2{\cdot}(H_2O)_x$) and calcite (a crystalline form of calcium carbonate), and only about 0.5% of carbonate ion (the carbonate content of modern bone is 3–5%). The carbonate component is of interest because of the possible use of carbon-14 dating and in dietary analysis from carbon isotope ratios. Changes occurring during bone diagenesis, can alter conclusions concerning dating and diet. The ^{13}C CPMAS spectrum of the bone has a strong signal at 168 ppm characteristic of calcite. A rough estimate based on comparison with a standard calcite sample, indicates that calcite constitutes about 10% of the total. There is not a clear signal from normal carbonate in the hydroxyapatite matrix, in agreement with the low amount found by XRD analysis. The only other signals found are in the 0–50 ppm region, and are from organic material. NMR and XRD results were found to be in a good agreement, however the diffraction data gives no indication of the considerable amount of organic material present. NMR and XRD combined techniques indicated that the diagenesis process involved the production of calcite and calcium phosphate hydrate and diminished amounts of normal bone carbonate.

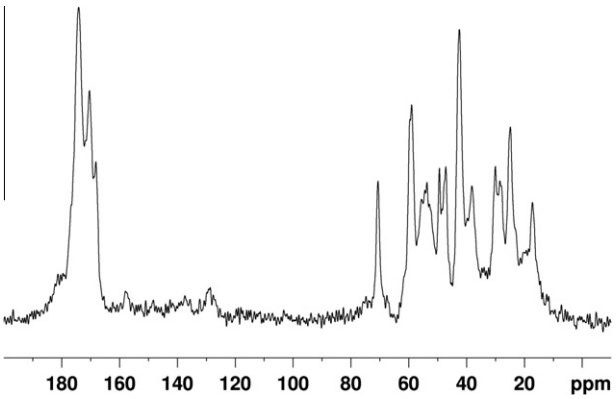

Fig. 36. ^{13}C CPMAS NMR spectrum at 100.13 MHz of an untreated ancient animal bone from an archaeological excavation site in Southern Italy. (D. Capitani, N. Proietti, V. Di Tullio, unpublished data.)

A later study on the diagenetic alteration of archaeological bones was carried out by combining complementary spectroscopy techniques such as solid state ^1H and ^{13}C NMR, IR spectroscopy and XRD [175]. Four archaeological human bones found in three Necropolises of Poseidonia (Paestum, Italy) were studied. Before the analysis, each archaeological bone fragment was cleaned by abrasion to remove any surface mineral, dried to remove surface hydration water, and treated with an acetic acid solution to evaluate the diagenetic alteration. The ^1H MAS NMR spectrum of an archaeological bone after the mechanical cleaning shows a rather broad resonance, centred at about 5 ppm, resulting from the presence of a considerable amount of hydration water. After drying, the hydration water was partially removed and an intense signal at 4.8 ppm, typical of $CaCO_3{\cdot}\ nH_2O$ and $NaHCO_3$ was observed. This signal can be assigned to the absorbed calcite which was deposited on the bone by groundwater during the burial. After the acid treatment, the signal at 4.8 ppm disappeared, confirming the elimination of the absorbed carbonate and bicarbonate salts by acidification. The ^{13}C MAS NMR spectrum has signals between 0 and 70 ppm ascribed to amino acidic residues in collagen, and two signals at 170 ppm and 174 ppm. After treatment with acetic acid, the signal at 170 ppm disappeared, suggesting that this signal is from adsorbed calcite, whereas the signal at 174 ppm is from structural CO_3^{2-} and organic carbonyls. This information was also correlated with the relative content of carbonate in the lattice of bone obtained by measuring the CO_3/PO_4 ratio by FTIR measurements. The ^1H MAS NMR spectrum of a contemporaneous

human bone has several signals ascribable to type 1 collagen. The comparison between the spectra of archaeological human bones and those from a contemporaneous bone, indicated a strong reduction of the organic fraction in buried bones, mainly due to natural degradation of proteins and lipids. In particular the intensity of the signal at 1.7 ppm seems to be correlated to collagen degradation. In the same paper ^{1}H and ^{13}C NMR spectroscopy was also used to characterize a sample of dentine after a drying process. In particular the ^{1}H NMR MAS spectrum has a narrow peak from the hydroxyl group, corresponding to highly crystalline material, associated with the absence of the characteristic signals of adsorbed carbonate and bicarbonate salts and the low amount of hydration water. This result was confirmed by ^{13}C CPMAS NMR analysis since the characteristic signal at 170 ppm of adsorbed carbonate is absent. These data confirmed that tooth enamel is more resistant to diagenesis alteration than bone.

Historical mummies and skeletons have also been studied. Ancient mummies have long been fascinating subjects of scientific researches, and it is not surprising that non-invasive diagnostic imaging has been widely applied to study them. Since the late 1970s computed tomography has been established as the most useful non-invasive method in this field. However, MRI which detects water protons, has met with only partial success with a limited subset of mummified samples. In the early reports of mummy MRI, no signal or image was obtained from a variety of pulse sequences unless there was an invasive re-hydration by acetone in water to increase NMR signal intensity [176]. It is worth noting that different type of mummies, reflecting various mummification processes, have been found in the world. Some were artificially mummified by well-trained embalmers (i.e. Egyptian mummies), whereas others were naturally mummified in dry (i.e. Taklimakan or northen Chile) permafrost (i.e. 15th century Greenland and Otzi the Iceman) or waterlogged conditions (i.e. bog bodies) [177]. Some of these types of mummies, such as Otzi the Iceman or bog bodies, belong to the so-called hydrated mummy category, as their tissue retained humidity. The MRI technique, which produces particularly clear images when applied to relatively well-hydrated tissue, can be a better diagnostic option for investigating the hydrated mummy category, as reported in the case of an MRI study on a hydrated mummy of medieval Korea [177]. In this study excellent MRI images of tissue and of well preserved internal organs were obtained, pointing out that MRI can be considered a powerful and non invasive tool for the investigation of hydrated mummies.

Nevertheless, recently some papers have reported successful MRI applications to dehydrated Egyptian mummies without artificial re-hydration, using newly available pulse sequences [178,179]. A non invasive ^{1}H and ^{23}Na MRI study of a mummified right first digit of an Egyptian human adult, was reported by Munnemann et al. [179]. In this study the feasibility of spatial ^{1}H and ^{23}Na imaging to visualize archaeological dry human tissue was demonstrated. The artificial mummification was done in ancient Egypt by dehydrating the corpse in Natron (e.g. a blend of NaCl and $NaCO_3.10H_2O$), and the authors expected ^{23}Na as a main component

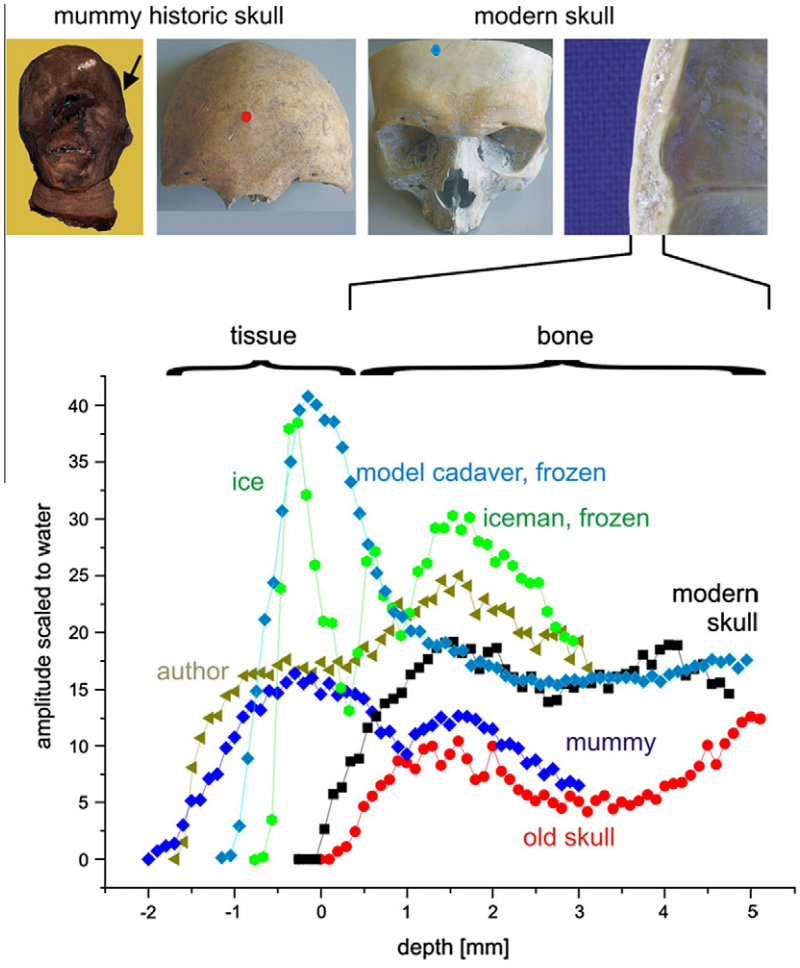

Fig. 37. Modern and historic (ca. 1100 AD) skulls and mummy head (top) with points of measurements and corresponding depth profiles (bottom). (Reproduced with permission from [37].)

of Natron to be found in the mummified tissues. In the collected images, protons were visualized primarily in the skin and soft tissue of the digit, whereas sodium accumulated inside the bone of the finger.

Although MRI is a non-destructive and non invasive technique, it cannot be used when mummies cannot leave the museum or need to be chilled as the case of Otzi The Iceman. Portable Profile NMR-MOUSE was used to analyze Otzi directly in the museum [37]. NMR depth profiles allowed the differentiation of various anatomical layers such as extra-corporal ice, skin, subcutaneous layers and skull bone compartments in both wet and dry tissues, see Fig. 37. In the same figure the depth profiles of a model frozen cadaver, an Egyptian mummy, a modern and an old skull, and a living human being (one of the authors), are also reported for comparison. The bone profiles of the model frozen cadaver and the modern skull overlap perfectly. The intensity of the NMR profiles of the Egyptian mummy and an old skull are lower than the intensity measured in Otzi and in the living human being profiles. It is worth noting that NMR depth profiles were also used to discriminate between textile wrapping from tissue and bone in Egyptian mummies [20,37]. In the case of the Otzi mummy the authors proposed a new NMR protocol for assessing the state of conservation by measuring the change of the signal of the water contained in frozen bone over time.

14. Plant exudates

Since ancient times plant exudates, including resins, gums, and gum resins, have been widely used in objects which are of interest to Cultural Heritage because of their artistic and/or historic value. Exudates have been used as jewelry, for religious purposes, as construction materials, for imparting luster to paper and textiles, as adhesives, lubricants, as bow rosin for some musical instruments. The most frequently used resins are colophony, Burgundy pitch, Venice and Strasbourg turpentine, sandarac and copals. Vegetable gums were used by the Egyptians, Greeks, and Romans and throughout the Middle Age as a binder for wall decorations. Water colours were also prepared from pigments tempered with water-soluble gums. Pigments were mixed with Arabic gum to paint motifs on an ivory surface. Rubber, turpentine, perfumes, paint solvents and cosmetics contain exudates. Plant exudates are produced by epithelial derivative cells adjacent to parenchymatous cells, whose content is released into elongated resin canals (gymnosperms) or into more globular resin pockets or blisters (angiosperms). These materials may be picked or scraped from the surface of plants. Resins are water–insoluble mixtures mostly of terpenes, and the fossilization process makes them extremely resistant to dissolution. These materials are usually referred to as fossil resins, or, inappropriately, as amber. Gums are water soluble or water-dispersible mixtures of polysaccharides. Gum resins such as myrrh and frankincense contain both terpenoid and carbohydrate components. Latexes are usually milky fluids consisting of droplets of organic compounds suspended or dispersed in an aqueous medium. The naturally occurring latex material called gum elastic, from the plant *Castilla elastica*, was firstly processed in pre-Hispanic South America. Note that latexes are easily identified by their characteristic carbon NMR spectrum of polyisoprene. The identification of these materials allows one to obtain information on the technology employed by artists and to understand the deterioration processes occurring in the object as well as the nature of alteration products. Exudates may have a very similar physical appearance and properties although they may have a very different molecular structures.

Lambert et al. [180] used solid state ^{13}C CPMAS NMR to investigate exudates collected from 65 species of gymnosperms and angiosperms. They developed a valuable library of spectral signatures for distinguishing types of exudates by NMR spectroscopy. The spectral signatures also provide a way of proving the authenticity of resinous materials of unknown provenance. In fact, the spectra of resins and gums are distinct from those of synthetic polymers that in appearance resemble natural materials but are fakes. Nuclear Magnetic Resonance applied to investigate bulk exudates, readily identified the materials as resins, gums, and gum resins. Lambert and coworkers [180] defined nine grouping of resins, each with a unique spectral signature, including dammars and many Bursera incense species. In particular these species are small to medium-sized trees frequently with a highly aromatic sap, the trunk and branches exude fragrant oleoresins used for incense by native Americans. For instance the Protium copal that belongs to this family, has probably been the main source of copal incense used by the Maya of Guatemala Highlands. The complex mixture of terpenes found in all resins varies across many families of plants, however they are characterized by specific fingerprints reflecting the specific terpene constituents. Taxonomically related genera tend to have similar or identical spectra. Gums have fully different NMR spectra from resins, such that resonances of saturated carbons are absent, but those from carbons characteristic of sugars are well observable. The spectra of gums, unlike those of resins, are very similar to each other, nevertheless they show defining features. Gum resins have characteristics of both resins and gums, as shown by their spectra which contain peaks from both saturated hydrocarbons and sugars. The investigated gum resins include mastic, myrrh, frankincense and Mexican mesquito.

14.1. Amber

Amber is a fossilized form of terpenoid resin found in many parts of the world and used by people of many different cultures as a raw material for decorative objects over several millennia. Amber samples have been associated with burials, and as a consequence the question arises as to the provenance of the material. A knowledge of the chemical structure of a sample of amber may allow one to associate a given object with its geographical

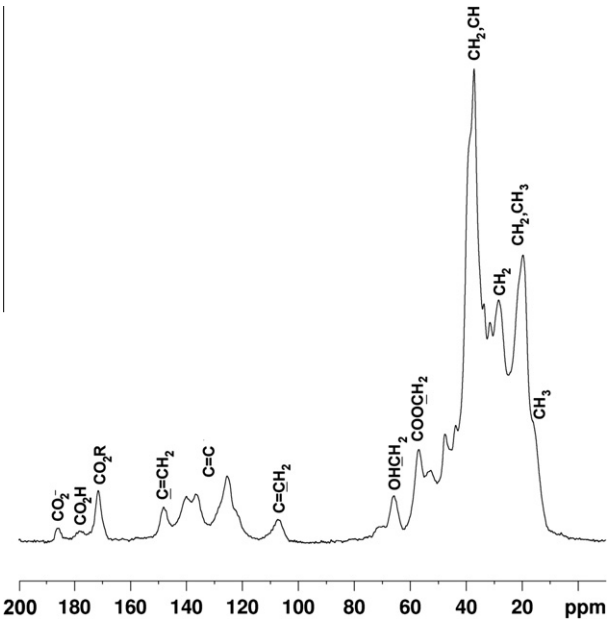

Fig. 38. ^{13}C CPMAS NMR spectrum at 100.13 MHz of a sample of amber. Assignment from [181]. (D. Capitani, N. Proietti, V. Di Tullio unpublished data.)

origin and to draw maps of cultural and trade networks, and provides information on the authenticity of artifacts. The chemical characteristics of amber depend on both its biological origin and geological environment. The non crystalline nature of amber and its poor solubility in most solvents have prevented the use of many characterization techniques. In 1982 Lambert and Frye published the ^{13}C CPMAS NMR spectrum of Baltic amber with the assigned carbon functionalities [181]: the spectrum shows signals in the aliphatic, olefinic and carbonyl regions. Baltic amber samples have essentially identical spectra, characterized by three weak peaks in the carbonyl region (carboxylate ion, carboxylate acid and carboxylate ester), exomethyelene resonances at 110 and 150 ppm from TMS, di and tri-substituted alkene resonances at 128 and 140 ppm, oxygen-substituted carbons at about 60 and 70 ppm, and a saturated carbon region with three major resonances. As an example, the ^{13}C CPMAS NMR spectrum of a sample of amber, is shown in Fig. 38.

The analysis of a large number of European ambers [182] allowed the samples to be assigned to two sets: one grouping materials from the northern European regions, including Baltic amber, and the other grouping materials from the southern European regions. The latter set was characterized by weaker carboxyl resonances than those found in the former group, by an alkene region with peaks at 127 and 138 ppm and the absence of exomethylene resonances, variable oxygen-substituted regions, and a saturated carbon region often showing only two major peaks.

Lambert et al. [183] also investigated Domenican ambers which have a significant variability of carbon functionalities. In particular, the intensity of the methylene carbon resonance at 30 ppm from TMS, varies from insignificant in most samples to quite appreciable in others. The intensities of ether/ester peaks between 45 and 75 ppm were found to be also rather variable, and there are small variations in the carboxyl resonances between 170 and 190 ppm. However the most variable region is that containing alkene carbons between 110 and 150 ppm, with different spectral patterns for almost every investigated sample.

Mexican amber was characterized and compared with Baltic and Domenican amber [184]. The ^{13}C CPMAS analysis of ambers from two sites in the state of Chiapas, Mexico established that samples from these sites are essentially identical, suggesting that Mexican amber might be a relatively homogeneous family of materials with a common paleobotanical source. Mexican and Baltic ambers have distinguishable spectra, with the latter having stronger carboxyl resonances, a dominant ester peak at 173 ppm ($-CO_2R$), and a peak at 180 ppm (–COOH) of acids compounds and their derivatives, along with stronger exomethylene resonances at 110 and 150 ppm, a strong methylene resonance between 28 and 30 ppm, and a weak peak at 67 ppm of methylene carbons next to an OH group. Spectral editing with dipolar dephasing experiments [8] which preferentially select quaternary and methyl carbons, accentuate the differences between the spectra of Mexican and Baltic ambers [185]. The spectra of Mexican and Domenican amber have different intensities of the exomethylene peaks that, in the spectra of Domenican amber varied in intensity but were always stronger than those of Mexican amber. There is also an ether peak (methylene carbons next to OC) at 75 ppm in the spectra of Domenican amber which is always very weak in the spectra of Mexican amber [184]. The spectra of Mexican and Domenican amber are very similar in the saturated region between 10 and 50 ppm.

The ^{13}C CPMAS NMR spectra of a wide variety of North American ambers can be used to distinguish these samples from those obtained from other locations in Mexico, the Domenican Republic and Europe [185]. The spectra of samples from Arkansas strongly contrast with those of other amber samples: the exomethylene resonances and a sharp resonance at 145 ppm are absent in amber from Arkansas, whereas a strong, diagnostic peak is located at 150 ppm, and the carbonyl region is of almost negligible intensity.

Lambert and coworkers [186] have compared the ^{13}C CPMAS NMR spectra of fossil resins from New Zealand and Australia with those of modern and semi-fossilized materials. Most of the spectra of the fossilized samples have strong similarities to those from modern *Agathis* resins, and to North American fossil resins. The spectra of a few samples dated from Late Cretaceous period from Australia and Papua New Guinea, indicate a different botanical source and have strong similarities to amber from Arkansas. In this paper the authors also proposed to use the intensity of resonances of exomethylene carbons to provide an approximate evaluation of the geological age of *Agathis*-related fossil resins.

A large number of fossil resins dated to the Cretaceous period have been investigated by ^{13}C CPMAS NMR spectroscopy [187]. Samples from Alaska, Canada, regions of United States, Greenland, France, Switzerland, Lebanon, Jordan and Israel have very similar spectra, which is consistent with their having a common, paleobotanical source related to *Agathis* that had a broad geographical distribution during Triassic, Cretaceous, and Early Tertiary times. Spectra from samples belonging to this group have a variation in spectral linewidths which suggests differences in sample age or maturity.

Copal is a hardened non-fossilized version of amber which differs from fossilized amber in its physical properties such as colour and its resistance to heat and organic solvents. Copals are young resins aged for only centuries or millennia. Martinez-Richa et al. [188] used ^{13}C CPMAS NMR spectroscopy to investigate Colombian copalite and commercial ambers from Chiapas, Domenican Republic and Poland. It was found that the spectrum of Colombian copalite is very similar to that of the resin obtained from the genus of the African species *H. Verrucosa* and to the spectra of ambers from other *Hymenea* species. In the same paper, the spectral features of the other samples were also reported and discussed.

Jet is probably the most important organic gemstone after amber, and it has been investigated by ^{13}C CPMAS NMR spectroscopy [189]. Its attractive black colour and ease of working made it a popular material for ornamentation in the past, even back to the Palaeolithic period. The ^{13}C CPMAS NMR spectra of jet samples from England and Spain resemble those of carbonaceous materials from lignitic and sub-bituminous ranks of coal. Coal is an organic sedimentary rock originating from the accumulation and preservation of plant materials usually in a swamp environment. As plant debris is exposed to the heat and pressure of burial it changes in composition and properties. The rank of a coal is a measure of how much change has occurred. In particular lignite is the lowest rank of coal with a carbon content ranging between 60% and 70% on a dry ash-free basis. Sub-bituminous coal is a lignite with an increased level of organic metamorphism, with a carbon content ranging between 71% and 77% on a dry ash-free basis. NMR has become a preferred method for the assessment of coal rank from the relative amount of aromatic and aliphatic resonances.

The spectra of jet samples from England and Spain [189] have aliphatic and aromatic carbon resonances in an roughly equal relative amount with maximum intensities at about 40 ppm, and 130 ppm respectively. The most characteristic resolved peaks of the jet spectra are the phenolic-like resonances at 155 and 120 ppm in the aromatic region and the methyl resonances at 10–20 ppm in the aliphatic region. Under conditions of dipolar dephasing, the entire aliphatic region disappears for Spanish jet, whereas for English jet a significant signal from rapidly moving methyl groups remains in the aliphatic region.

A ^{13}C CPMAS NMR investigation allowed the determination of the origin of two jet beads found in association with the burial of children in a Christian cemetery at Tipu, a colonial-period Maya site in Belize, Central America, and the determination of the origin

of an amber bead found in a midden from the early years of Spanish occupation. The analysis indicated that these materials are of European origin, more specifically the amber is clearly of Baltic origin and the jet spectrum is consistent with a Spanish origin [190].

14.2. Rubber

Ancient Mesoamerican people made solid rubber artifacts, used liquid rubber for medicine and painted with it. A ball game played with a solid rubber ball was a key event in ancient Mesoamerican society. The raw material for most Mesoamerican rubber artifacts was a latex obtained from the *Castilla elastica* tree which is indigenous to tropical lowland Mexico and Central America. Sixteenth century historical documents report that to improve the elastic properties, the ancient Mesoamerican people processed the raw material by mixing the latex with the juice obtained from *Ipomoea alba*, a species of morning glory vine, and then heated the processed rubber when forming it. Hosler et al. [191] analyzed samples obtained from unprocessed latex, processed according to the ancient technology, and ancient samples obtained from artifacts recovered from the Manati archaeological site at Veracruz, Mexico. The mechanical properties of unprocessed and processed latex were investigated by mechanical analysis, whereas solid state ^{13}C MAS and ^{13}C CPMAS NMR spectroscopy were applied to investigate the chemical structure of the samples. All ^{13}C MAS spectra show the five resonances characteristic of cis-1,4-polyisoprene which is the polymer component of natural rubber and latex, and in the case of the ancient sample a small amount of trans-1,4-polyisoprene was also detected. The ^{13}C CPMAS spectrum of unprocessed latex shows additional resonances, not detectable in the ^{13}C MAS spectrum, which suggests the presence of other carbon components, including proteins. These additional components are not present in the ^{13}C CPMAS spectrum of the latex processed with *Ipomoea alba*, indicating that the ancient processing of latex was possibly, in part, a purification process. Hosler and co-workers [191] have suggested that the elastic behaviour of latex processed with *Ipomoea alba* extract, originated from a combination of two processes, namely the purification of cis-1,4-polyisoprene by separation of the aqueous phase and dissolution of organic agents acting as plasticizers that impaired the interaction between polymeric chains, and an increase of interchain interactions favoured by reactions with sulfonyl chloride and sulfonic acid moieties found in *Ipomoea alba*. In contrast, simple drying of latex produces a brittle material without elastic behaviour.

14.3. Oriental lacquer

^{13}C CPMAS NMR spectroscopy has been applied to characterize oriental lacquer used as a decorative and protective coating for artifacts found in China and Japan [192]. This coating has been used in China for about the last 4000 years and in Japan since the 9th century AD. Oriental lacquer has a low solubility in almost all solvents except in a destructive sense with turpentine, and therefore analytical techniques which require the solubilization of samples are excluded. The raw lacquer contains up to 65–70% of urushiol, which is composed of catechols (ortho-dihyroxybenzenes substituted with a 15 carbon side chain containing from zero to three double bonds). The curing process of oriental lacquer, has been suggested to be a mechanism involving oxidation and polymerization to form certain oligomeric units [193], and this mechanism is supported by the observed ^{13}C CPMAS spectra. The most diagnostic carbon resonance is that at about 75 ppm from TMS, indicative of a carbon with an attached oxygen. Such a C–O group is not present in the starting urushiol, but is present in the oligomers. As a consequence, the intensity of this resonance was proposed as a marker indicating variation in the degree of polymerization. One of the historic samples analyzed by Lambert et al. [192] was found to have a spectrum remarkably different from the others, with the lowest intensity of the resonance at 75 ppm and the highest intensity of resonances due to unsaturated carbons, possibly indicating a lower degree of oligomerization and a higher proportion of the more unsaturated starting material.

15. Synthetic resins

Unsaturated polyester resins (UPR) have been widely used as contemporary art materials. Unfortunately, these materials age faster than traditional craft materials. Even objects in museums stored under controlled thermo-hygrometric conditions degrade very fast. The chemical composition and the manufacturing process play an important role in the degradation of these materials. A powerful analytical technique such as NMR can be successfully used to identify the materials constituting modern art objects and to investigate the degradation processes occurring in UPR-based materials. Stamatakis et al. [194] studied soluble acetone extracts by sonication of UPR resins obtained from two contemporary art installations. The surface of these artifacts was exposed to weathering and was therefore continuously subject to chemical alteration by environmental factors. At the same time the surface was the interface through which volatile chemicals components formed during the ageing escaped from the polymer matrix. UPR oligomers were identified by high resolution 1D and 2D NMR analysis as a main component of the acetone extracts, and are comprised of esterified phthalate or isophthalate, and esterified 1,2-propylene glycol units. Propylene glycol units bearing a hydroxyl end group, e.g. either primary or secondary propylene glycol, were also identified. Low molecular weight compounds were also identified such as styrene, dimethylphthalate, benzaldehyde, benzoic acid, and 2-hydroxy-4-methoxy-benzophenone. The presence of significant amounts of residual styrene in the resin indicates that a complete curing had not been achieved by the procedure applied by the artist when creating the art installation. Statistical analysis applied to the compositional data obtained by NMR showed that the styrene and benzaldehyde contents can be used to differentiate between fresh and aged UPR samples. Also, the detection of the phthalate and propylene glycol units in the extracts, along with the use of suitable reference samples, provided evidence of the commercial resin used to realize the art installations.

16. Identification of various organic residues in archaeological samples

The identification of the nature and composition of organic residues in archaeological samples can provide direct evidence of ancient activities and can help in determining their provenance. These compounds were of importance in everyday life, and, when extracted from archaeological findings and identified, enable archaeologists to shed light into the lives of ancient people and on their practices, such as diet, food processing and storage. In particular, pottery assemblages are often studied by archaeologists to obtain information about different aspects of ancient societies, such as the organization of production, trade and exchange, social complexity, and technological evolution. The archaeological information stored in any assemblage of artifacts may be interpreted only if the past use of the object is known. The most direct way of identifying the use of an original vessel is by detecting alterations resulting from use of the vessel. The chemical characterization of organic remains found in direct association with vessels is therefore considered to be a useful method in the functional study of ceramics.

One of the first published paper on the use of NMR spectroscopy in solution to identify a sample obtained from an archaeological finding, dates back to 1974 [195]. A liquid contained in a flask found in Syria, dated sixth–fourth century BC, was investigated by ^{1}H NMR spectroscopy. The spectrum clearly indicates that the substance is mainly oleic acid together with some saturated analogues. The NMR spectrum matches that of oleic acid and those of calcium and potassium oleate, whereas signals of the glycerol unit characteristic of olive oil are missing, indicating that, if the original sample had been olive oil, it underwent hydrolysis. However, despite the age of the sample complete polymerization or oxidation had not occurred.

During excavations to recover the relic of an ancient boat wrecked in 1629 AD in the Abrolhos Islands, a majolica jar containing a solid lump of resin was found. The NMR analysis of the material indicated the presence of unsaturated fatty esters, wax esters and a small amount of pine resin showing signals corresponding to those observed in spectra of modern pine rosins [196].

One of the first archaeological applications of ^{13}C NMR spectroscopy in solution to the analysis of organic material investigated the composition of non-metallic seals stored in collections in Britain [197]. The interest in the composition of these seals arose out of the desire to use materials which should closely match the original components in restoration works. The carbon spectrum of the chloroform soluble fraction of three seals matched the spectrum of modern beeswax except in the region at about 130 ppm where loss of the signal indicated loss of unsaturation through oxidation. The spectrum of the fourth seal shows only traces of beeswax, and the intense signals in the 130–150 ppm region indicate the presence of aromatic compounds similar to those present in rosin.

The combination of ^{13}C MAS and CPMAS NMR spectroscopy and isotopic analysis has been applied to characterize black encrustations from two forms of a late prehistoric pottery, flat plates and round pots, found in archaeological sites in Manitoba and southern Ontario, Canada [198]. These encrustations were presumed to be remains of prehistoric meals. The principal resonances observed in the spectra of encrustations from round pots are similar to those in spectra of samples produced by charring of meat and fish, and differ significantly from the spectra of uncharred foods. As a consequence, the interpretation of the aliphatic region of the solid state carbon spectra of these encrustations indicates that either meat or fish had been cooked in those pots, and that no significant amount of plant material is present in the residues. NMR spectra of encrustations from flat plates clearly indicate the presence of a greater amount of fat with respect to encrustations from round pots, possibly indicating that flat plates could have been used as frying pans or fat burning lamps.

^{13}C CPMAS NMR spectroscopy and FTIR have been applied [199] to characterize organic residues in ceramic vessels recovered from the settlement of Uitgeest-Groot Dorregeest, The Netherlands, which dates back to the Roman period. According to NMR spectra, three groups of residues can be defined on the basis of the extent of aromatization, i.e. aromatic charred residues, mildly condensed and highly condensed, non-aromatic residues, and soot residues containing polyaromatic hydrocarbons. The spectra of mildly condensed charred residues contain characteristics peaks of lipids and proteins, whereas those of highly condensed charred residues have a minimal number of lipid signals and, sometimes, carbohydrate peaks. Spectra of non-charred residues show only aliphatic and carboxylic resonances.

17. Conclusion

Many applications of various NMR methods to characterize and monitor Cultural Heritage have been reported. The various cases reported clearly show how NMR is not confined to a few specific applications, but its use can be successfully extended to a wide number of different issues regarding Cultural Heritage. In fact NMR is a very powerful tool in the chemical characterization of materials which allows light to be shed on the techniques used by artists, and can provide knowledge about the materials constituting artifacts. A knowledge of the causes of degradation of artifacts may also be achieved by NMR through the study of the chemical–physical transformation and structural modifications caused by ageing. NMR investigations may also help in planning proper restoration works. The reported investigations on archaeological bones, mummies, amber, and the identification of residues in archaeological findings, clearly show how NMR can also play an important role in a specific field of Cultural Heritage known as archaeometry which concerns the application of scientific techniques to the analysis of archaeological materials. NMR has not yet been widely used in this field. However, in the view of the possibility of using ever lower amounts of sample for the analysis of solutions, swollen samples and solids, NMR will probably become more and more competitive with other conventional analytical techniques.

An actual breakthrough has surely been the availability of portable NMR instrumentation which allows one to investigate large objects *in situ* without any sampling. Successful NMR applications to monitor *in situ* the state of degradation of artifacts and the effectiveness of restoration treatments show the real potentialities of portable NMR devices.

A number of experiments have already been developed and adapted for use in inhomogeneous magnetic field generated by portable NMR devices. Mobile instruments are already available for performing bi- and tri-dimensional imaging, and for obtaining high resolution depth profiles as well as for chemical-shift resolved spectroscopy. The technology may be further refined and focused on studies involving many new NMR applications, and possibly extended to include ESR *in situ*. The building of new sensors to investigate ever deeper depths inside the object with portable devices, and, maybe, the availability of sensors with enhanced sensitivity capable of successful detection of nuclei other than hydrogen with mobile instruments, will be possible future developments.

References

[1] R.R. Ernst, G. Bodenhausen, A. Wokaun, Principles of Nuclear Magnetic Resonance in One and Two dimensions, Clarendon Press, Oxford, 1987.
[2] P. Stilbs, Fourier transform pulsed-gradient spin-echo studies of molecular diffusion, Prog. Nucl. Magn. Reson. Spectrosc. 19 (1987) 1–45.
[3] K.F. Morris, C.S. Johnson, Diffusion-ordered two-dimensional nuclear magnetic resonance spectroscopy, J. Am. Chem. Soc. 114 (1992) 3139–3141.
[4] S. Braun, H.O. Kalinowski, S. Berger, 150 and More Basic NMR Experiments A Practical Course, Wiley-VCH Weinheim, Germany, 1998.
[5] M. Spraul, A.S. Feund, R.E. Nast, R.S. Withers, W.E. Maas, O. Corcoran, Advancing NMR sensitivity for LC-NMR-MS using a cryoflow probe: application to the analysis of acetaminophen in urine, Anal. Chem. 75 (2003) 1546–1551.
[6] G. Schlotterbeck, A. Ross, R. Hochstrasser, H. Senn, T. Kühn, D. Marek, O. Schett, High-resolution capillary tube NMR. A miniaturized 5-(L high-sensitivity TXI Probe for mass-limited samples, off-line LC NMR, and HT NMR, Anal. Chem. 74 (2002) 4464–4471.
[7] K.J.D. MacKenzie, M.E. Smith, in: R.W. Cahn (Ed.), Multinuclear Solid-State NMR of Inorganic Materials, Pergamon Materials Series 6, The Netherlands, 2002.
[8] K. Schmidt-Rohr, H.W. Spiess, Multidimensional Solid-State NMR and Polymers, Academic Press, London, 1994.
[9] B. Blümich, NMR Imaging of Materials, Monographs on the Physics and Chemistry of Materials 57, Clarendon Press, Oxford, 2003.
[10] A.T. Watson, C.T. Chang, Characterizing porous media with NMR methods, Progr. Nucl. Magn. Reson. Spectrosc. 31 (1997) 343–386.
[11] P. Galvosas, P.T. Callaghan, Multi-dimensional inverse Laplace spectroscopy in the NMR of porous media, C. R. Phys. 11 (2010) 172–180.
[12] R.L. Kleinberg, Utility of NMR T_2 distributions, connection with capillary pressure, clay effect, and determination of the surface relaxivity parameter $\rho 2$, Magn. Reson. Imag. 14 (1996) 761–767.

[13] K.J. Dunn, D.J. Bergman, G.A. Latorraca, Nuclear Magnetic Resonance Petrophysical and Logging Applications, vol. 32, Pergamon Press, 2002.
[14] M.D. Hürlimann, Effective gradients in porous media due to susceptibility differences, J. Magn. Reson. 131 (1998) 232–240.
[15] Y.Q. Song, L. Venkataramanan, M.D. Hürlimann, M. Flaum, P. Frulla, C. Straley, T_1–T_2 correlation spectra obtained using a fast two-dimensional Laplace inversion, J. Magn. Reson. 154 (2002) 261–268.
[16] M.D. Hürlimann, L. Venkataramanan, Quantitative measurement of two-dimensional distribution functions of diffusion and relaxation in grossly inhomogeneous fields, J. Magn. Reson. 157 (2002) 31–42.
[17] M.D. Hürlimann, L. Venkataramanan, C. Flaum, The diffusion-spin relaxation time distribution as an experimental probe to characterize fluid mixtures in porous media, J. Chem. Phys. 117 (2002) 10223–10232.
[18] A.E. English, K.P. Whittall, M.L.G. Joy, R.M. Henkelman, Quantitative two-dimensional time correlation relaxometry, Magn. Reson. Med. 22 (1991) 425–434.
[19] J.H. Lee, C. Labadie, C.S. Springer Jr, G.S. Harbison, 2-dimensional inverse Laplace transform NMR – altered relaxation-times allow detection of exchange-correlation, J. Am. Chem. Soc. 115 (1993) 7761–7764.
[20] B. Blümich, J. Perlo, F. Casanova, Mobile single-sided NMR, Progr. Nucl. Magn. Reson. 52 (2008) 197–269.
[21] R.L. Kleinberg, A. Sezginer, D.D. Griffin, M. Fukuhara, Novel NMR apparatus for investigating an external sample, J. Magn. Reson. 97 (1992) 466–485.
[22] G. Eidmann, R. Savelsberg, P. Blümer, B. Blümich, The NMR-MOUSE, a mobile universal surface explorer, J. Magn. Reson. A 122 (1996) 104–109.
[23] J. Mitchell, P. Blümer, P.J. McDonald, Spatially resolved nuclear magnetic resonance studies of planar samples, Progr. Nucl. Magn. Reson. 48 (2006) 161–181.
[24] R. Kimmich, NMR Tomography, Diffusometry, Relaxometry, Springer-Verlag, Berlin, 1997.
[25] T.J. Norwood, R.A. Quilter, A robust NMR method for studying diffusion, J. Magn. Reson. 97 (1992) 99–110.
[26] M. Klein, R. Fechete, D.E. Demco, B. Blümich, Self-diffusion measurements by a constant-relaxation methods in strongly inhomogeneous magnetic fields, J. Magn. Reson. 164 (2003) 310–320.
[27] A. Marko, B. Walter, W. Arnold, Application of a portable nuclear magnetic resonance surface probe to porous media, J. Magn. Reson. 185 (2007) 19–27.
[28] J. Perlo, V. Demas, F. Casanova, C.A. Meriles, J. Reimer, A. Pines, B. Blümich, High resolution NMR spectroscopy with a portable single-sided sensor, Science 308 (2005) 1279.
[29] D. Sakellariou, C.A. Meriless, A. Pines, Advances in *ex situ* nuclear magnetic resonance, C. R. Phys. 5 (2004) 337–347.
[30] J. Perlo, F. Casanova, B. Blümich, *Ex situ* NMR in highly homogeneous fields: ^{1}H spectroscopy, Science 315 (2007) 1110–1112.
[31] J. Perlo, F. Casanova, B. Blümich, Profiles with microscopic resolution by single-sided NMR, J. Magn. Reson. 176 (2005) 64–70.
[32] F. Presciutti, J. Perlo, F. Casanova, S. Glöggler, C. Miliani, B. Blümich, B.G. Brunetti, A. Sgamellotti, Noninvasive nuclear magnetic resonance profiling of painting layers, Appl. Phys. Lett. 93 (2008) 033505-1–033505-3.
[33] B. Blümich, F. Casanova, J. Perlo, F. Presciutti, C. Anselmi, B. Doherty, Noninvasive testing of art and cultural heritage by mobile NMR, Acc. Chem. Res. 43 (2010) 761–770.
[34] E. Del Federico, S.A. Centeno, C. Kehlet, P. Currier, D. Stockman, A. Jerschow, Unilateral NMR applied to the conservation of works of art, Anal. Bioanal. Chem. 396 (2010) 213–222.
[35] N. Proietti, F. Presciutti, V. Di Tullio, B. Doherty, A.M. Marinelli, B. Provinciali, N. Macchioni, D. Capitani, C. Miliani, Unilateral NMR, ^{13}C CPMAS NMR spectroscopy and micro-analytical techniques for studying the materials and state of conservation of an ancient Egyptian wooden sarcophagus, Anal. Bioanal. Chem. 399 (2011) 3117–3131.
[36] V. Di Tullio, N. Proietti, D. Capitani, I. Nicolini, A.M. Mecchi, NMR depth profiles as a non-invasive analytical tool to probe the penetration depth of hydrophobic treatments and inhomogeneities in treated porous stones, Anal. Bioanal. Chem. 400 (2011) 3151–3164.
[37] F.J. Rühli, T. Böni, J. Perlo, F. Casanova, M. Baias, E. Egarter, B. Blümich, Non-invasive spatial tissue discrimination in ancient mummies and bones *in situ* by portable nuclear magnetic resonance, J. Cult. Heritage 8 (2007) 257–263.
[38] D. Camuffo, Physical weathering of stones, Sci. Tot. Environ. 167 (1995) 1–14.
[39] G.C. Borgia, V. Bortolotti, M. Camaiti, F. Cerri, P. Fantazzini, F. Piacenti, Performance evolution of hydrophobic treatments for stone conservation investigated by MRI, Magn. Reson. Imag. 19 (2001) 513–516.
[40] G.C. Borgia, M. Camaiti, F. Cerri, P. Fantazzini, F. Piacenti, Study of water penetration in rock materials by nuclear magnetic resonance tomography: hydrophobic treatment effects, J. Cult. Heritage 1 (2000) 127–132.
[41] M. Gombia, V. Bortolotti, R.J.S. Brown, M. Camaiti, P. Fantazzini, Models of water imbibition in untreated and treated porous media validated by quantitative magnetic resonance imaging, J. Appl. Phys. 103 (2008) 094913-1–094913-8.
[42] M. Alesiani, S. Capuani, B. Maraviglia, R. Giorgi, P. Baglioni, Effects induced in marbles by water repellent compounds: the NMR contributions, Appl. Magn. Reson. 23 (2002) 63–73.
[43] M. Alesiani, S. Capuani, B. Maraviglia, NMR applications to low porosity carbonate stones, Magn. Reson. Imag. 21 (2003) 799–804.
[44] M. Alesiani, S. Capuani, B. Maraviglia, NMR study on the early stages of hydration of a porous carbonate stone, Magn. Reson. Imag. 21 (2003) 333–335.
[45] P.T. Callaghan, Principles of Nuclear Magnetic Resonance Microscopy, Oxford University Press, Oxford, 1991.
[46] L. Apollonia, G.C. Borgia, V. Bortolotti, R.J.S. Brown, P. Fantazzini, G. Rezzaro, Effects of hydrophobic treatments of stone on pore water studied by continuous distribution analysis of NMR relaxation times, Magn. Reson. Imag. 19 (2001) 509–512.
[47] P. López-Arce, L.S. Gomez-Villalba, L. Pinho, M.E. Fernández-Valle, M. Álvarez de Buergo, R. Fort, Influence of porosity and relative humidity on consolidation of dolostone with calcium hydroxyde nanoparticles: effectiveness assessment with non-destructive techniques, Mater. Charact. 61 (2010) 168–184.
[48] J. Arnold, C. Clauser, R. Pechnig, S. Anferova, V. Anferov, B. Blümich, Porosity and permeability from mobile NMR core-scanning, Petrophysics 47 (2006) 306–314.
[49] S. Anferova, V. Anferov, D.G. Rata, B. Blümich, J. Arnold, C. Clauser, P. Blümer, H. Raich, A Mobile NMR device for measurements of porosity and pore size distributions of drilled core samples, Concepts Magn. Reson. Part B Magn. Reson. Eng. 23B (2004) 26–32.
[50] B. Blümich, S. Anferova, R. Pechnig, H. Pape, J. Arnold, C. Clauser, Mobile NMR for porosity analysis of core sections, J. Geophys. Eng. 1 (2004) 177–180.
[51] S. Sharma, F. Casanova, W. Wache, A. Segre, B. Blümich, Analysis of historical porous building materials by the NMR-MOUSE, Magn. Reson. Imag. 21 (2003) 249–255.
[52] B. Blümich, S. Anferova, K. Kremer, S. Sharma, V. Herrmann, A. Segre, Unilateral NMR for quality control: the NMR-MOUSE®, Spectroscopy 18 (2003) 18–34.
[53] N. Proietti, D. Capitani, S. Cozzolino, M. Valentini, E. Pedemonte, E. Princi, S. Vicini, A.L. Segre, *In situ* and frontal polymerization for the consolidation of porous stones: an unilateral NMR and a magnetic resonance imaging study, J. Phys. Chem. B 110 (2006) 23719–23728.
[54] S. Chen, H.K. Liaw, A.T. Watson, Fluid saturation-dependent nuclear magnetic resonance spin–lattice relaxation in porous media and pore structure analysis, J. Appl. Phys. 74 (1993) 1473–1479.
[55] V. Bortolotti, M. Camaiti, C. Casieri, F. De Luca, P. Fantazzini, C. Terenzi, Water absorption kinetics in different wettability conditions studied at pore and sample scales in porous media by NMR with portable single-sided and laboratory imaging devices, J. Magn. Reson. 181 (2006) 287–295.
[56] M. Brai, C. Casieri, F. De Luca, P. Fantazzini, M. Gombia, C. Terenzi, Validity of NMR pore-size analysis of cultural heritage ancient building materials containing magnetic impurities, Solid State Nucl. Magn. Reson. 32 (2007) 129–135.
[57] J.R. Clifton, G.J.C. Frohnsdorf, Stone-Consolidating Materials: A Status Report, Conservation of Historic Stone Building and Monuments, National Academy Press, Washington, DC, 1982. pp. 287–311.
[58] L. Pel, H. Huinink, K. Kopinga, Ion transport and crystallization in historical objects as studied by NMR, Appl. Phys. Lett. 81 (2002) 2893–2895.
[59] L. Pel, H. Huinink, K. Kopinga, Ion transport and crystallization in porous materials as studied by magnetic resonance imaging, in: J.M. Huyghe (Ed.), IUTAM Proceedings on Physicochemical and Electromechanical Interactions in Porous Media, Springer, 2005, pp. 149–158.
[60] K. Kopinga, L. Pel, One-dimensional scanning of moisture in porous materials with NMR, Rev. Sci. Instrum. 65 (1994) 3673–3681.
[61] L.A. Rijniers, L. Pel, H.P. Huinink, K. Kopinga, Salt crystallization as damage mechanism in porous building materials: a nuclear magnetic resonance study, Magn. Reson. Imag. 23 (2005) 273–276.
[62] L.A. Rijniers, H.P. Huinink, L. Pel, K. Kopinga, Experimental evidence of crystallization pressure inside porous media, Phys. Rev. Lett. 94 (2005) 075503-1–075503-4.
[63] K.R. Brownstein, C.E. Tarr, Importance of classical diffusion in NMR studies of water in biological cells, Phys. Rev. A 19 (1979) 2446–2453.
[64] L.A. Rijniers, P.C.M.M. Magusin, H.P. Huinink, L. Pel, K. Kopinga, Sodium NMR in porous building materials, J. Magn. Reson. 167 (2004) 25–30.
[65] M. Gombia, V. Bortolotti, R.J. Brown, M. Camaiti, L. Cavallero, P. Fantazzini, Water vapor absorption in porous media polluted by calcium nitrate studied by time domain nuclear magnetic resonance, J. Phys. Chem. B 113 (2009) 10580–10586.
[66] G.C. Borgia, R J.S. Brown, P. Fantazzini, Uniform-penalty inversion of multiexponential decay data, J. Magn. Reson. 1321 (1998) 65–77.
[67] G.C. Borgia, R.J.S. Brown, P. Fantazzini, Uniform-penalty inversion of multiexponential decay data: II data spacing, T_2 data, systematic data errors, and diagnostics, J. Magn. Reson. 147 (2000) 273–285.
[68] T. Diaz Gonçalves, L. Pel, J.D. Rodrigues, Influence of paints on drying and salt distributions processes in porous building materials, Constr. Build. Mater. 23 (2009) 1751–1759.
[69] M. Matteini, An assessment of florentine methods of wall painting conservation based on the use of mineral treatments in the conservation of wall paintings, in: Sharon Cather (Ed.), The Proceedings of a Symposium Organized by the Courtauld Institute of Art and the Getty Conservation Institute, London, Tien Vah Press, Singapore, July 13–16, 1987.
[70] V.G.G. Amoroso, V. Fassina, Stone Decay and Conservation, Elsevier, Lausanne, 1983.
[71] A. Sansonetti, E. Rosina, N. Ludwig, Moisture damage new tools for the protection of cultural heritage in Italy: innovative techniques for *in situ* diagnostics, Mater. Eval. 69 (1) (2011) 41–46.
[72] E. Rosina, N. Ludwig, Optimal thermographic procedure for moisture analysis in buildings materials, in: Diagnostic Imaging Technologies and Industrial

Applications 1999, Munich, Germany, SPIE Proceedings, vol. 3827, SPIE ed. WA, USA, pp. 22–33.
[73] N. Proietti, D. Capitani, E. Rossi, S. Cozzolino, A.L. Segre, Unilateral NMR study of a XVI century wall painted, J. Magn. Reson. 186 (2007) 311–318.
[74] D. Capitani, N. Proietti, M. Gobbino, L. Soroldoni, U. Casellato, M. Valentini, E. Rosina, An integrated study for mapping the moisture distribution in an ancient damaged wall painting, Anal. Bioanal. Chem. 395 (2009) 2245–2253.
[75] R. Olmi, S. Priori, D. Capitani, N. Proietti, L. Capineri, P. Falorni, R. Negrotti, C. Riminesi, Innovative techniques for sub-surface investigation, Mater. Eval. 69 (2011) 89–96.
[76] V. Di Tullio, N. Proietti, M. Gobbino, D. Capitani, R. Olmi, S. Priori, C. Riminesi, E. Giani, Non-destructive mapping of dampness and salts in degraded wall paintings in hypogeous buildings: the case of St. Clement at mass fresco in St. Clement Basilica, Rome, Anal. Bioanal. Chem. 396 (2010) 1885–1896.
[77] V. Di Tullio, N. Proietti, G. Gentile, E. Giani, D. Poggi, D. Capitani, Unilateral NMR, a non-invasive tool for monitoring *in situ* the effectiveness of intervention to reduce the capillary rise of water in an ancient deteriorated wall painting, Int. J. Spectrosc., in press, doi: 10.1155/2012/494301.
[78] B. Blümich, A. Haber, F. Casanova, E. Del Federico, V. Boardman, G. Wahl, A. Stilliano, L. Isolani, Noninvasive depth profiling of walls by portable nuclear magnetic resonance, Anal. Bioanal. Chem. 397 (2010) 3117–3125.
[79] N. Proietti, D. Capitani, F. Presciutti, E. Rossi, A.L. Segre, G. Botticelli, Analysis of the conservation state of frescoes by unilateral NMR, in: U. Baldini, P.A. Vigato, (Eds.), The discovery of a forgotten pictorial cycle: Casa Vasari in Florence. An Interdisciplinary approach to the Restoration Project, Edizion Polistampa, Firenze, 2006, pp. 117–130.
[80] N. Proietti, D. Capitani, R. Lamanna, F. Presciutti, E. Rossi, A.L. Segre, Fresco Paintings studied by unilateral NMR, J. Magn. Reson. 177 (2005) 111–117.
[81] F. Presciutti, D. Capitani, A. Sgamellotti, B.G. Brunetti, F. Costantino, S. Viel, A. Segre, Electron paramagnetic resonance, scanning electron microscopy with energy dispersion X-ray spectrometry, X-ray powder diffraction, and NMR characterization of iron-rich fired clays, J. Phys. Chem. B 109 (2005) 22147–22158.
[82] L. Frydman, J.H. Harwood, Isotropic spectra of half-integer quadrupolar spins from bidimensional magic-angle spinning NMR, J. Am. Chem. Soc. 117 (1995) 5367–5368.
[83] C. Fernandez, J.P. Amoureux, Triple-quantum MAS-NMR of quadrupolar nuclei, Solid State Nucl. Magn. Reson. 5 (1996) 315–321.
[84] D. Massiot, F. Fayon, M. Capron, I. King, S. LeCalvé, B. Alonso, J.O. Durand, B. Bujoli, Z. Gan, G. Hoatson, Modelling one and two-dimensional solid-state NMR spectra, Magn. Reson. Chem. 40 (2002) 70–76.
[85] L. Pel, K. Kopinga, G. Bertram, G. Lang, Water absorption in a fired-clay brick observed by NMR scanning, J. Phys. D: Appl. Phys. 28 (1995) 675–680.
[86] P.J. McDonald, J. Mitchell, M. Mulheron, L. Monteilhet, J.P. Korb, Two-dimensional correlation relaxation studies of cement pastes, Magn. Reson. Imag. 25 (2007) 470–473.
[87] P.J. McDonald, P.S. Aptaker, J. Mitchell, M. Mulheron, A unilateral NMR magnet for sub-structure analysis in the built environment: the surface GARField, J. Magn. Reson. 185 (2007) 1–11.
[88] S. Anferova, V. Anferov, J. Arnold, E. Talnishnikh, M.A. Voda, K. Kupferschläger, P. Blümer, C. Clauser, B. Blümich, Improved Halbach sensor for NMR scanning of drill cores, Magn. Reson. Imag. 25 (2007) 474–480.
[89] Y.Q. Song, Novel two-dimensional NMR of diffusion and relaxation for material characterization, in: S. Stapf, S. Han (Eds.), NMR in Chemical Engineering, Wiley-VCH, Weinheim, 2006, pp. 163–183.
[90] C. Casieri, C. Terenzi, F. De Luca, Two-dimensional longitudinal and transverse relaxation time correlation as a low-resolution nuclear magnetic resonance characterization of ancient ceramics, J. Appl. Phys. 105 (2009). 034901-1-8.
[91] C. Terenzi, C. Casieri, A.C. Felici, M. Piacentini, M. Venditelli, F. De Luca, Characterization of elemental and firing-dependent properties of Phlegrean ceramics by non-destructive ED-XRF and NMR techniques, J. Archaeol. Sci. 37 (2010) 1403–1412.
[92] V. Tudisca, C. Casieri, F. Demma, M. Diaz, L. Piñol, C. Terenzi, F. De Luca, Firing technique characterization of black-slipped pottery in Praeneste by low field 2D NMR relaxometry, J. Archaeol. Sci. 38 (2011) 352–359.
[93] M. R. Gillespie, M.T. Stiles, BGS Rock Classification Scheme, Vol. 1 Classification of Igneous Rocks British Geological Survey, Research Report RR 96-0, Keyworth, Nottingham, UK, 1999.
[94] P. Ciccioli, P. Plescia, D. Capitani, ^{1}H, ^{29}Si, ^{27}Al MAS NMR as a tool to characterize volcanic tuffs and assess their suitability for industrial applications, J. Phys. Chem. C 114 (2010) 9328–9343.
[95] M. de Gennaro, A. Langella, Italian zeolitized rocks of technological interest, Miner. Deposita 31 (1996) 452–472.
[96] P. Ciccioli, C. Cattuto, P. Plescia, V. Valentini, R. Negrotti, Geochemical and engineering geological properties of the volcanic tuffs used in the Etruscan Tombs of Norchia (Northern Latium, Italy) and a study of the factors responsible for their rapid surface and structural decay, Archaeometry 52 (2010) 229–251.
[97] J. Klinowski, S. Ramdas, J.M. Thomas, C.A. Fyfe, J.S. Hartmann, A re-examination of Si, Al, ordering in zeolites NaX and NaY, J. Chem. Soc. Faraday Trans. 2 (78) (1982) 1025–1050.
[98] J. Cervantes, G. Mendoza-Díaz, D.E. Alvarez-Gasca, A. Martinez-Richa, Application of ^{29}Si and ^{27}Al magic angle spinning nuclear magnetic resonance to studies of the building materials of historical monuments, Solid State Nucl. Magn. Reson. 13 (1999) 263–269.
[99] G. Demortier, PIXE, PIGE and NMR study of the masonry of the pyramid of Cheops at Giza, Nucl. Instrm. Meth. Phys. Res. B 226 (2004) 98–109.
[100] M.P. Colombini, A. Andreotti, I. Bonaduce, F. Modugno, E. Ribechini, Analytical strategies for characterizing organic paint media using gas chromatography/mass spectrometry, Acc. Chem. Res. 43 (2010) 715–727.
[101] L. Mannina, A.P. Sobolev, A. Segre, Olive oil as seen by NMR and chemometrics, Spectrosc. Eur. 15 (2003) 6–14.
[102] R. Sacchi, M. Patumi, G. Fontanazza, P. Barone, P. Fiordiponti, L. Mannina, E. Rossi, A.L. Segre, A high-field ^{1}H nuclear magnetic resonance study of the minor components in virgin olive oils, J. Am. Oil. Chem. Soc. 73 (1996) 747–758.
[103] L. Mannina, F. Presciutti, N. Proietti, D. Capitani, A. Sgamellotti, B.B. Brunetti, unpublished results.
[104] A. Spyros, D. Anglos, Study of aging in oil paintings by 1D and 2D NMR spectroscopy, Anal. Chem. 76 (2004) 4929–4936.
[105] A. Spyros, D. Anglos, Studies of organic paint binders by NMR spectroscopy, Appl. Phys. A 83 (2006) 705–708.
[106] G. Cipriani, A. Salvini, L. Dei, A. Macherelli, F.S. Cecchi, C. Giannelli, Recent advances in swollen-state NMR spectroscopy for the study of drying oils, J. Cult. Heritage 10 (2009) 388–395.
[107] M. Paci, C. Federici, D. Capitani, N. Perenze, A.L. Segre, NMR study of paper, Carbohyd. Polym. 26 (1995) 289–297.
[108] D. Capitani, A.L. Segre, D. Attanasio, B. Blicharska, B. Focher, G. Capretti, ^{1}H NMR relaxation study of papers a system of cellulose and water, Tappi Journal 79 (1996) 113–122.
[109] D. Capitani, M.C. Emanuele, J. Bella, A.L. Segre, D. Attanasio, B. Focher, G. Capretti, ^{1}H NMR relaxation study of cellulose and water interaction in paper, Tappi J. 82 (1999) 117–124.
[110] D. Attanasio, D. Capitani, C. Federici, A.L. Segre, Electron spin resonance study of paper samples dating from the XV to the XVIII century, Archeometry 37 (1995) 377–384.
[111] D. Attanasio, D. Capitani, C. Federici, M. Paci, A.L. Segre, Electron paramagnetic resonance and ^{1}H and ^{13}C NMR study of paper, ACS Symp. Ser. 598 (1995) 333–353.
[112] D.L. VanderHart, R.H. Atalla, Studies of microstructure in native celluloses using solid state ^{13}C NMR, Macromolecules 17 (1984) 1465–1472.
[113] A. Isogai, M. Usuda, T. Kato, T. Uryu, R.H. Atalla, Solid state CP MAS ^{13}C NMR study of cellulose polymorphs, Macromolecules 22 (1989) 3168–3172.
[114] K. Overloop, L. Van Gerven, Freezing phenomena in adsorbed water as studied by NMR, J. Magn. Reson. A 101 (1993) 179–187.
[115] D. Capitani, N. Proietti, F. Ziarelli, A.L. Segre, NMR study of water-filled pores in one of the most widely used polymeric material: the paper, Macromolecules 35 (2002) 5536–5543.
[116] J. Clauss, K. Schmidt-Rohr, A. Adam, C. Boeffel, H.W. Spiess, Stiff macromolecules with aliphatic side chains: side-chain mobility, conformation, and organization from 2D solid-state NMR spectroscopy, Macromolecules 25 (1992) 5208–5214.
[117] D. Radloff, C. Boeffel, H.W. Spiess, Cellulose and cellulose/poly(vinyl alcohol) blends. 2. Water organization revealed by solid-state NMR spectroscopy, Macromolecules 29 (1996) 1528–1534.
[118] J. Clauss, K. Schmidt Rohr, H.W. Spiess, Determination of domain sizes in heterogeneous polymers by solid-state NMR, Acta Polym. 44 (1993) 1–17.
[119] M.P. Coughlan, M.G. Touhy, X.F. Filho, J. Puls, M. Claeyssens, M. Vrsanska, M.M. Hughes, Enzymological aspects of microbial emphasis on fungal system, in: M.P. Coughlan, G.P. Hazlewood (Eds.), Hemicellulose and Hemicellulases, Portland Press, London, 1993, pp. 53–85.
[120] D. Capitani, M.C. Emanuele, A.L. Segre, C. Fanelli, A.A. Fabbri, D. Attanasio, B. Focher, G. Capretti, Early detection of enzymatic attack on paper by NMR relaxometry, EPR spectroscopy and X-ray powder spectra, Nord. Pulp Pap. Res. 13 (1998) 95–100.
[121] C. Boileau, S. Pessanha, C. Tardif, K. Castro, N. Proietti, D. Capitani, S. Vicini, J.M. Madariaga, M.L. Carvahlo, E. Princi, Efficacy of waterborne polyurethane to prevent the enzymatic attack on paper-based materials, J. Appl. Polym. Sci. 113 (2009) 2030–2040.
[122] D. Capitani, A.L. Segre, M. Pentimalli, M. Bicchieri, P.F. Munafò, Ancient deteriorated paper: washing and restoring processes as studied by ^{13}C CP-MAS NMR spectroscopy, Quinio 2 (2000) 37–43.
[123] S. Margutti, S. Vicini, N. Proietti, D. Capitani, G. Conio, E. Pedemonte, A.L. Segre, Physical chemical characterization of acrylic polymers grafted on cellulose, Polymer 43 (2002) 6183–6194.
[124] R.K. Harris, Relaxation and double-resonance in solid-state NMR, in: R.K. Harris, P. Granger (Eds.), Multinuclear Magnetic Resonance in Liquids and Solids-Chemical Application, NATO ASI Series 322, Kluwer, Dordrecht, 1988, pp. 291–309.
[125] B. Blümich, S. Anferova, S. Sharma, A.L. Segre, C. Federici, Degradation of historical paper non destructive analysis by the NMR-MOUSE, J. Magn. Reson. 161 (2003) 204–209.
[126] N. Proietti, D. Capitani, E. Pedemonte, B. Blümich, A.L. Segre, Monitoring degradation in paper: non-invasive analysis by unilateral NMR. Part II, J. Magn. Reson. 170 (2004) 113–120.
[127] K. Castro, E. Princi, N. Proietti, M. Manso, D. Capitani, S. Vicini, J.M. Madariaga, M.L. Carvahlo, Assessment of the weathering effects on cellulose based materials trhough a multianalytical approach, Nucl. Instrm. Meth. Phys. Res. B 269 (2011) 1401–1410.
[128] K. Castro, S. Pessanha, N. Proietti, E. Princi, D. Capitani, M.L. Carvalho, J.M. Madariaga, Noninvasive and nondestructive NMR, Raman and XRF analysis of

a Blaeu coloured map from the seventeenth century, Anal. Bioanal. Chem. 391 (2008) 433–441.
[129] K. Castro, N. Proietti, E. Princi, S. Pessanha, M.L. Carvalho, S. Vicini, D. Capitani, J.M. Madariaga, Analysis of a coloured Dutch map from the eighteenth century: the need for a multi-analytical spectroscopic approach using portable instrumentation, Anal. Chim. Acta 622 (2008) 187–194.
[130] E. Del Federico, S.A. Centeno, C. Kehelet, P. Currier, D. Stockman, A. Jerschow, Unilateral NMR Applied to the conservation of works of art, Anal. Bioanal. Chem. 396 (2010) 213–220.
[131] I. Viola, S. Bubici, C. Casieri, F. De Luca, The codex major of the Collectio Altaempsiana: a non-invasive NMR study of paper, J. Cult. Heritage 5 (2004) 257–261.
[132] C. Casieri, S. Bubici, I. Viola, F. De Luca, A low-resolution non-invasive NMR characterization of ancient paper, Solid State Nucl. Magn. Reson. 26 (2004) 65–73.
[133] R.H. Newman, J.A. Hemmingson, Determination of the degree of cellulose crystallinity in wood by carbon-13 NMR spectroscopy, Holzforschung 44 (1990) 351–355.
[134] P.T. Larsson, K. Wickholm, T. Iversen, A CP/MAS ^{13}C NMR investigation of molecular ordering in celluloses, Carbohydr. Res. 302 (1997) 19–25.
[135] S.L. Mannu, NMR studies of wood and wood products, Progr. Nucl. Magn. Reson. Spectrosc. 40 (2002) 151–174.
[136] J.F. Haw, G.E. Maciel, E.A. Schroeder, Carbon-13 nuclear magnetic resonance spectrometric study of wood and wood pulping with cross polarization and magic-angle spinning, Anal. Chem. 56 (1984) 1323–1329.
[137] M. Bardet, K. Lundquist, J. Parkas, D. Robert, S. von Unge, ^{13}C assignments of the carbon atoms in the aromatic rings of lignin model compounds of the arylglycerol beta-aryl ether type, Magn. Reson. Chem. 44 (2006) 976–979.
[138] M. Bardet, D. Robert, K. Lundquist, S. von Unge, Distribution of erythro and threo forms of different types of β-O-4 structures in aspen lignin by ^{13}C NMR using the 2D INADEQUATE experiment, Magn. Reson. Chem. 36 (1998) 597–600.
[139] D.S. Argyropoulos, in: D.S. Argyropoulos (Ed.), Advances in Lignocellulosics Characterization, TAPPI Press, Atlanta, 1999.
[140] A.M. Gil, C. Pascoal Neto, Solid state NMR studies of wood and other lignocellulosic materials, Annu. Rep. NMR Spectrosc. 37 (1999) 75–117.
[141] M. Bardet, G. Gerbaud, M. Giffard, C. Doan, S. Hedger, G. Le Pape, ^{13}C high-resolution solid-state NMR for structural elucidation of archaeological woods, Prog. Nucl. Magn. Reson. Spectrosc. 55 (2009) 199–214.
[142] C.D. Araujo, A.L. MacKey, J.R.T. Hailey, K.P. Whittal, H. Le, Proton magnetic resonance techniques for characterization of water in wood: application to white spruce, Wood Sci. Technol. 26 (1992) 101–113.
[143] A. Pournou, Deterioration assessment of waterlogged archaeological lignocellulosic material via ^{13}C CP/MAS NMR, Archaeometry 50 (2008) 129–141.
[144] M. Bardet, M.F. Foray, Q.K. Tran, High-resolution solid-state CPMAS NMR study of archaeological woods, Anal. Chem. 74 (2002) 4386–4390.
[145] M. Bardet, M.F. Foray, S. Maron, P. Goncalves, Q.K. Tran, Characterization of wood components of Portuguese medieval dugout canoes with high-resolution solid-state NMR, Carbohyd. Polym. 57 (2004) 419–424.
[146] M. Alesiani, F. Proietti, S. Capuani, M. Paci, M. Fioravanti, B. Maraviglia, ^{13}C CPMAS NMR spectroscopic analysis applied to wood characterization, Appl. Magn. Reson. 29 (2005) 177–184.
[147] M. Bardet, G. Gerbaud, Q.K. Tran, S. Hediger, Study of interactions between polyethylene glycol and archaeological wood components by ^{13}C high-resolution solid state CP-MAS NMR, J. Archaeol. Sci. 34 (2007) 1670–1676.
[148] S. Viel, D. Capitani, N. Proietti, F. Ziarelli, A.L. Segre, NMR spectroscopy applied to the Cultural Heritage: a preliminary study on ancient wood characterization, Appl. Phys. A 79 (2004) 357–361.
[149] A. Salanti, L. Zoia, E.L. Tolppa, G. Giachi, M. Orlandi, Characterization of waterlogged wood by NMR and GPC techniques, Microchem. J. 95 (2010) 345–352.
[150] C. Crestini, N.M.N. El Hadidi, G. Palleschi, Characterization of archaeological wood: a case study on deterioration of a coffin, Microchem. J. 92 (2009) 150–154.
[151] L. Braunschweiler, R.R. Ernst, Coherence transfer by isotropic mixing: application to proton correlation spectroscopy, J. Magn. Reson 53 (1983) 521–528.
[152] A. Bax, D.G. Davis, MLEV-17-based two-dimensional homonuclear magnetization transfer spectroscopy, J. Magn. Reson. 65 (1985) 355–360.
[153] M.B. Robertson, K.J. Packer, Diffusion of D_2O in archaeological wood measured by 1-D NMR profiles, Appl. Magn. Reson. 17 (1999) 49–64.
[154] D.J. Cole-Hamilton, B. Kaye, J.A. Chudek, G. Hunter, Nuclear magnetic resonance imaging of waterlogged wood, Studies in Conservation 40 (1995) 41–50.
[155] J. Nagyvary, J.A. DiVerdi, N.L. Owen, H.D. Tolley, Wood used by Stradivari and Guarneri, Nature 444 (2006) 565.
[156] R. Chûiô, A. Shimaoka, K. Nagaoka, A. Kurata, M. Inoue, Primary structure of archeological silk and ancient climate, Polymer 37 (1996) 3693–3696.
[157] R.D.B. Fraser, T.P. MacRae, Conformation in Fibrous Proteins, Academic Press, New York, 1973.
[158] J. Kümmerlen, J.D. van Beek, F. Vollrath, B.H. Meier, Local structure in spider dragline silk investigated by two-dimensional spin-diffusion, Nucl. Mag. Reson. Macromol. 29 (1996) 2920–2928.
[159] R. Chûiô, K. Fukutani, Y. Magoshi, Estimation of physical properties of archaeological silk with NMR relaxation time and fluctuation–dissipation theorem in NMR spectroscopy of polymers in solution and in solid state, ACS Symp. Ser. 834 (2002) 83–91.
[160] E. Princi, S. Vicini, N. Proietti, D. Capitani, Grafting polymerization on cellulose based textiles: a ^{13}C solid state NMR characterization, Eur. Polym. J. 41 (2005) 1196–1203.
[161] E. Princi, S. Vicini, E. Pedemonte, N. Proietti, D. Capitani, A.L. Segre, L. D'Orazio, G. Gentile, C. Polcaro, E. Martuscelli, Physical and chemical characterization of cellulose based textiles modified by periodate oxidation, Macromol. Symp. 218 (2004) 343–352.
[162] G.N. Ramachandran, A.H. Reddi, Biochemistry of Collagen, Plenum Press, New York, 1976.
[163] A.E. Aliev, Solid-state NMR studies of collagen-based parchments and gelatin, Biopolymers 77 (2005) 230–245.
[164] H. Kalinowski, S. Berger, S. Braun, Carbon-13 NMR Spectroscopy, J. Wiley & Sons, New York, 1988.
[165] M. Kamihira, A. Naito, K. Nishimura, S. Tuzi, H. Saitô, A high-resolution solid-state ^{13}C and ^{15}N NMR study on crystalline Leu- and Met-enkephalins distinction of polymorphs, backbone dynamics and local conformational rearrangements induced by dehydration or freezing motions of bound solvent, J. Phys. Chem. B 102 (1998) 2826–2834.
[166] M. Odlyha, N.S. Cohen, G.M. Foster, A. Aliev, E. Verdonck, D. Grandy, Dynamic mechanical analysis (DMA), ^{13}C solid state NMR and micro-thermomechanical studies of historical parchment, J. Therm. Anal. Calorim. 71 (2003) 939–950.
[167] E. Badea, L. Miu, P. Budrugeac, M. Giurginca, A. Mašic, N. Badea, G. Della Gatta, Study of deterioration of historical parchments by various thermal analysis techniques complemented by SEM, FTIR, UV–VIS–NIR and unilateral NMR investigations, J. Therm. Anal. Calorim. 91 (2008) 17–27.
[168] M. Bardet, G. Gerbaud, L. La Pape, S. Hediger, Q.-K. Trân, N. Boumlil, Nuclear magnetic resonance and electron paramagnetic resonance as analytical tools to investigate the structural features of archaeological leathers, Anal. Chem. 81 (2009) 1505–1511.
[169] W.D. Armstrong, L. Singer, Composition and constitution of the mineral phase of bone, Clin. Orthop. Relat. Res. 38 (1965) 179–196.
[170] A.L. Boskey, A.S. Posner, Bone structure, composition and mineralization, Orthop. Clin. N. Am. 15 (1984) 597–612.
[171] W.E. Brown, L.C. Chow, Chemical properties of bone mineral, Ann. Rev. Mater. Sci. 6 (1976) 213–250.
[172] R.E.M. Hedges, Bone diagenesis: an overview of processes, Archaeometry 44 (2002) 319–328.
[173] M.I. Kay, R.A. Young, A.S. Posner, Crystal structure of hydroxyapatite, Nature 204 (1964) 1050–1052.
[174] A.P. Lee, J. Klinowski, E.A. Marseglia, Application of nuclear magnetic resonance spectroscopy to bone diagenesis, J. Archeol. Sci. 22 (1995) 257–262.
[175] D. Alfano, A.R. Albunia, O. Motta, A. Proto, Detection of diagenetic alterations by spectroscopic on archaeological bones from the Necropolis of Poseidonia (Paestum): a case study, J. Cult. Heritage 10 (2009) 509–513.
[176] D.N. Notman, J. TashJian, A.C. Aufderheide, O.W. Cass, O.C. Shane, T.H. Berquisit, J.E. Gray, E. Gedgaudas, Modern imaging and endoscopic biopsy techniques in Egyptian mummies, AJR 146 (1986) 93–96.
[177] D.H. Shin, I.S. Lee, M.J. Kim, C.S. Oh, J.B. Park, G.D. Bok, D.S. Yoo, Magnetic resonance imaging performed on a hydrated mummy of medieval Korea, J. Anatom. 216 (2010) 329–334.
[178] F.J. Rűhli, H. Von Waldburg, S. Nielles-Vallespin, T. Böni, P. Speier, Clinical magnetic resonance imaging of ancient dry human mummies without rehydration, JAMA 298 (2007) 2618–2620.
[179] K. Munnemann, T. Böni, G. Colacicco, B. Bluemich, F.J. Ruhli, Non-invasive ^{1}H and ^{23}Na nuclear magnetic resonance imaging of ancient Egyptian human mummified tissue, Mag. Reson. Imag. 25 (2007) 1341–1345.
[180] J.B. Lambert, Y. Wu, J.A. Santiago-Blay, Taxonomic and chemical relationships revealed by nuclear magnetic resonance spectra of plant exudates, J. Nat. Prod. 68 (2005) 635–648.
[181] J.B. Lambert, J.S. Frye, Carbon functionalities in amber, Science 217 (1982) 55–57.
[182] J.B. Lambert, C.W. Beck, J.S. Frye, Analysis of European amber by carbon-13 nuclear magnetic resonance spectroscopy, Archaeometry 30 (1988) 248–263.
[183] J.B. Lambert, J.S. Frye, G.O. Poinar, Amber from the Dominican republic: analysis by nuclear magnetic resonance spectroscopy, Archaeometry 27 (1985) 43–51.
[184] J.B. Lambert, J.S. Frye, T.A. Lee, C.J. Welch, G.O. Poinar, Analysis of Mexican amber by carbon-13 NMR spectroscopy, in: Archaeological Chemistry, in: R. Allen (Ed.), Advances in Chemistry Ser. 220, vol. IV, American Chemical Society, Washington, DC, 1989, pp. 381–388.
[185] J.B. Lambert, J.S. Frye, G.O. Poinar, Analysis of North American amber by carbon-13 NMR spectroscopy, Geoarchaeology 5 (1990) 43–52.
[186] J.B. Lambert, S.C. Johnson, G.O. Poinar, J.S. Frye, Recent and fossil resins from New Zealand and Australia, Geoarchaeology 8 (1993) 141–155.
[187] J.B. Lambert, S.C. Johnson, G.O. Poinar, Nuclear magnetic resonance characterization of Cretaceous amber, Archaeometry 38 (1996) 325–335.
[188] A. Martinez-Richa, R. Vera-Graziano, A. Rivera, P. Joseph-Nathan, A solid-state carbon-13 NMR analysis of ambers, Polymer 41 (2000) 743–750.
[189] J.B. Lambert, J.S. Frye, A. Jurkiewicz, The provenance and coal rank of jet by carbon-13 nuclear magnetic resonance spectroscopy, Archaeometry 34 (1992) 121–128.

[190] J.B. Lambert, E. Graham, M.T. Smith, J.S. Frye, Amber and Jet from Tipu, Belize, Ancient Mesoamerica 5 (1994) 55–60.
[191] D. Hosler, S.L. Burkett, M.J. Tarkanian, Prehistoric polymers: rubber processing in Ancient Mesoamerica, Science 284 (1999) 1988–1991.
[192] J.B. Lambert, J.S. Frye, G.W. Carriveau, The structure of oriental lacquer by solid-state nuclear magnetic resonance spectroscopy, Archaeometry 33 (1991) 87–93.
[193] J. Kumanotani, Laccase-catalyzed polymerization of urushiol in precisely confined Japanese lacquer system, Makromol. Chem. 179 (1978) 47–61.
[194] G. Stamatakis, U. Knuutinen, K. Laitinen, A. Spyros, Analysis and aging of unsaturated polyester resins in contemporary art installations by NMR spectroscopy, Anal. Bioanal. Chem. 398 (2010) 3203–3214.
[195] C.W. Beck, C.A. Fellows, E. MacKennan, Nuclear magnetic resonance spectrometry in archaeology, Archaeol. Chem. 138 (1974) 226–235.
[196] E.L. Ghisalberti, I. Godfrey, The application of nuclear magnetic resonance spectroscopy to the analysis of pitches and resins from marine archaeological sites, Bull. Aust. Inst. Marit. Archaeol. 14 (1990) 1–8.
[197] M. Cassar, G.V. Robins, R.A. Fletton, A. Alstin, Organic components in historical non-metallic seals identified using ^{13}C NMR spectroscopy, Nature 303 (1983) 238–239.
[198] B.L. Sherriff, M.A. Tisdale, B.G. Sayer, H.P. Schwarz, M. Knif, Nuclear magnetic resonance spectroscopic and isotopic analysis of carbonized residues from subarctic Canadian prehistoric pottery, Archaeometry 37 (1995) 95–111.
[199] T.F.M. Oudemans, J.J. Boon, R.E. Botto, FTIR and solid-state ^{13}C CP/MAS NMR spectroscopy of charred and non-charred solid organic residues preserved in roman iron age vessels from The Netherlands, Archaeometry 49 (2007) 571–594.